CRC Report No. A-89-4

Properties of an Ozone Metamodel for the Continental United States

Deliverable 2D

June 2016

COORDINATING RESEARCH COUNCIL, INC.
5755 NORTH POINT PARKWAY·SUITE 265·ALPHARETTA, GA 30022

The Coordinating Research Council, Inc. (CRC) is a nonprofit corporation supported by the petroleum and automotive equipment industries. CRC operates through the committees made up of technical experts from industry and government who voluntarily participate. The four main areas of research within CRC are: air pollution (atmospheric and engineering studies); aviation fuels, lubricants, and equipment performance, heavy-duty vehicle fuels, lubricants, and equipment performance (e.g., diesel trucks); and light-duty vehicle fuels, lubricants, and equipment performance (e.g., passenger cars). CRC's function is to provide the mechanism for joint research conducted by the two industries that will help in determining the optimum combination of petroleum products and automotive equipment. CRC's work is limited to research that is mutually beneficial to the two industries involved. The final results of the research conducted by, or under the auspices of, CRC are available to the public.

P. Steven Porter
Porter-Gego
Idaho Falls, Idaho 83401
pporter@uidaho.edu

ABSTRACT

A metamodel is a mathematical relationship between the inputs and outputs of an air quality model. This report describes a metamodel that was fit to a 21-year ozone simulation (1990-2010) for the continental United States. Predictors included the Principal Component Scores (PCS) of emission and meteorological variables, while the predictand was the monthly mean of 8-hour daily maximum ozone for the ozone season at each model grid. The PCS form an orthogonal basis for the metamodel predictors. In addition, a few PCS incorporate most of the variability of emissions and meteorology, thereby reducing the dimensionality of the predictor space. Stochastic kriging was used to estimate the model.

The metamodel was used to (1) separate variability due to meteorology from that due to emissions, (2) estimate meteorologically-independent temporal trends in ozone for the 21 years, and (3) estimate the ozone response to particular emission sources. Meteorological and emission effects were separated by running the metamodel with emissions constant (ozone dependent on meteorology), or constant meteorology (ozone dependent on emissions). Years with ozone-conducive meteorology were identified, and the meteorological variables that best explain meteorologically-dependent ozone were identified. Meteorology accounted for 19% to 55% of total ozone variability in the eastern U.S., and 39% to 92% in the western U.S. Variability attributed to emissions, on the other hand, ranged from 46% to 74% in the eastern US and 1 to 33% in the west. Much of the variability attributed to emissions in the eastern US is due to the downward trend there. Most of the emission-driven ozone trend in the eastern U.S. occurred after 2000. Emission driven changes for the period 2000-2010 were between 6.4 and 10.9 ppb for the eastern U.S. and 1.4 to 2.5 ppb for the western U.S. Temporal trends estimated for CMAQ and emission-dependent ozone were both negative but confidence intervals for emission-dependent ozone are much smaller.

The ozone response to emissions was assessed by regressing emission-dependent ozone against emission sources. There was no improvement in emission-dependent ozone air quality during 1990-2000 despite reductions in emissions (representing about 30% of the reductions during 1990-2010). The years 2001-2005, representing roughly 30% of emission changes, saw significant reductions in emission-dependent ozone followed by modest improvements during 2006-2010, with the latter period having about 40% of emission reductions.

The largest responses in the eastern U.S. (NE, MA, MW, S) were to mobile sources and the smallest responses were usually for non-road mobile in parts of the eastern U.S., which trended steadily downward during the period of study. The ozone response to anthropogenic emissions was largest in the eastern U.S., with large areas declining by more than 15 ppb. For much of the western U.S., the responses are much smaller. Area sources, due to wildfires, produced ozone responses in the western U.S. of 6-8 ppb

I. INTRODUCTION

A metamodel was developed from a 21-year Community Multiscale Air Quality (CMAQ) model simulation experiment for the continental U.S. (CONUS). A metamodel is a mathematical relationship between the inputs and outputs of an air quality model, permitting estimation of additional modeling scenarios without having to run costly new simulations. Ozone predictors for the metamodel included monthly mean emissions and meteorology, while the CMAQ outputs of interest are the monthly means of daily maximum 8-hour summer season surface ozone (May-September). The metamodel was fit by stochastic kriging (Ankenman, 2010) applied to the Principal Component Scores (PCS) of the emissions and meteorology. The PCS form an orthogonal basis for the metamodel inputs (Eder et al, 1993, Bakshi, 1998). In addition, a few PCS incorporate most of the variability of emissions and meteorology, thereby reducing the dimensionality of the problem.

The 21-year model run was created for a variety of purposes that did not initially include metamodel development. Therefore, the meteorological fields and emission inventories did not represent extra effort. In addition, the NOx and VOC emissions for some sources (mobile for example) are correlated to a degree because they tend to occur together. Ozone simulations dedicated to metamodel development, on the other hand, are typically designed to capture the ozone response to a range of emissions for a fixed set of meteorological conditions. The metamodel described in USEPA (2006), for example, is based on 155 one-month model runs with emissions selected via statistical sampling of a wide range of emissions; in this case the emissions are orthogonal and the meteorology is fixed.

During the simulation period, CMAQ monthly average ozone values declined in much of the eastern U.S. and were little changed in the western U.S. At the same time, anthropogenic VOC and NOx emissions declined by roughly 50%. The western US also saw significant trends in several CMAQ meteorological variables.

The metamodel was used to (1) separate variability due to meteorology from that due to emissions, (2) estimate meteorologically-independent temporal trends in ozone for the 21 years, and (3) estimate the ozone response to particular emission sources. The years with ozone-conducive meteorology were identified and ozone variability was attributed to emissions or meteorology. Temporal trends in emission-dependent ozone were estimated and compared with CMAQ ozone. The ozone response to emissions (emission-dependent ozone) was negligible during 1990-2000 despite reductions in emissions (representing about 30% of the reductions during 1990-2010. The years 2001-2005, representing roughly 30% of emission changes, saw significant reductions in emission-dependent ozone air quality followed by modest improvements during 2006-2010, with this period having about 40% of emission reductions.

The largest responses in the eastern U.S. (NE, MA, MW, S) were to mobile sources and the smallest responses were usually for non-road mobile in parts of the eastern U.S. The ozone response to anthropogenic emissions was largest in the eastern U.S., with large areas declining by more than 15 ppb. For much of the western U.S., the responses are much smaller. Area sources, mostly due to wildfires, produced ozone responses in the western U.S. of 6-8 ppb.

II. Methods

A. Photochemical model setup

Photochemical model simulations were done for the years 1990-2010 with the on-line coupled weather research and forecasting (WRF) - Community Multiscale Air Quality (CMAQ) version 5.0 modeling system (Wong et al, 2012). The WRF simulation was derived from the NCEP/NCAR Reanalysis (2.5^{o} x 6h temporal resolution).

The outer domain was the northern hemisphere (108 km resolution, 44 vertical layers of variable thickness between the surface and 50 mb), while the inner domain was the CONUS with a grid cell size of 36 km. The inner domain was divided into eight (8) regions (Figure 1) which were fit to separate metamodels. The sub-regions considered include Northeast (NE), Middle Atlantic (MA), Midwest (MW), South (S), West (W), Northwest (NW), West Coast (WC), and Southwest (SW).

The emissions were based on the U.S. EPA National Emissions Inventory (NEI) for the years 1990, 1995, 1996, 1999, 2001, 2002 and 2005. For other years, emissions were scaled depending on the trends of activity data and emission controls over the entire period (Xing et al., 2013).

The predicted variables were monthly averages of the daily maximum 8-hour average ozone concentrations at each grid cell for the ozone season, defined as 1 May to 30 September (153 days or 5 months). Predictors included monthly means of emission and meteorological variables. Table 1 lists the emission sources while meteorological variables are shown in Table 2. All predictors were scaled (0 to 1 basis).

B. Metamodel Development

Metamodels were fit to the Principal Components Scores (PCS) of the predictor variables using Stochastic Kriging (SK) (Ankenman, 2010). The PCS form an orthogonal basis for the predictors and replace the original set of predictors (*X*) with scores (*XS*):

$$\boldsymbol{XS} = (\boldsymbol{X} - \overline{\boldsymbol{X}}) * \boldsymbol{XW} \quad , \quad \boldsymbol{X} = \boldsymbol{XS} * \boldsymbol{XW'} + \overline{\boldsymbol{X}} \tag{1}$$

Scores are the orthogonal representation of X in the principal component space, while *XW* are the weights (coefficients applied to X) that accomplish the transformation between X and XS. Dimension reduction is accomplished when a few 'scores' (PCS) explain much of the variability in X (see Eder et al, 1993 for other air quality applications of principal component analysis).

A single set of PCS was created for each region of the model domain from anthropogenic emissions, meteorology and biogenic emissions (all rescaled to 0 to 1) at each model cell. The set of scores explaining more than 95% of the variability of set of predictors was retained. The number of PCS used ranged from 14 to 28 depending on region.

SK is a geostatistical method for which emissions and meteorology have the role of location coordinates. Ozone values coincident with a particular set of emission and meteorological values are interpolated from nearby ozone values (Ankenman et al, 2010). An interpolation estimate looks like:

$$\widehat{\boldsymbol{Y}} = \boldsymbol{\mu} + \boldsymbol{B_1 Y_1} + \boldsymbol{B_2 Y_2} + \boldsymbol{B_3 Y_3} + \boldsymbol{B_4 Y_4} + \boldsymbol{B_5 Y_5} \ldots + \boldsymbol{B_n Y_n} + \boldsymbol{\varepsilon_i} \tag{2}$$

The Y_i are neighbors of an ozone value at a location of interest ($\hat{Y}$) in the sense that they are close to $\hat{Y}$ in terms of the PCS of emissions and meteorology. The B_i are constants derived from the correlation between different ozone values as a function of their distance apart (as noted, distance in terms of emissions and/or meteorology). While equation (2) is linear, SK ozone response is nonlinear with respect to emissions and meteorology (unlike projection onto latent structures, which is a linear model based on PCS (Wold et al, 2001)).

While the PCS are indeed orthogonal, highly collinear variables are separated in an arbitrary fashion. Monthly mobile source VOC and NOx are highly correlated in every sub-domain (average R2 > 0.95). Therefore, for the metamodel applications that follow, the effects of NOx and VOC on ozone are considered jointly.

C. Metamodel application

After SK estimation with the 21-year set of predictor and output variables, the metamodel was run with either meteorology or emissions fixed. To determine the ozone response to emissions, for example, the model was driven with meteorology from a particular year while emissions (one or more sources) were varied. Conversely, the ozone response to meteorology was determined from a metamodel run with a single year of emissions and meteorology varying over the 21 years.

III. RESULTS AND DISCUSSION

A. Overview of metamodel predictand and predictor variables

1. CMAQ ozone

Temporal trends for CMAQ monthly mean 8 hour ozone concentrations for July (1990 - 2010) are shown in Figure 2 (ppb/year, upper panel), and slope p values (lower panel). Trends were larger and more often statistically significant ($p<0.05$) in the eastern half of the U.S. A large percentage of model cells in the eastern U.S. have negative trends, while most of the western U.S. is trend-free (Table 3, Row 1). For the eastern U.S. (NE, MA, MW, S) the percentage of model cells with negative trends ranges from 35% to 87% ($p\leq0.05$). None of the cells have positive trends. For each of the western U.S. sub-domains (W, NW, WC, SW), there are 11% or fewer cells with significant trends, up or down. This pattern is consistent with those in observed ozone (Porter, 2015). Jaffe and Ray (2007) speculate that ozone increases in western states may be due, among other things, to increased biomass burning and increasing ozone background levels due to emissions from Asia.

2. CMAQ emissions

Time series of regional mean anthropogenic emissions are also mostly downward trending (Figures 3-10). Exceptions include non-road mobile source VOC (all regions), EGU VOC (everywhere except NE), non-EGU point source NOx (W) and area source NOx (MW, S, W, WC, SW). Mobile source NOx and VOC are smoothly trending downward for all regions making them nearly indistinguishable. Table 3 (Rows 2-13) highlights regions with more than 25% of model cells with positive or negative trends in emissions (red and blue highlights, respectively). For some emission sources and regions, nearly all cells have decreasing trends. For example, mobile source VOC and NOx have downward trends in at least 96% of model cells for all regions. Biogenic VOC and NOx emissions increased in much of the W and WC regions.

The algorithms used to create the emission profiles used in CMAQ start with temporally coarse profiles provided by states and insert periodic diurnal, weekly, and annual cycles. Emissions from EGU’s are an exception to this practice as measured EGU emissions, collected since the late 1990’s, are now often used in ozone simulations. In an example of a monthly EGU NOx time series used in this ozone simulation, it is obvious where measured NOx begins (blue line Figure 11). By comparison, a mobile source time series for the same CMAQ cell maintains the regular seasonal pattern superimposed on the downward trend found in the state emission inventories. Measured EGU NOx values change with weather. In addition, the noisy appearance of measured NOx may make attribution of ozone responses to changes in EGU NOx emissions more difficult than for other emission sources.

3. CMAQ meteorology

Meteorological trends and p values appear in Figures 12-15. Significant upward trends in temperature and solar radiation (Figure 12 and Figure 13 where $p<0.05$) in much of the western U.S. may have contributed to increases in ozone in there. The western U.S. also has downward trends in soil moisture and convective precipitation (Figures 14 and 15). As with emissions, meteorological trends can also be indicated by the percentage of model cells with up- or downward trends (Table 4). By this measure, temperature in the MW, W and WC regions had substantial areas with upward trends during 1990-2010. The MW, W and NW regions had large areas with upward trends in solar radiation. The W and NW regions had large areas with downward trends in relative humidity and soil moisture. More than half of the SW region saw decreased v wind velocity (Vautard etal, 2010 discusses the phenomena of decreasing worldwide wind speeds).

B. Separating meteorological and emission effects

One use of the metamodel is to separate ozone responses to meteorology from those due to emissions. Trends in emission-dependent ozone (Figure 16) can be compared with those in CMAQ ozone (Figure 2). While the upper panels in those two figures are similar, the aerial extent of significant ($p<0.05$) emission-dependent ozone trends is much greater (lower panels of Figures 2 and 16).

The separation also provides a smooth trending response to emissions and a highly variable response to meteorology, as seen in Figures 17-24 (one for each region), which display CMAQ ozone (blue lines), emission-dependent ozone (green lines) and meteorologically dependent ozone (red lines). When emissions are fixed, years of ozone-conducive meteorology are indicated by large values for the red line. The years least and most meteorologically-conducive to ozone production are summarized in Table 5.

The regional emission-dependent ozone time series are displayed together in Figure 25. Four of the eight regions (NE, MA, MW and S) showed substantial reductions in ozone beginning about 2000, which coincides with the beginning of NO_x controls in the eastern U.S. (NO_x SIP call). Slope estimates (linear regression against year, ppb/year) and confidence intervals for each region for the years 2000-2010 are given in Table 6. The emission-dependent slopes, all of which are significant at the 1% or 5% level, have confidence intervals that are much smaller than those for CMAQ ozone.

Meteorologically-dependent ozone (red lines in Figures 17-24), as expected, is highly correlated with the meteorological variables that explain 77% to 98% of this component (Table 7, first two lines). Ozone variability attributable to meteorology ranged from 19% to 55% in the eastern U.S., and 39% to 92% in the western U.S. (Row 3 of Table 7). Variability attributed to emissions (Row 4 of Table 7) were between 46% and 74% in the eastern US and 1% to 33% in the western US (Row 5 of Table 7). The 5th row of Table 7 is the variability explained by both meteorology and emissions in a multivariate model. This latter value exceeded 96% in all but the western region (66%).

Much of the effect of emissions on ozone variability in the eastern U.S. is due to the downward trend in both ozone and emissions. To quantify the impact of trends, ozone, emissions, and meteorology were detrended prior to estimating explained variance. In the eastern US, the relative variability due to meteorology increases (compare Rows 3 and 6, Table 7), while that due to emissions decreases (compare Rows 4 and 7, Table 7). The balance between meteorology- and emission-based variability in western U.S. regions is much less affected by detrending.

What stands out for the emission-dependent components are the large changes in the eastern U.S. beginning about 2000 as compared with the western U.S. (Figure 25). For a closer look, the time span was broken into two periods: 1990-2000 and 2000-2010. Figures 26 and 27 contrast CMAQ ozone trend estimates for the two time spans, Figures 28-29 do the same for emission-dependent ozone trends. Summaries for each region appear in Table 8.

The CMAQ ozone trends were upward for most of the domain for 1990-2000 (Figure 26). Though none of the regional trends were significant (Table 8), some individual model cells were (lower panel Figure 26). Emission-dependent ozone trends had the same sign as CMAQ trends for this period, with the exception of the NW region (Figure 28 and Table 8). Emission-dependent ozone has a larger areal extent of significant trends ($p<0.05$) and smaller slope confidence intervals than CMAQ ozone because meteorological variation has been removed.

For 2000-2010, most of the domain was seeing significant downward trends. However, many of the CMAQ ozone trends were not significant, while many of the emission-dependent were (Figures 27 and 29, Table 8). All regional trends for emission-dependent ozone were significant, in contrast to CMAQ ozone trends, which were significant in only five of the eight regions. Once again, the emission-dependent confidence intervals are much smaller, by factors as large as 20 (WC region).

During 1990-2000, few CMAQ ozone model cells have significant trends (no more than 15% in any region, line one of Table 9). With respect to emission-dependent ozone, several regions (MA, MW, S and NW) have large percentages of positive trends (line two, Table 9). As noted above, the earlier period also saw increases in some emission sources in some places. NOx from non-EGU point sources, EGU point sources, and area sources increased in 25% or more of the model cells in MA, MW, W, NW, and SW. CMAQ and emission-dependent ozone as well as most emissions were down over most of the model domain in 2000-2010 (Table 10).

A last word on the subject of temporal trends is the idea that their detection depends on the starting time and duration of the data used. Walker (2016) introduced a method for displaying trends for all available starting times and durations. Figure 30 shows trends and p values in CMAQ ozone for each region (ppb/year). The x-axis is the starting year and the y-axis is the duration, ranging from 5 to 21 years. For example, the upper left corner of each panel is a 21-year span beginning in 1990 (the whole duration). The lower right corner is a 5 year time interval beginning in 2006. The upper panels gradually turn from yellow (upward trends) to blue (downward trends) as the starting time advances. Notice that not many slope estimates are significant ($p<0.05$). The same information for emission-dependent ozone appears in Figure 31. The transition from upward to downward trends in the eastern US is smooth, and many of the trends are significant, even some with the shortest durations (5 years).

C. Ozone response to emissions

The ozone response to emissions was assessed by plotting regionally-averaged emission-dependent ozone against each emission source (scaled, 0-1). The ozone values have been shifted by subtracting the maximum value (usually near the beginning of the plot) to show changes over time as emissions change. Separate plots for VOC and NOx emissions were created by fixing meteorology and all but one emission source at 2010 levels and letting the other source vary (Figures 32-39). Responses to all anthropogenic emissions (fixing meteorology and letting all anthropogenic sources vary together) appear in Figure 40. In addition, because VOC and NOx emissions from a given source are in some cases nearly indistinguishable, additional plots were created for which both VOC and NOx for a given source were allowed to vary (Figures 41-48).

The slopes in linear regressions from the lines in these plots were used to compare the ozone response to each source (Table 11). More than 80% of the slopes were statistically significant ($p<0.05$). For most regions, the largest responses were to mobile source NOx and VOC. The response to non-road VOC was negative in seven of eight regions.

The response to changes in all anthropogenic emissions typically has a plateau on the right (corresponding to 1990-2000), a steep mid-portion, and a gradual reduction in slope in the lower left of the plot (Figure 40). The shape of these plots can be interpreted as there being no improvement in ozone air quality during the period 1990-2000, despite reductions in emissions (representing about 30% of the reductions during 1990-2010, as indicated by the 0-1 emission scale). The years 2001-2005, representing roughly 30% of emission changes, saw significant reductions in air quality followed by modest improvements during 2006-2010, with this period having about 40% of the emission reductions.

When VOC and NOx sources are combined, the largest responses in the eastern U.S. (NE, MA, MW, S) were to mobile sources and the smallest responses were usually to non-road mobile (NE, MA, S) (last five Rows of Table 11 and Figures 41-48). Non-road NOx and VOC ozone responses are often opposite in sign, leading to ozone response plots that have no discernible pattern. Such is the case for the eastern U.S. (upper left panels of figures 41-44).

The mobile source plots for all regions are the least noisy and most linear. Mobile source emissions trend smoothly downward due to steady fleet turnover. As seen in Figure 3-10, reductions in other emission sources were not steadily downward, and, as noted above, measured EGU emissions were used in the CMAQ emission inventory beginning about 1999.

Spatial representations of the ozone response to emissions are displayed in Figures 49-54. The largest ozone responses to anthropogenic emissions (greater than about 10 ppb) are limited to the eastern half of the U.S. (Figure 49). For much of the western U.S., the responses are much smaller. Area sources, due to wildfires, produced ozone responses in the W region of 6-8 ppb (Figure 53). The largest responses to mobile sources occurred in Washington DC, New Jersey and southeastern Pennsylvania (Figure 54).

IV. Summary

A metamodel was fit to the ozone, emissions and meteorology of a CMAQ simulation for the CONUS for the years 1990-2010. During this time ozone declined in much of the eastern U.S., while in the west ozone was little changed. Emissions also declined for most sources in all regions.

The metamodel was used to separate ozone variability due to meteorology from that attributable to emissions. Downward trends in emission-dependent ozone occurred in the eastern U.S. during 2000-2010 and ranged from -0.65±0.06 to -1.07±0.20 ppb/year, depending on region. Trends in the western U.S. ranged from -0.05±0.02 to -0.25±0.04 ppb/year. Trends estimated from CMAQ ozone were also mostly negative but with much larger confidence intervals.

Meteorology explains between 19% and 55% of ozone variance in the eastern U.S., and emissions account for 46% to 74% of ozone variance. Much of the ozone variability due to emissions was connected to the downward trend in emissions. In the western U.S., meteorology was responsible for 39% to 92% of ozone variation, with emission dependent variation ranging between 1% and 33%.

Of all the individual sources considered in this study, the mobile sector has the clearest (most linear) connection to emission-dependent ozone because of steady fleet turnover. The other emission sources do not have a clear trend for the period of study. In addition, as stated in Section II A, the metamodel developed in this study does not account for the effects of emission changes in one region on air quality in a different region.

V. References

Ankenman, B., Nelson, B.L. and J.Staum. 2010. Stochastic Kriging For Simulation Metamodeling. Operations Research Vol. 58, No. 2, March–April, pp. 371–382

Bakshi, B. 1998. Multiscale PCA with application to MSPC monitoring, AIChE J. 44, pp. 1596–1610.

Eder, B. K., Davis, J. M. and P. Bloomfield. 1993. A characterization of the spatiotemporal variability of non-urban ozone concentrations over the eastern United States. Atmospheric Environment Part A General Topics 27(16):2645-2668, October

Foley, K. M., Napelenok, S.L., Jang, C., Phillips, S. Hubbell, B.J., and C.M. Fulcher. 2014. Two reduced form air quality modeling techniques for rapidly calculating pollutant mitigation potential across many sources, locations and precursor emission types. Atmospheric Environment 98: 283-289

Jaffe, D. and J. Ray. 2007. Increase in surface ozone at rural sites in the western U.S. Atmospheric Environment 41: 5452–5463

Porter, P.S. 2015. Ozone RFM for the Continental US: Model Inputs, Development and Performance. Report for CRC Project A-89

U.S. Environmental Protection Agency. 2006. Technical Support Document for the Proposed Mobile Source Air Toxics Rule: Ozone Modeling, Office of Air Quality Planning and Standards Research Triangle Park, NC

Walker, S. 2016. Investigating global warming using a new graph style. http://wattsupwiththat.com/2016/03/12/investigating-global-warming-using-a-new-graph-style

Wong, D. C., Pleim, J., Mathur, R., Binkowski, F., Otte, T., Gilliam, R., Pouliot, G. Xiu A. Young J. O., and D. Kang. 2012. *Geosci. Model Dev.*, **2012**, 5, 299-312, doi:10.5194/gmd-5-299-2012.

Xing, J.; Pleim, J.; Mathur, R.; Pouliot, G.; Hogrefe, C.; Gan, C.-M.; and Wei, C. 2013. Historical gaseous and primary aerosol emissions in the United States from 1990 to 2010 Atmos. Chem. Phys. 13, 7531-7549, doi:10.5194/acp-13-7531-2013.

Acknowledgements

Although this presentation has been reviewed and approved by the EPA and approved for publication, it does not necessarily reflect EPA's policies or views.

This work was made possible by Coordinating Research Council contract A-89.

Legal Notice

List of Tables

Table 1. Emissions

emission source (VOC and NOx)	time scale	space scale
area	monthly mean	36 km
non-EGU point		
EGU point		
non-road mobile		
biogenic		

Table 2. Meteorology

	time scale	space scale
planetary boundary layer	monthly mean	36 km
pressure		
temperature, 2m		
solar radiation, 2m		
water vapor mixing ratio, 2m		
relative humidity		
precipitation		
soil moisture		
u wind		
v wind		

Table 3. Temporal trends in ozone and emissions (1990 – 2010): percent of model cells in a given region with trends significant at the 95% level).
Blue: downtrends > 24%; red: uptrends > 24%

region:	NE		MA		MW		S		W		NW		WC		SW	
emission	+	-	+	-	+	-	+	-	+	-	+	-	+	-	+	-
O3	0	56	0	87	0	35	0	35	4	0	11	3	5	0	2	2
VNR	30	3	71	0	29	19	46	3	22	4	40	0	23	2	53	2
VNE	5	83	2	86	6	84	7	79	24	55	19	50	10	73	20	69
VEG	18	40	40	2	26	14	46	9	27	25	67	22	39	7	47	13
VAR	0	97	0	96	3	95	0	83	2	24	0	38	15	27	10	33
VMO	0	100	0	100	0	100	0	100	0	100	0	100	0	100	0	98
VBI	1	0	0	0	17	0	1	0	76	0	0	3	47	0	19	0
NNR	0	84	0	89	1	91	0	91	2	88	0	91	2	86	2	88
NNE	8	67	9	60	13	52	12	65	36	34	15	40	5	53	25	58
NEG	7	73	12	47	14	49	16	40	19	35	25	25	0	67	15	44
NAR	26	50	33	42	48	26	45	24	39	1	20	11	39	15	57	1
NMO	0	100	0	99	0	100	0	96	0	100	0	100	0	99	3	97
NBI	2	0	0	11	5	2	4	3	45	1	0	3	38	0	19	0

+ uptrend, - downtrend

Table 4. Temporal trends in meteorology (1990 – 2010): percent of model cells with trends significant at the 95% level).
Blue: downtrends > 24%; red: uptrends > 24%

region:	NE		MA		MW		S		W		NW		WC		SW	
	+	-	+	-	+	-	+	-	+	-	+	-	+	-	+	-
pb	1	14	5	1	2	10	0	6	1	3	0	11	0	25	0	7
pr	0	0	0	0	0	0	0	2	1	0	0	0	0	51	0	15
t2	2	0	0	0	26	0	2	0	83	0	9	6	53	0	20	0
r2	15	0	1	0	31	0	0	1	39	0	63	0	9	0	0	5
q2	22	0	0	0	3	0	4	3	1	0	0	0	0	0	7	0
prec	27	0	0	9	0	9	2	1	0	13	3	8	0	1	3	0
rh	10	0	0	10	1	10	0	3	0	25	0	28	0	1	5	5
sm	4	1	0	21	0	21	1	11	0	36	0	42	4	2	3	4
u	2	0	0	0	0	0	0	0	11	0	2	0	3	0	2	17
v	4	1	4	0	18	0	0	17	1	11	0	0	0	15	0	55

+ uptrend, - downtrend

Table 5. Meteorologically dependent ozone by region

region:	NE	MA	MW	S	W	NW	WC	SW
ozone								
least conducive year	1994	1994	2002	1992	1993	1993	1993	2008
most conducive year	2000	1993	2009	2000	1998	1996	2003	2009

Table 6. Temporal trends (ppb/year) in CMAQ ozone and emission-dependent ozone at 1% (**) and 5%(*) significance levels, along with a ± 95% confidence interval for the slope for the period 2000-2010.

ozone:	Original	emission-dependent
Region		
NE	-0.23 ± 0.63	-0.65**± 0.06
MA	-0.83** ± 0.59	-1.07 **± 0.20
MW	-1.00** ± 0.71	-0.69**± 0.08
S	-1.17** ± 0.76	-0.72**± 0.13
W	-0.40 ± 0.52	-0.15* ± 0.15
NW	0.00 ± 0.41	-0.12**± 0.05
WC	-0.01 ± 0.40	-0.05* ± 0.02
SW	-0.18* ± 0.10	-0.25**± 0.04

Table 7. Ozone variance attributed to meteorology and emissions

region:	NE	MA	MW	S	W	NW	WC	SW
met-dep. ozone by CMAQ meteorology (%)	98	96	95	85	77	91	91	96
met. variables (stepwise regression)	t, u	-p, t, -r, -u	t, -v	-rh, -u, v	r, -ws	t	t, -v	pb, t, -v, -ws
% total variability due to meteorology	36	19	55	54	39	86	90	92
% total variability due to emissions	51	74	46	52	33	9	1	19
% total due to meteorology and emissions	99	98	97	97	66	97	96	98
after detrending								
% total variability due to meteorology	88	51	85	82	34	95	94	97
% total variability due to emissions	8	34	43	43	59	11	2	39
% total due to meteorology and emissions	98	96	96	96	78	97	96	98

p = pressure, pb=boundary layer height, t = temperature, r = solar radiation, rh = relative humidity, u = u wind component, v = v wind component, ws = wind speed

Table 8. Temporal trends (ppb/year) in CMAQ ozone and emission-dependent ozone with a (95% confidence interval for the slope for different periods. Blue: significant negative slopes; red: significant positive slopes.

period:	1990-2010		1990-2000		2000-2010	
ozone:	CMAQ	emission-dep	CMAQ	emission-dep	CMAQ	emission-dep
Region						
NE	-0.39 (0.20)	-0.24 (0.02)	-0.25 (0.66)	-0.059(0.060)	-0.23 (0.63)	-0.65 (0.06)
MA	-0.62 (0.24)	-0.29 (0.03)	0. 10 (0.64)	0.09 (0.06)	-0.83 (0.59)	-1.07 (0.20)
MW	-0.29 (0.26)	-0.18 (0.02)	0. 25 (0.63)	0.080(0.079)	-1.00 (0.71)	-0.69 (0.08)
S	-0.33 (0.28)	-0.19 (0.02)	0.62 (0.73)	0.15 (0.09)	-1.17 (0.76)	-0.75 (0.14)
W	0.11 (0.16)	-0.03 (0.01)	0.27 (0.42)	0.03 (0.05)	-0.40 (0.52)	-0.151(0.150)
NW	-0.01 (0.11)	-0.023 (0.004)	-0.09 (0.42)	0.001 (0.03)	0.00 (0.41)	-0.12 (0.02)
WC	0.005 (0.114)	-0.007 (0.001)	-0.05(0.32)	-0.025(0.029)	-0.01 (0.40)	-0.05 (0.02)
SW	-0.05 (0.19)	-0.07 (0.01)	0.40 (0.51)	0.024 (0.31)	-0.18 (0.10)	-0.25 (0.04)

Table 9. Temporal trends in ozone and emissions (1990 – 2000): percent of model cells in a given region with trends significant at the 95% level.
Blue: downtrends > 25%; red: uptrends > 25%

region:	NE		MA		MW		S		W		NW		WC		SW	
	+	-	+	-	+	-	+	-	+	-	+	-	+	-	+	-
CMAQ O3	0	0	0	0	0	0	15	0	7	0	0	0	0	1	7	0
emission-dep.O3	7	40	51	0	41	3	61	2	8	1	32	8	1	17	10	5
emission																
VNR	0	26	0	36	5	35	1	34	16	17	1	2	0	59	0	30
VNE	12	42	11	43	10	49	20	44	42	27	44	16	16	48	27	40
VEG	20	4	65	1	52	2	66	3	47	6	78	0	22	9	51	4
VAR	20	63	0	91	4	90	1	73	3	18	0	23	1	16	2	26
VMO	0	100	0	100	0	100	0	100	0	100	0	100	0	100	0	98
VBI	0	0	0	0	1	0	5	0	9	0	0	0	0	1	6	0
NNR	0	45	0	72	1	66	0	71	3	65	0	45	0	77	0	81
NNE	17	45	34	20	30	19	34	17	52	5	59	7	19	29	27	12
NEG	10	35	28	7	34	21	51	10	39	16	58	8	18	53	40	13
NAR	47	19	51	22	79	2	65	3	36	0	39	0	17	7	45	0
NMO	4	80	0	84	0	82	0	78	0	91	0	100	0	91	0	81
NBI	0	0	0	11	3	0	1	2	4	0	0	0	0	4	5	0

+ uptrend, - downtrend

ANTH = anthropogenic, NNR = NOx, nonroad, NNE = NOx non-EGU point source, NEG = NOx EGU, NAR=NOx area, NMO = NOx mobile, VNR = VOC, nonroad, VNE = VOC non-EGU point source, VEG = VOC EGU, VAR = VOC area, VMO = VOC mobile.

Table 10. Temporal trends in ozone and emissions (2000 – 2010): percent of model cells in a given region with trends significant at the 95% level).
Blue: downtrends > 24%; red: uptrends > 24%

region:	NE		MA		MW		S		W		NW		WC		SW	
	+	-	+	-	+	-	+	-	+	-	+	-	+	-	+	-
CMAQ O3	0	3	0	57	0	67	0	76	0	25	0	0	2	1	1	26
emission-dep.O3	0	99	0	100	2	92	0	99	1	37	5	77	16	48	4	67
emission																
VNR	0	5	18	0	15	21	21	0	27	25	0	25	17	4	4	0
VNE	7	77	6	83	8	81	14	70	36	37	31	39	15	66	20	54
VEG	8	31	24	20	11	18	27	15	25	13	22	0	4	20	24	15
VAR	0	97	0	92	0	93	0	70	0	19	0	32	0	22	0	23
VMO	0	100	0	100	0	100	0	100	0	100	0	100	0	100	0	98
VBI	2	0	19	0	0	0	4	0	0	0			0	0	1	0
NNR	0	95	0	93	0	93	0	95	0	96	0	98	1	90	0	93
NNE	9	60	9	57	12	38	19	52	38	15	34	35	20	56	24	39
NEG	5	47	9	52	5	48	6	53	20	25	8	17	7	79	13	44
NAR	8	60	14	50	37	34	17	29	19	1	5	13	9	8	22	5
NMO	0	100	0	98	0	100	0	96	0	100	0	100	0	99	3	97
NBI	6	0	3	0	0	1	2	0	0	11	0	0	0	0	1	2

+ uptrend, - downtrend

ANTH = anthropogenic, NNR = NOx, nonroad, NNE = NOx non-EGU point source, NEG = NOx EGU, NAR=NOx area, NMO = NOx mobile, VNR = VOC, nonroad, VNE = VOC non-EGU point source, VEG = VOC EGU, VAR = VOC area, VMO = VOC mobile,

Table 11. Slope of emission-dependent ozone vs. scaled (0-1) emissions, with 95% confidence interval, 1990-2010.

Blue: significant positive slopes; red: significant negative slopes.

region: source	NE	MA	MW	S	W	NW	WC	SW
ANTH	8.91 (1.17)	13.48 (2.85)	7.46 (1.20)	14.14 (3.01)	1.98 (0.69)	1.36 (0.31)	0.80 (0.76)	2.47 (0.79)
NNR	0.64 (0.03)	1.37 (0.03)	1.14 (0.05)	1.02 (0.03)	0.11 (0.01)	0.01 (0.02)	0.01 (0.02)	0.04 (0.01)
NNE	0.81 (0.11)	1.28 (0.20)	0.50 (0.18)	1.36 (0.20)	0.08 (0.10)	0.03 (0.05)	-0.04 (0.05)	0.02 (0.01)
NEG	0.40 (0.06)	0.38 (0.07)	0.17 (0.15)	0.77 (0.11)	0.04 (0.01)	-0.009 (0.004)	0.02 (0.01)	0.062 (0.002)
NAR	0.44 (0.15)	0.72 (0.18)	0.54 (0.21)	0.93 (0.65)	1.02 (0.27)	0.34 (0.16)	-0.06 (0.18)	-0.02 (0.01)
NMO	2.31 (0.07)	3.84 (0.14)	2.59 (0.07)	3.27 (0.14)	0.51 (0.07)	0.94 (0.03)	0.15 (0.01)	0.06 (0.01)
VNR	-0.16 (0.11)	-1.75 (0.30)	-0.39 (0.33)	-1.32 (0.35)	0.18 (0.08)	-0.14 (0.29)	-0.10 (0.07)	-0.07 (0.04)
VNE	0.97 (0.03)	0.99 (0.03)	0.63 (0.05)	1.02 (0.11)	0.03 (0.02)	0.03 (0.01)	0.12 (0.02)	0.024 (0.004)
VEG	0.33 (0.14)	0.09 (0.11)	0.27 (0.12)	-0.01 (0.09)	0.02 (0.01)	-0.009 (0.002)	-0.06 (0.01)	0.004 (0.001)
VAR	2.05 (0.15)	0.98 (0.08)	0.80 (0.04)	1.31 (0.19)	1.24 (0.27)	0.49 (0.23)	0.06 (0.05)	0.02 (0.03)
VMO	2.66 (0.14)	2.05 (0.10)	1.16 (0.04)	1.40 (0.05)	0.46 (0.02)	0.29 (0.04)	-0.02 (0.03)	0.004 (0.005)
NR	0.50 (0.25)	-0.17 (1.75)	0.75 (0.66)	0.27 (0.86)	0.47 (0.11)	0.78 (0.23)	-0.10 (0.05)	0.38 (0.47)
NE	1.62 (0.11)	2.26 (0.31)	1.12 (0.22)	2.06 (0.31)	0.10 (0.07)	0.09 (0.03)	0.11 (0.13)	0.62 (0.11)
EG	0.78 (0.17)	0.63 (0.22)	0.22 (0.24)	0.98 (0.30)	0.03 (0.01)	-0.001 (0.012)	-0.05 (0.04)	0.10 (0.03)
AR	2.31 (0.18)	1.61 (0.34)	1.12 (0.17)	2.25 (0.42)	1.84 (0.30)	0.60 (0.13)	0.30 (0.14)	-0.02 (0.22)
MO	5.06 (0.23)	6.04 (0.24)	3.78 (0.14)	4.33 (0.31)	0.73 (0.10)	0.46 (0.10)	-0.15 (0.03)	1.57 (0.17)

ANTH = all anthropogenic, NNR = NOx, nonroad, NNE = NOx non-EGU point source, NEG = NOx EGU, NAR=NOx area, NMO = NOx mobile, VNR = VOC, nonroad, VNE = VOC non-EGU point source, VEG = VOC EGU, VAR = VOC area, VMO = VOC mobile,

List of Figures

Figure 14. July trend in meteorology (1990-2010): daily average soil moisture (fraction/year) upper left, convective precipitation ((cm/day)/year) upper center, non-convective precipitation ((cm/day)/year) upper right, daily average u wind ((m/s)/year, positive when wind is from the west) lower left, average v wind ((m/s)/year, positive when wind is from the south) lower center, scaler wind speed ((m/s)/year).

Figure 15. Slope p values (con., 1990-2010): daily average soil moisture, upper left; convective precipitation, upper center; non-convective precipitation, upper right; daily average u wind, lower left; average v wind, lower center.

Figure 16. Emission-dependent temporal trend in O3 (ppb/year, 1990-2010) (upper panel), p value of slope estimate (lower panel)

Figure 17. NE region: CMAQ ozone (CMAQ, blue), emission-dependent ozone (green), and meteorologically-dependent ozone (red).

Figure 18. MA region: CMAQ ozone (CMAQ, blue), emission-dependent ozone (green), and meteorologically-dependent ozone (red).

Figure 19. MW region: CMAQ ozone (CMAQ, blue), emission-dependent ozone (green), and meteorologically-dependent ozone (red).

Figure 20. S region: CMAQ ozone (CMAQ, blue), emission-dependent ozone (green), and meteorologically-dependent ozone (red).

Figure 21. W region: CMAQ ozone (CMAQ, blue), emission-dependent ozone (green), and meteorologically-dependent ozone (red).

Figure 22. NW region: CMAQ ozone (CMAQ, blue), emission-dependent ozone (green), and meteorologically-dependent ozone (red).

Figure 23. WC region: CMAQ ozone (CMAQ, blue), emission-dependent ozone (green), and meteorologically-dependent ozone (red).

Figure 24. SW region: CMAQ ozone (CMAQ, blue), emission-dependent ozone (green), and meteorologically-dependent ozone (red).

Figure 25. Emission-dependent ozone: regional means.

Figure 26. CMAQ ozone: 1990-2000 July trend (ppb/year, top panel), p value of slope estimate (lower panel)

Figure 27. CMAQ ozone: 2000-2010 July trend (ppb/year, top panel), p value of slope estimate (lower panel)

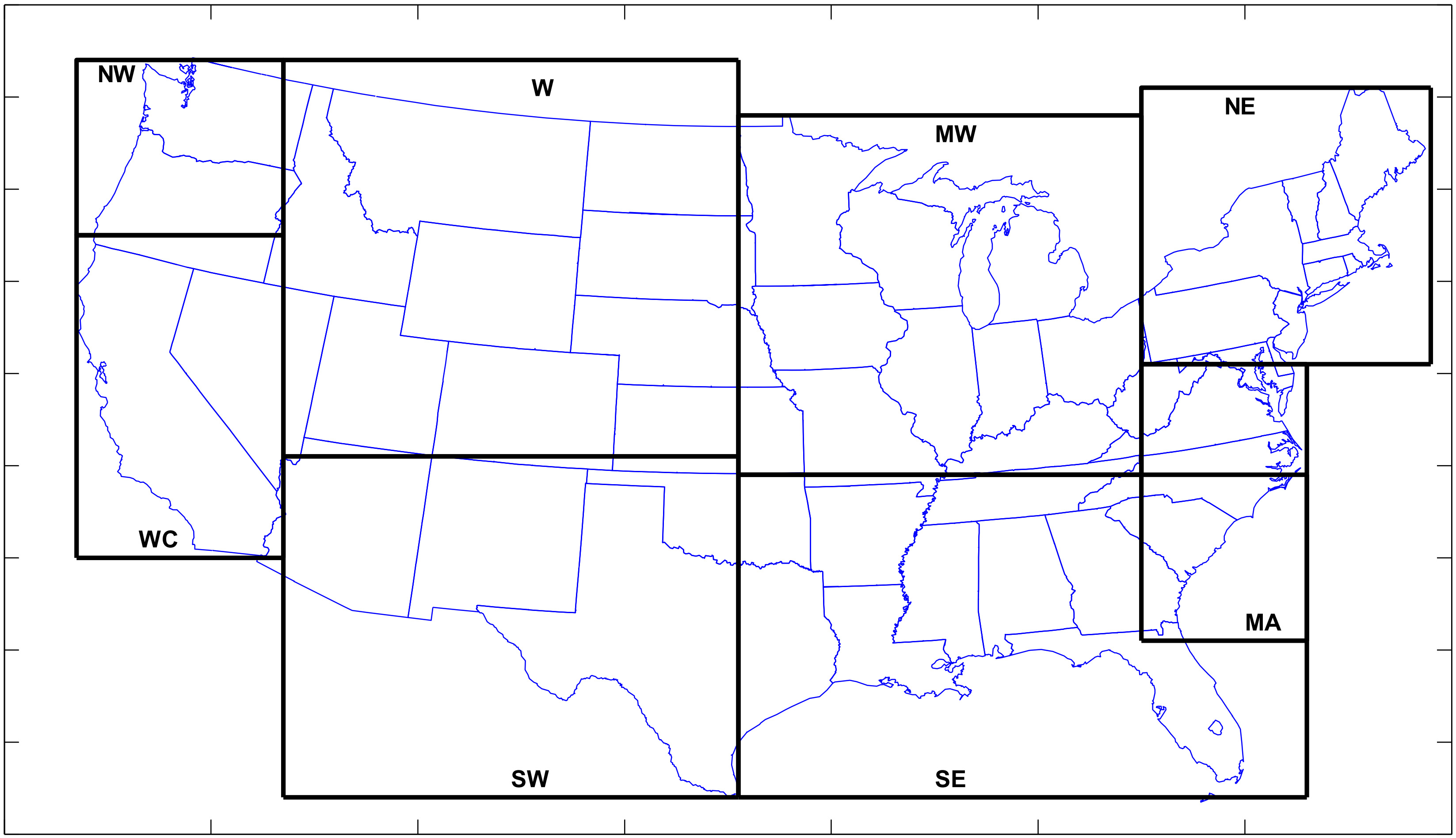

Figure 1. Model domain divided into eight regions: Northeast (NE), Mid-Atlantic (MA), Midwest (MW), South (S), West (W), Southwest (SW), Northwest (NW), and West Coast (WC). The MA region overlaps parts of the NE and S.

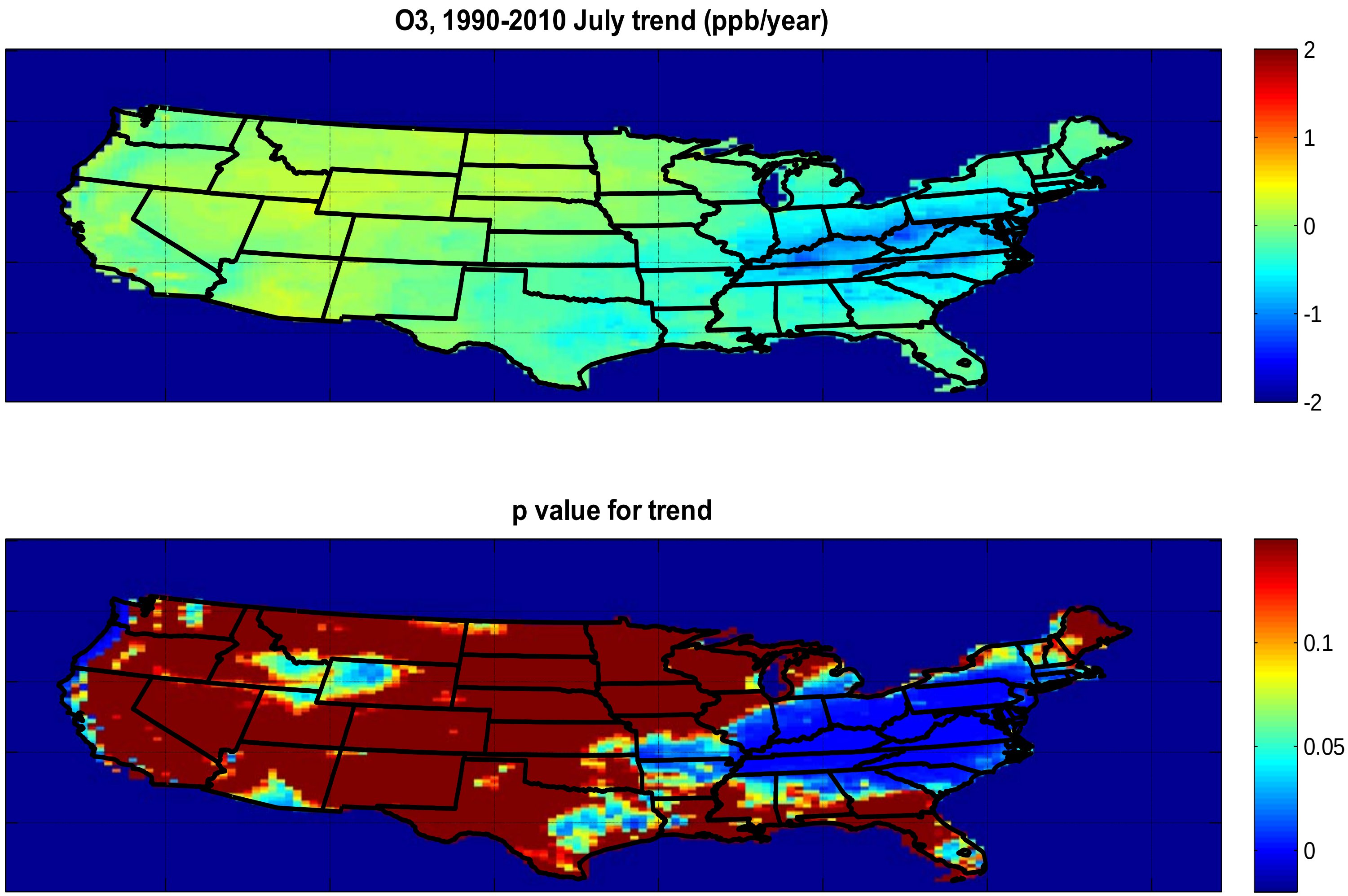

Figure 2. CMAQ Ozone: 1990-2010 July trend (ppb/year, upper panel), p value of slope estimate (lower panel)

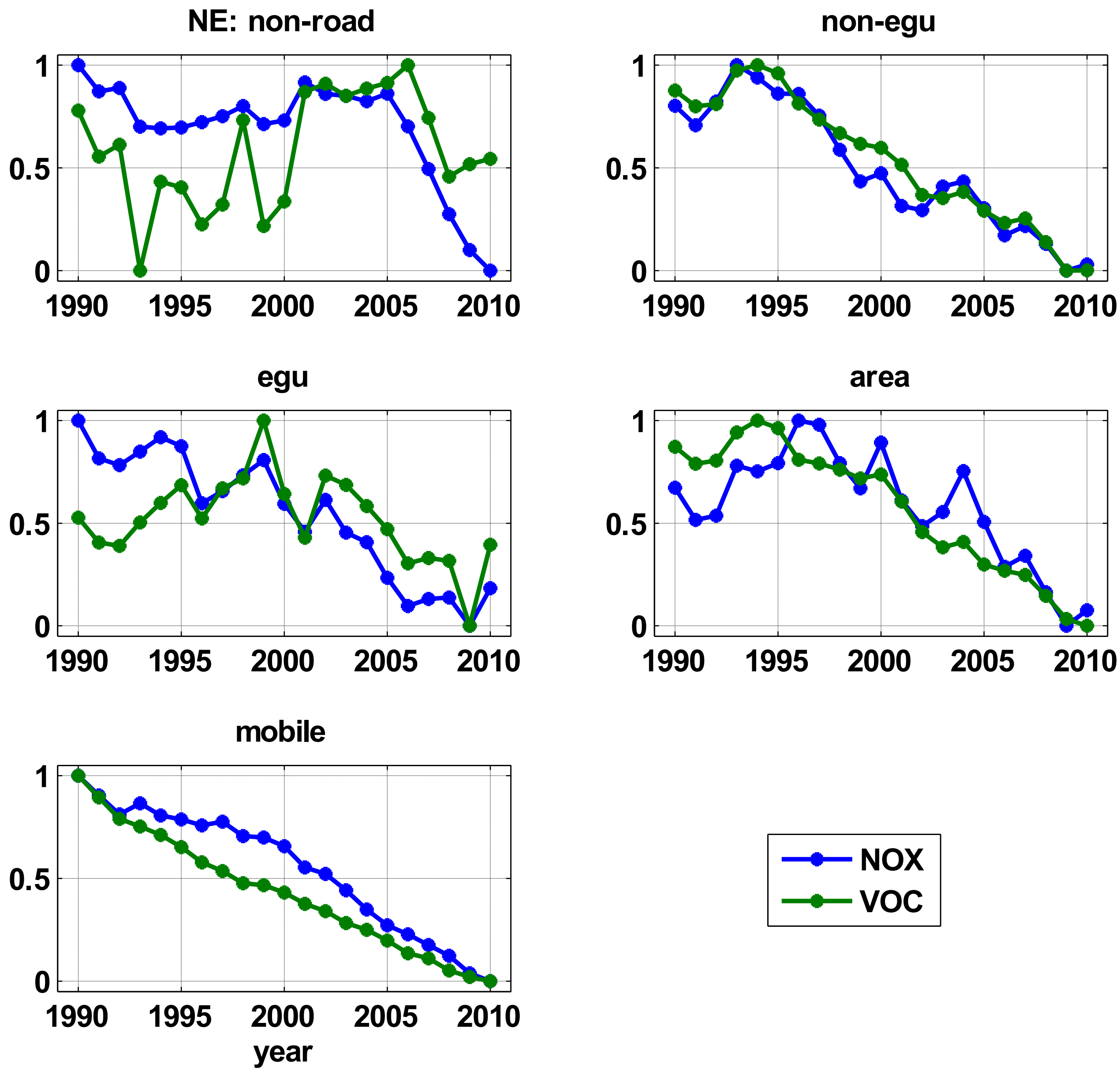

Figure 3. NE regional mean emissions

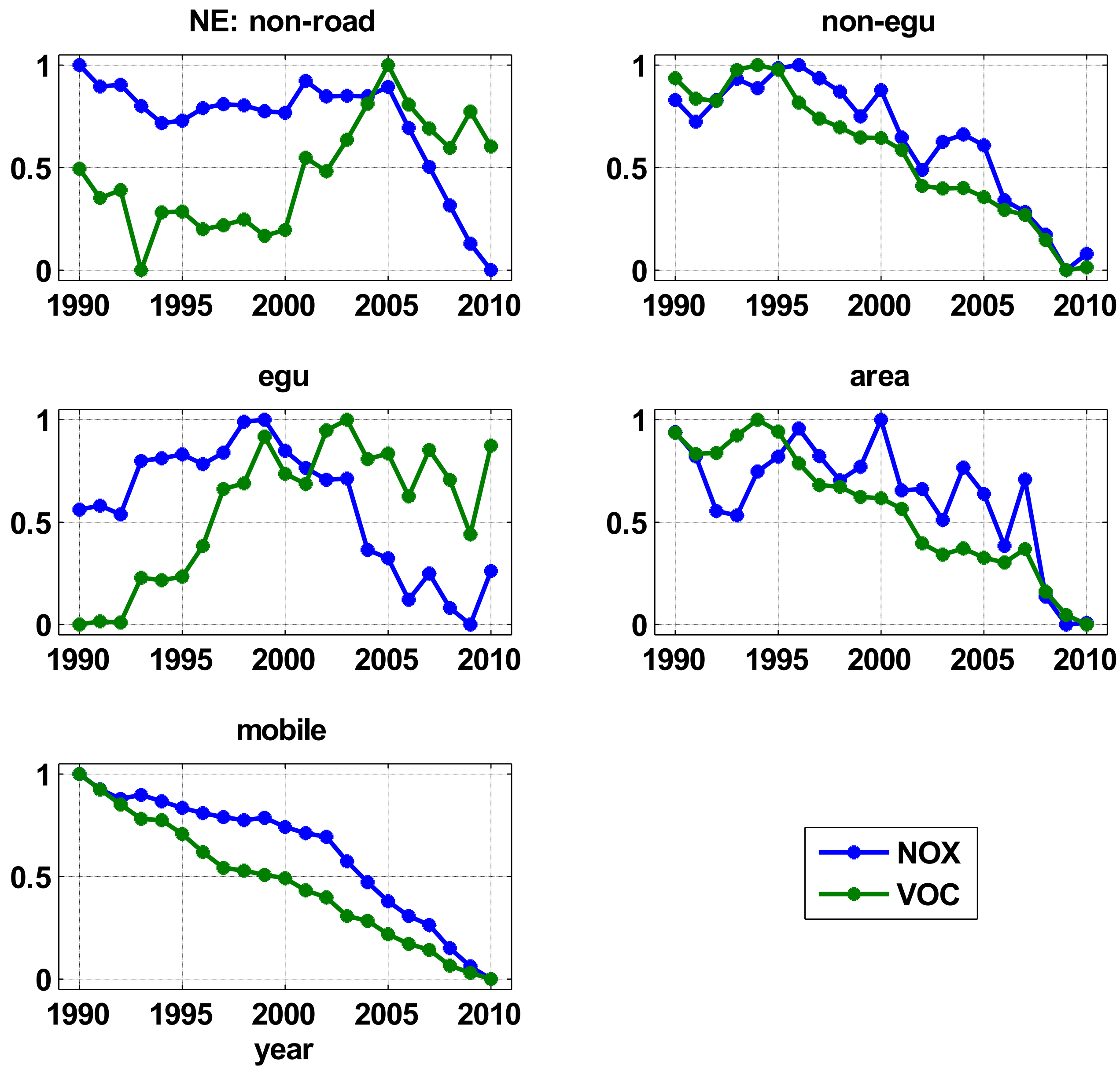

Figure 4. MA regional mean emissions

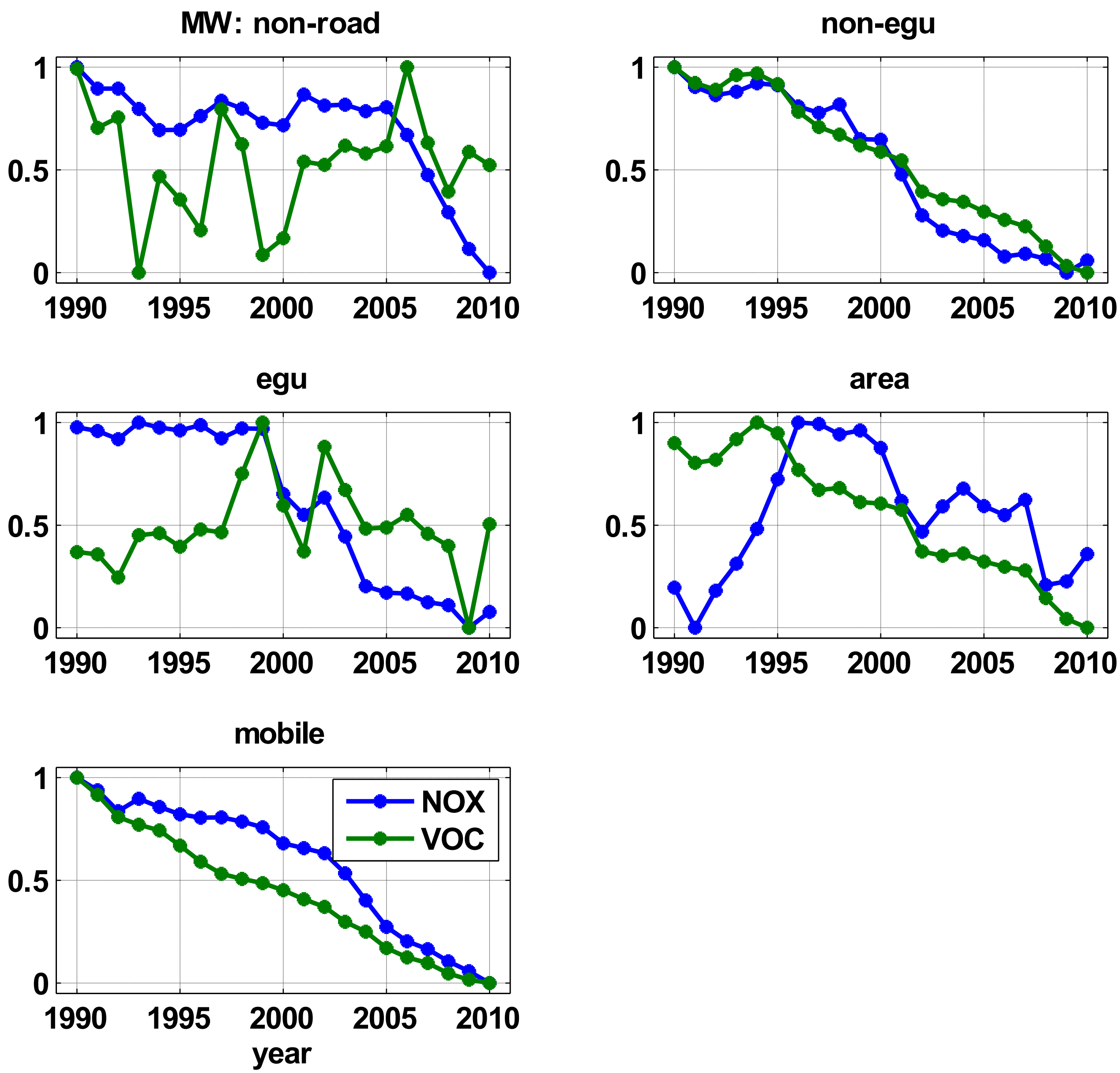

Figure 5. MW regional mean emissions

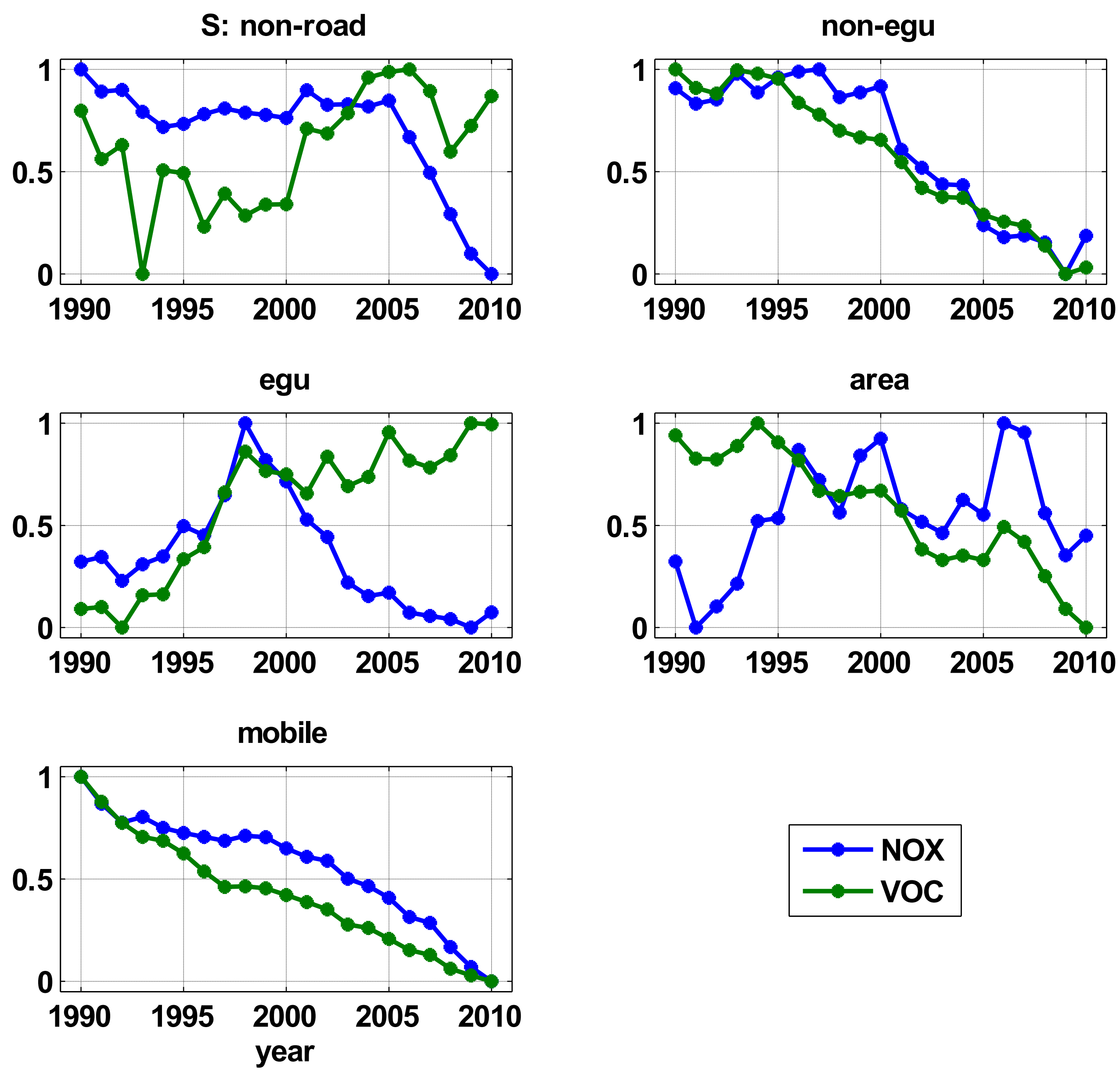

Figure 6. S regional mean emissions

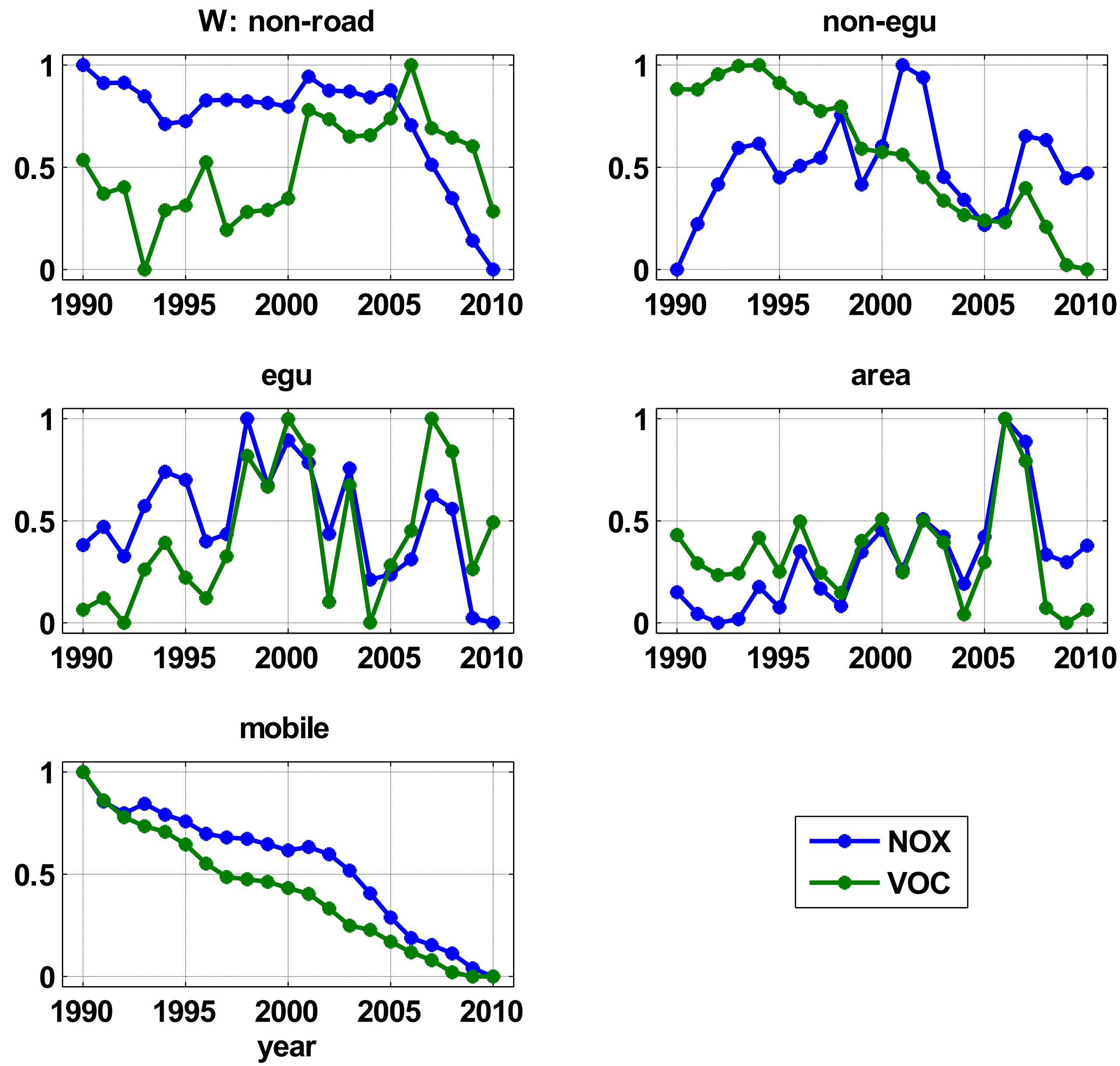

Figure 7. W regional mean emissions

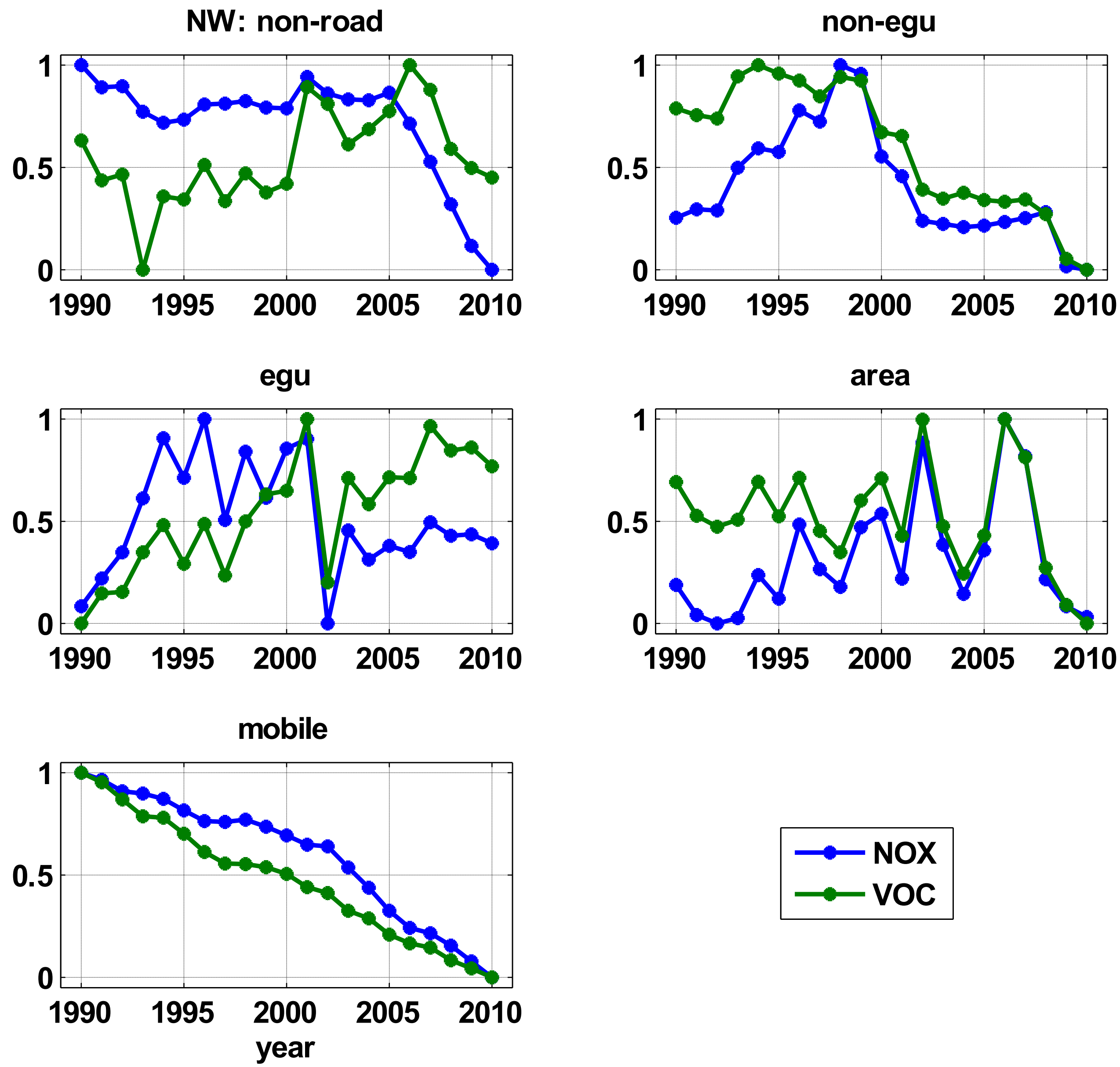

Figure 8. NW regional mean emissions

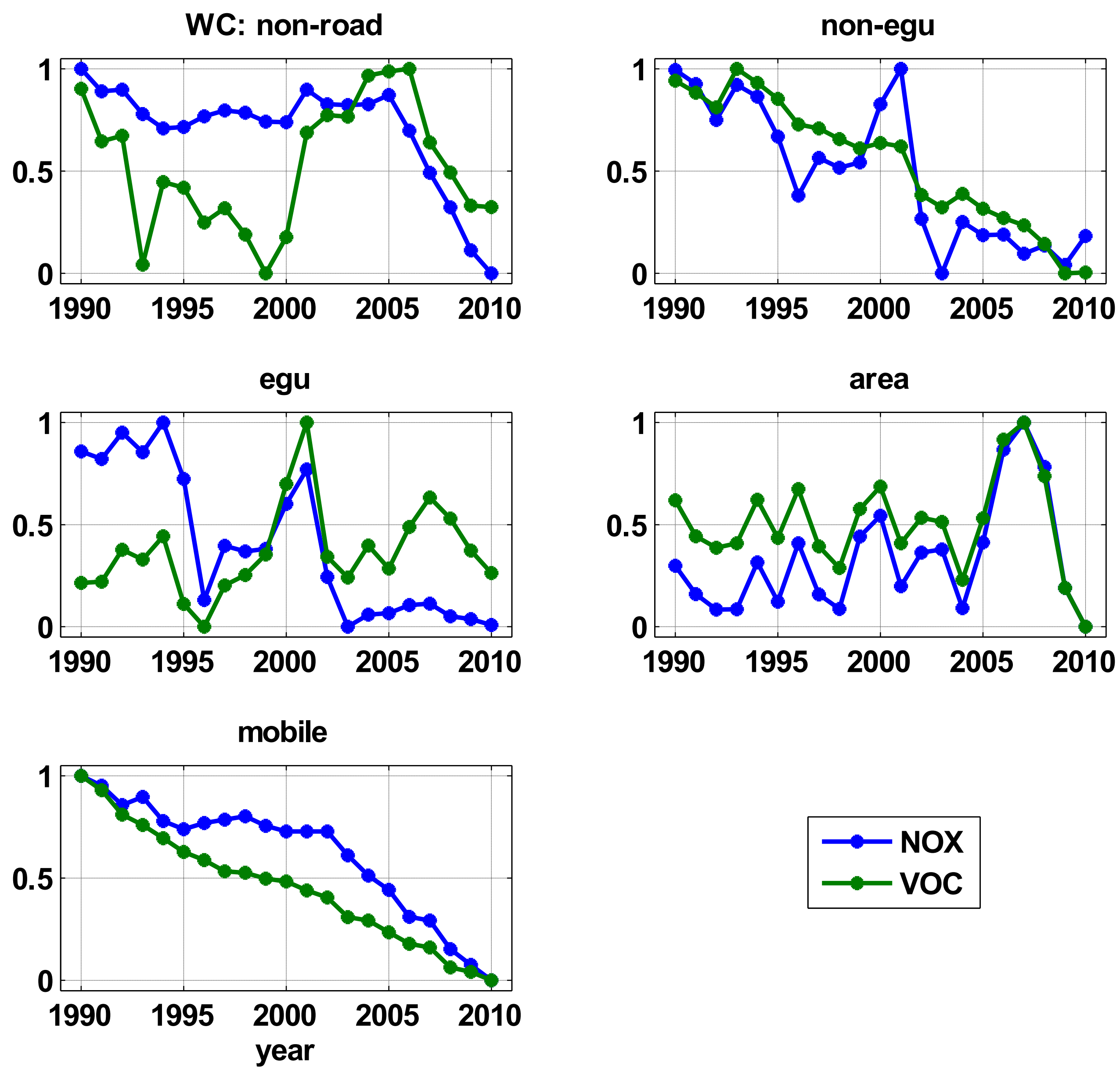

Figure 9. WC regional mean emissions

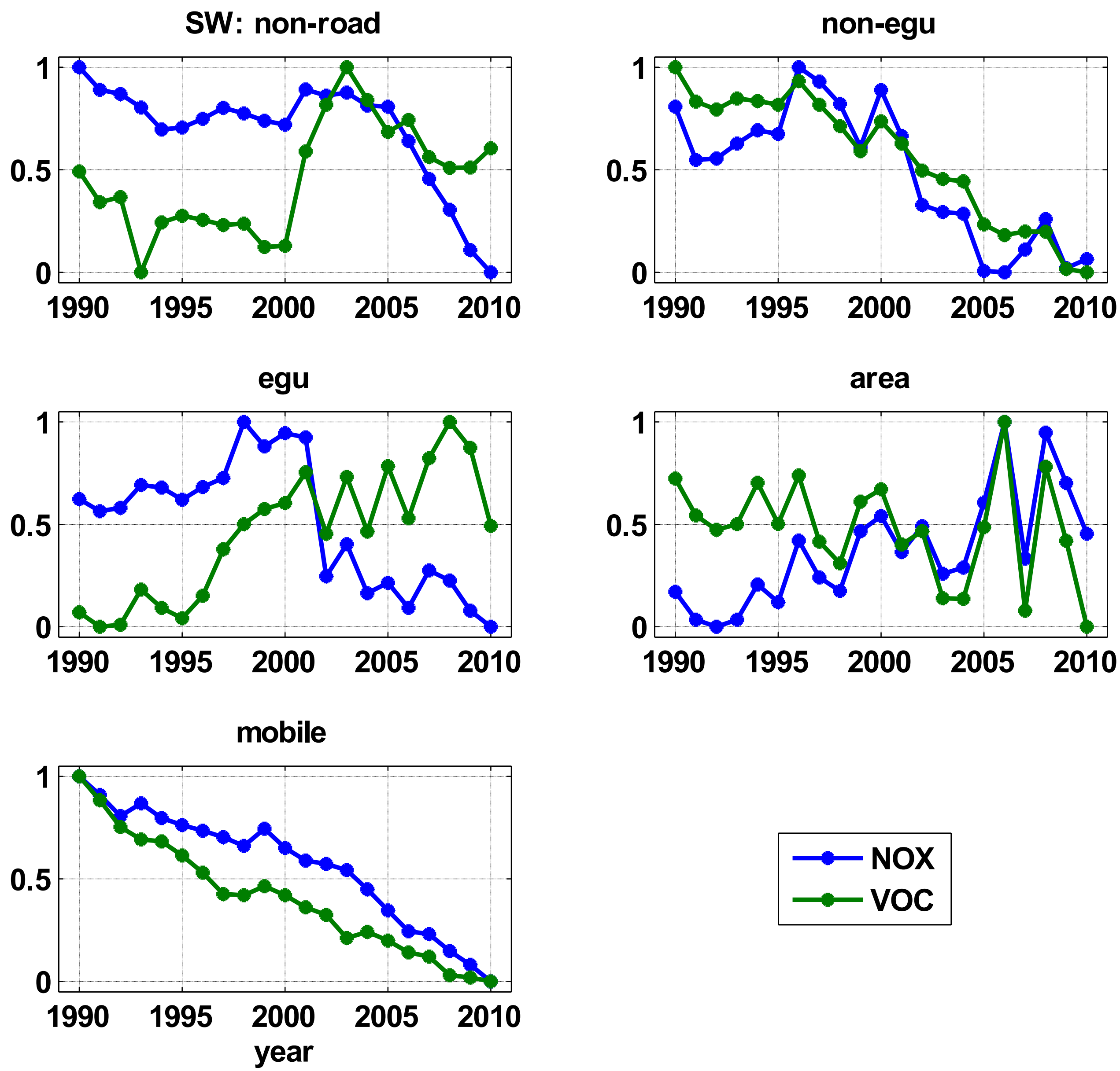

Figure 10. SW regional mean emissions

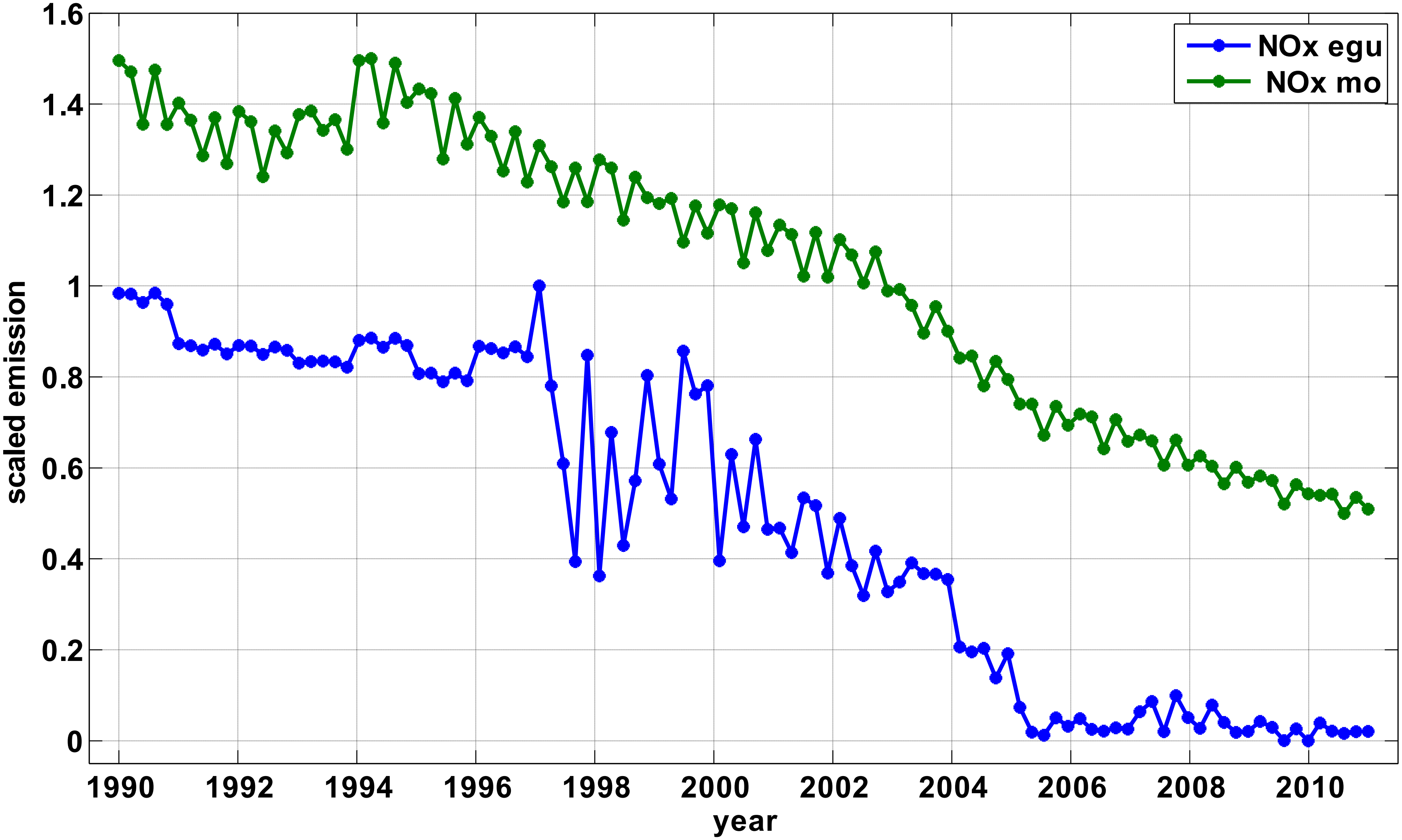

Figure 11. Examples of NOx EGU and mobile emissions at a single model cell.

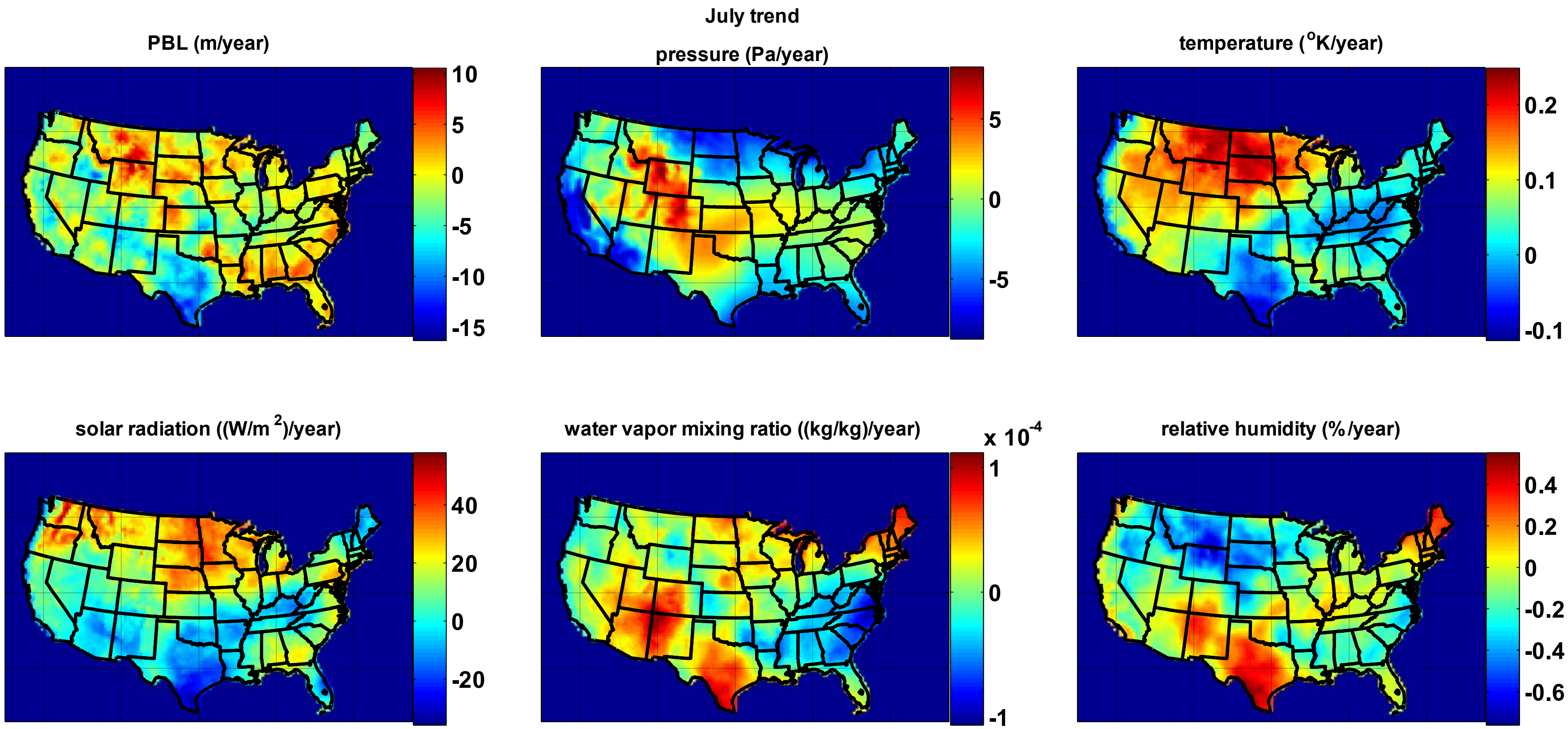

Figure 12. Trend in Meteorology (1990-2010): daily average PBL (m/year), upper left, daily average pressure (Pa/year), upper center, daily hourly maximum temperature (°K/year) upper right, daily total solar radiation ((W/m²)/yar), daily total), lower left, daily average water vapor mixing ratio ((kg/kg)/year), lower center, daily average relative humidity (%/year), lower right.

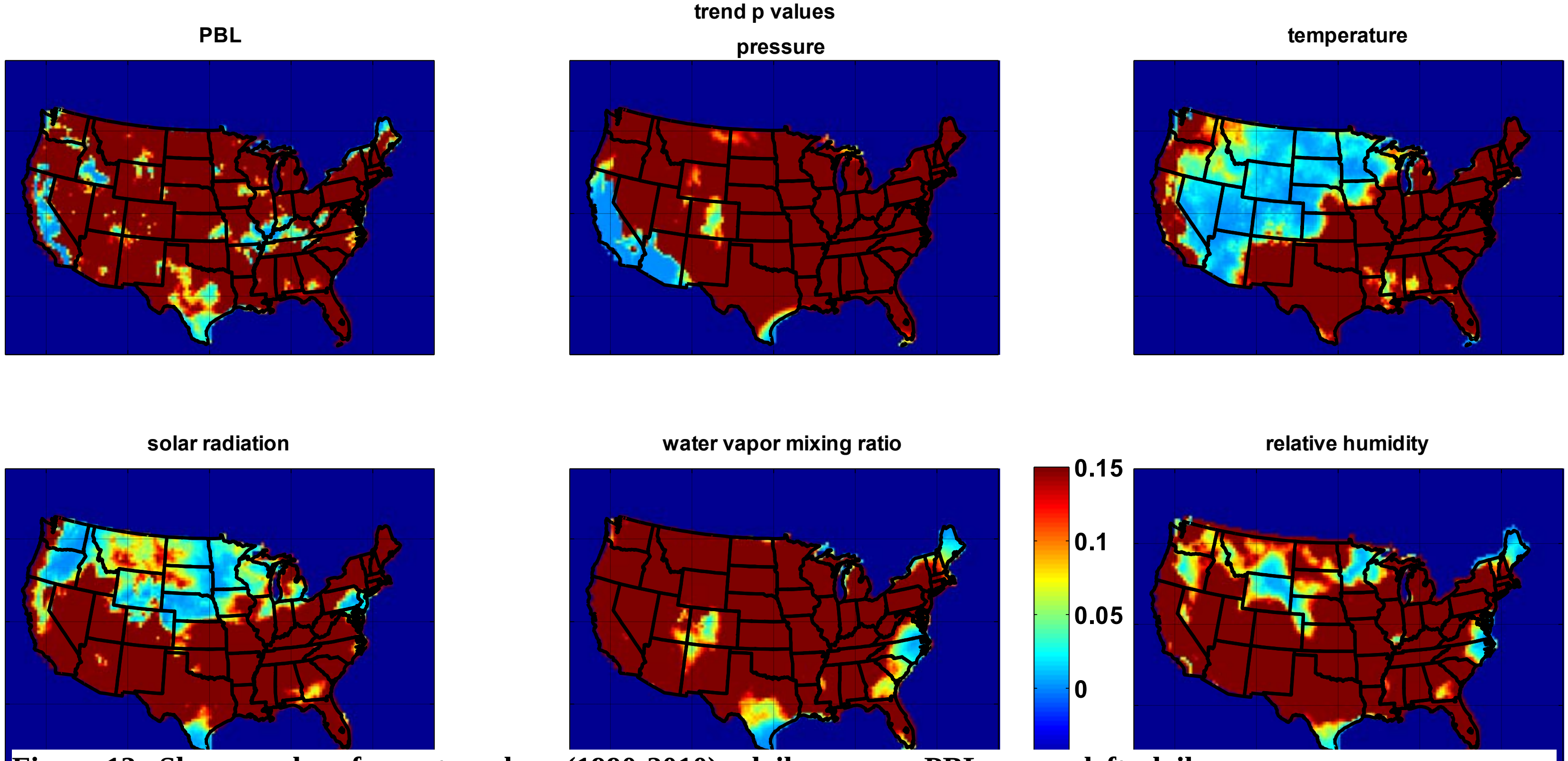

Figure 13. Slope p values for meteorology (1990-2010): daily average PBL, upper left; daily average pressure upper center; daily hourly maximum temperature, upper right; daily total solar radiation, lower left; daily average water vapor mixing ratio, lower center; daily average relative humidity, lower right.

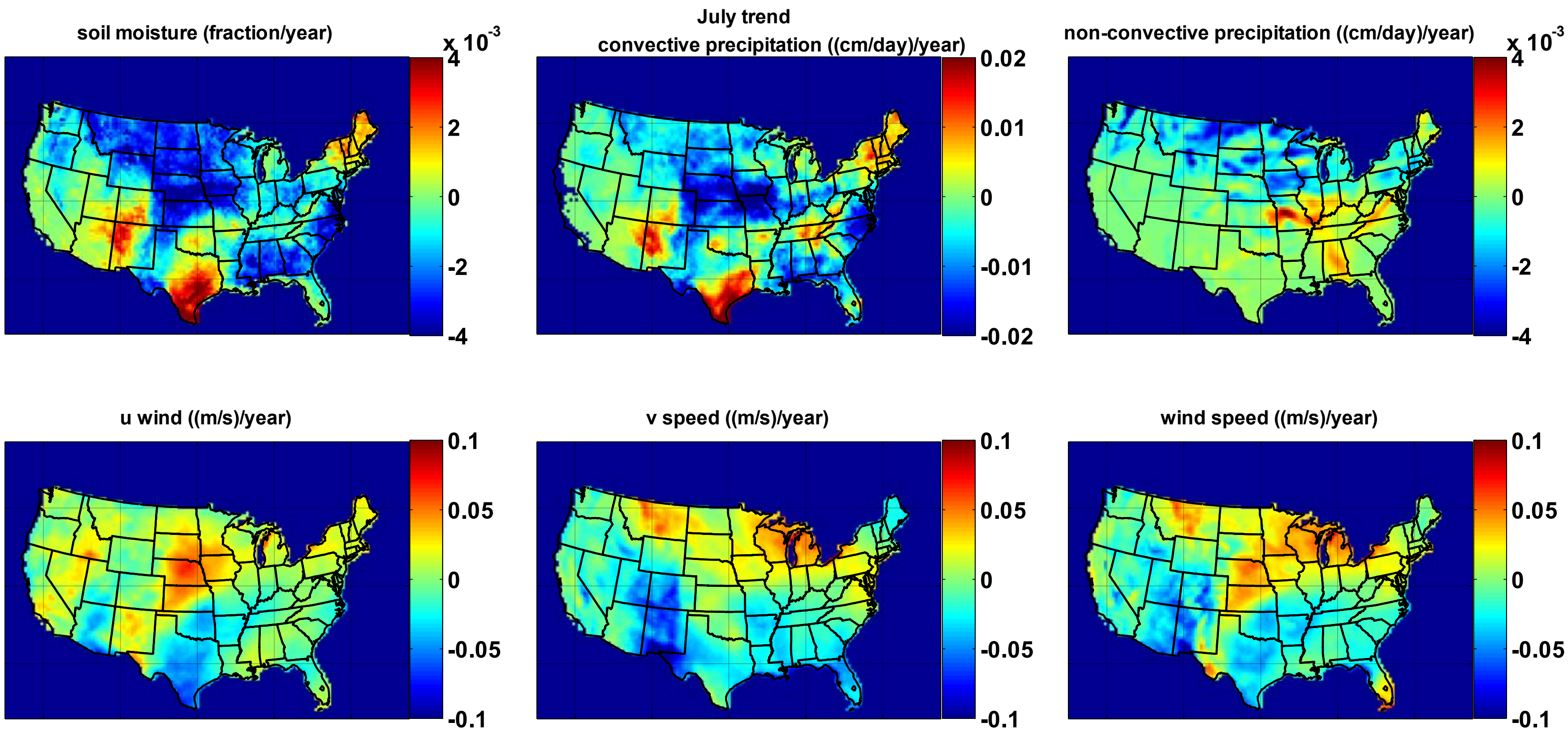

Figure 14. July trend in meteorology (1990-2010): daily average soil moisture (fraction/year) upper left, convective precipitation ((cm/day)/year) upper center, non-convective precipitation ((cm/day)/year) upper right, daily average u wind ((m/s)/year, positive when wind is from the west) lower left, average v wind ((m/s)/year, positive when wind is from the south) lower center, scaler wind speed ((m/s)/year).

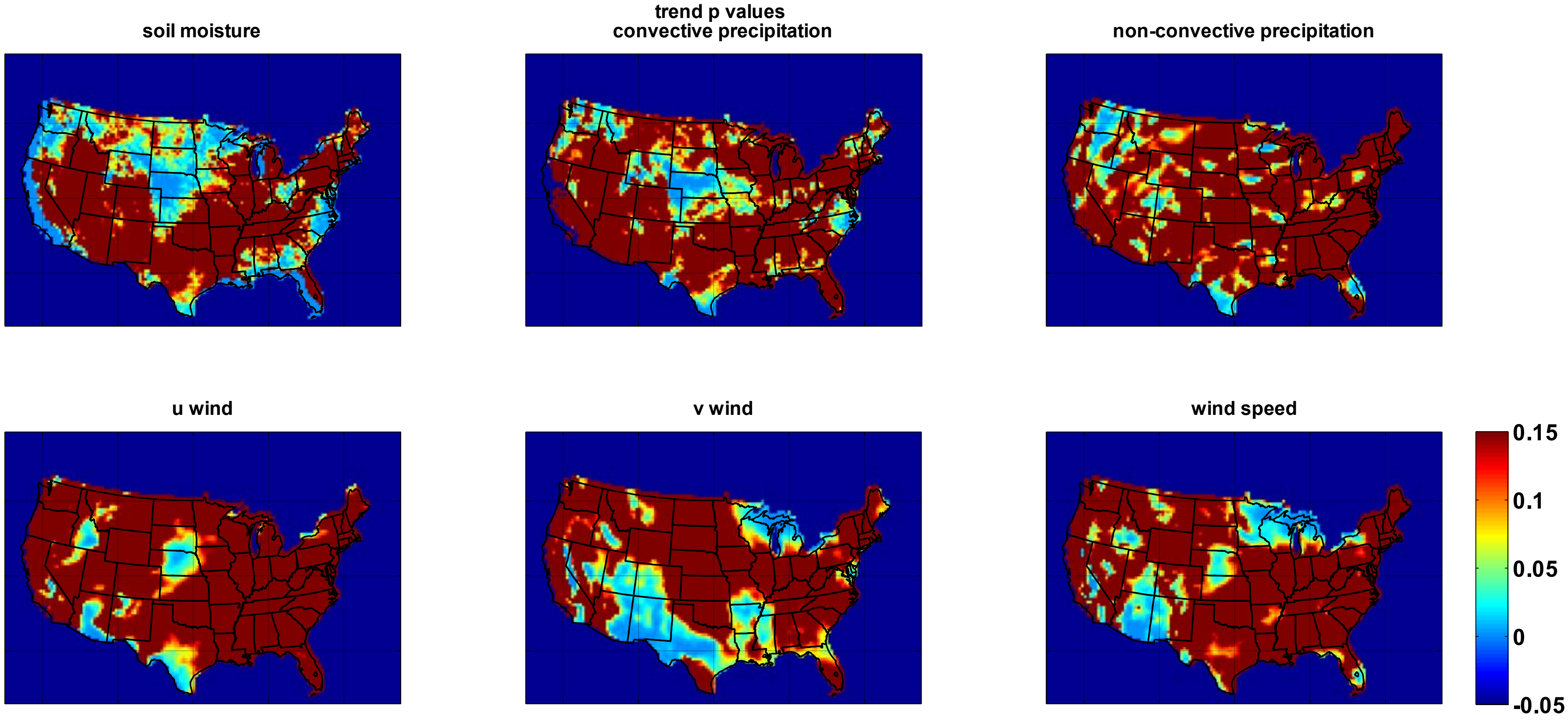

Figure 15. Slope p values (1990-2010): daily average soil moisture, upper left; convective precipitation, upper center; non-convective precipitation, upper right; daily average u wind, lower left; average v wind, lower center.

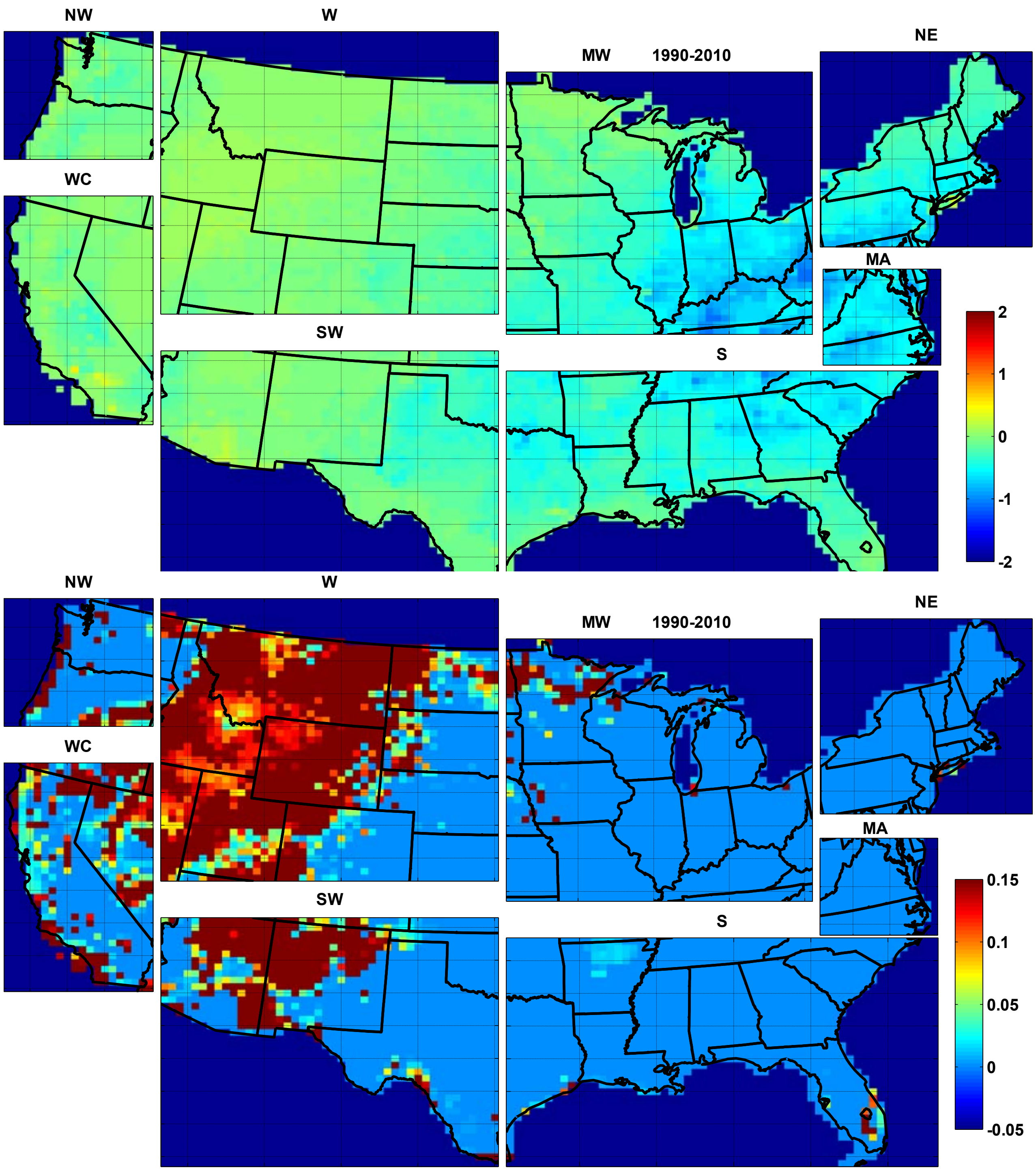

Figure 16. Emission-dependent temporal trend in O3 (ppb/year, 1990-2010) (upper panel), p value of slope estimate (lower panel)

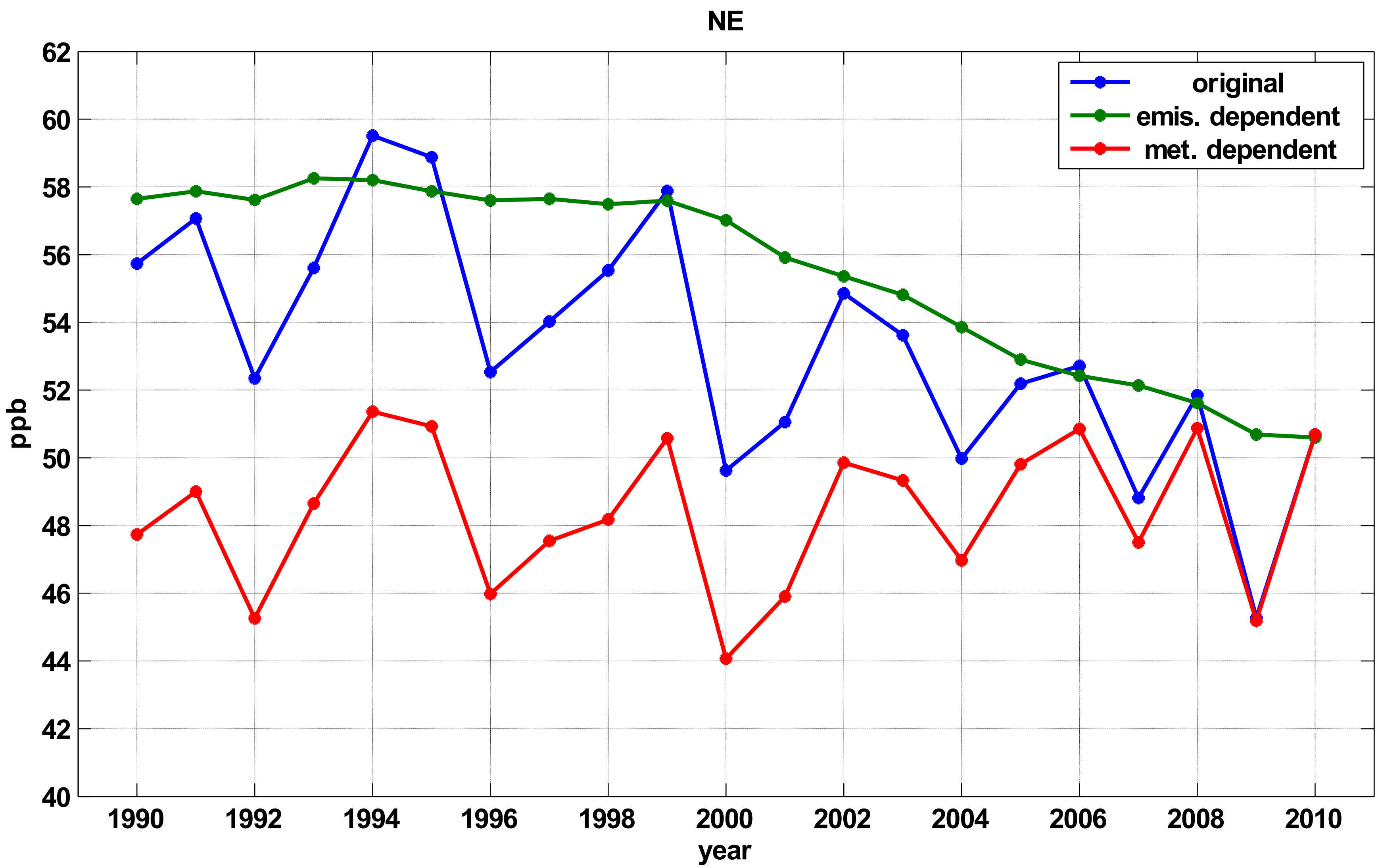

Figure 17. NE region: CMAQ ozone (CMAQ, blue), emission-dependent ozone (green), and meteorologically-dependent ozone (red).

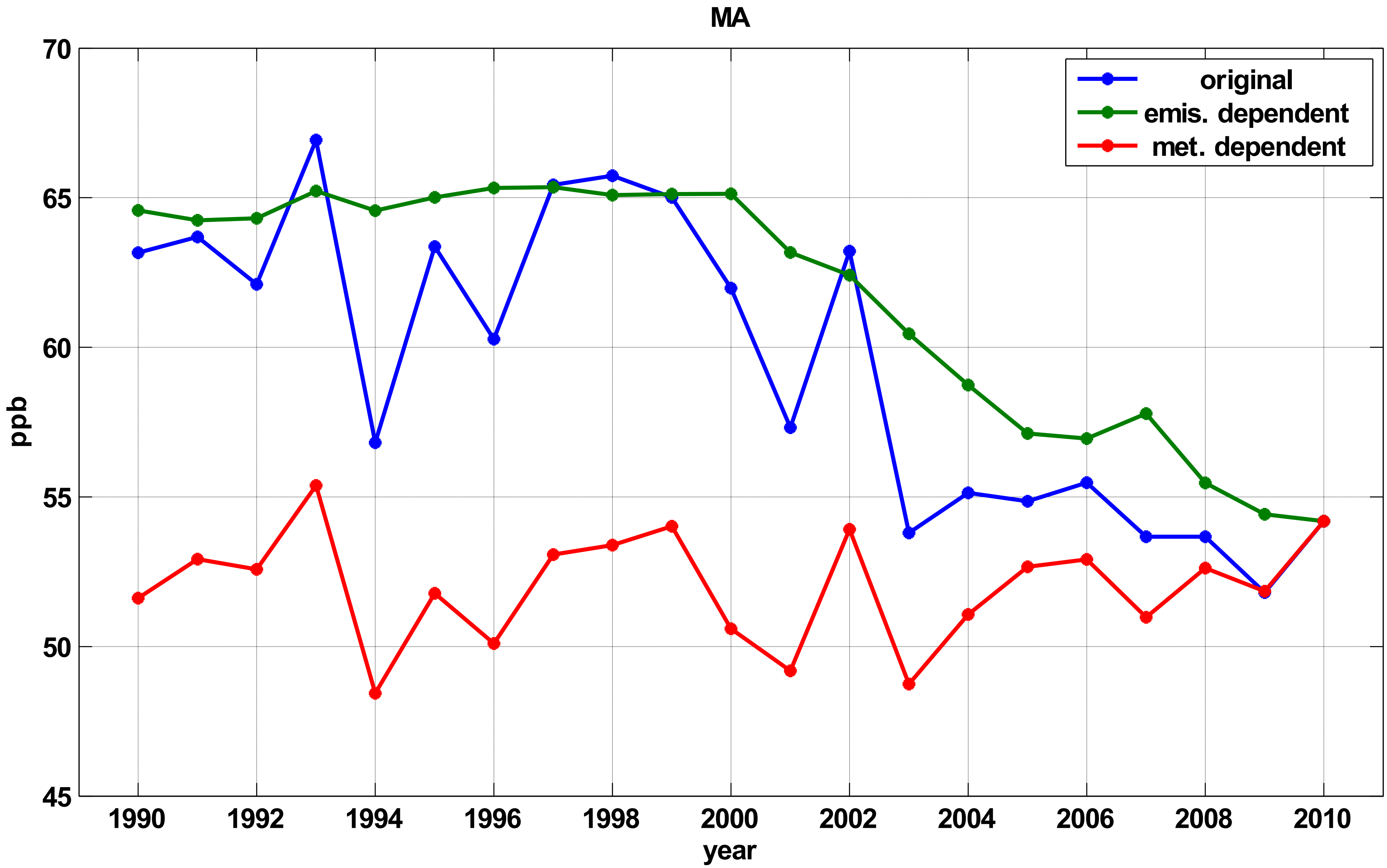

Figure 18. MA region: CMAQ ozone (CMAQ, blue), emission-dependent ozone (green), and meteorologically-dependent ozone (red).

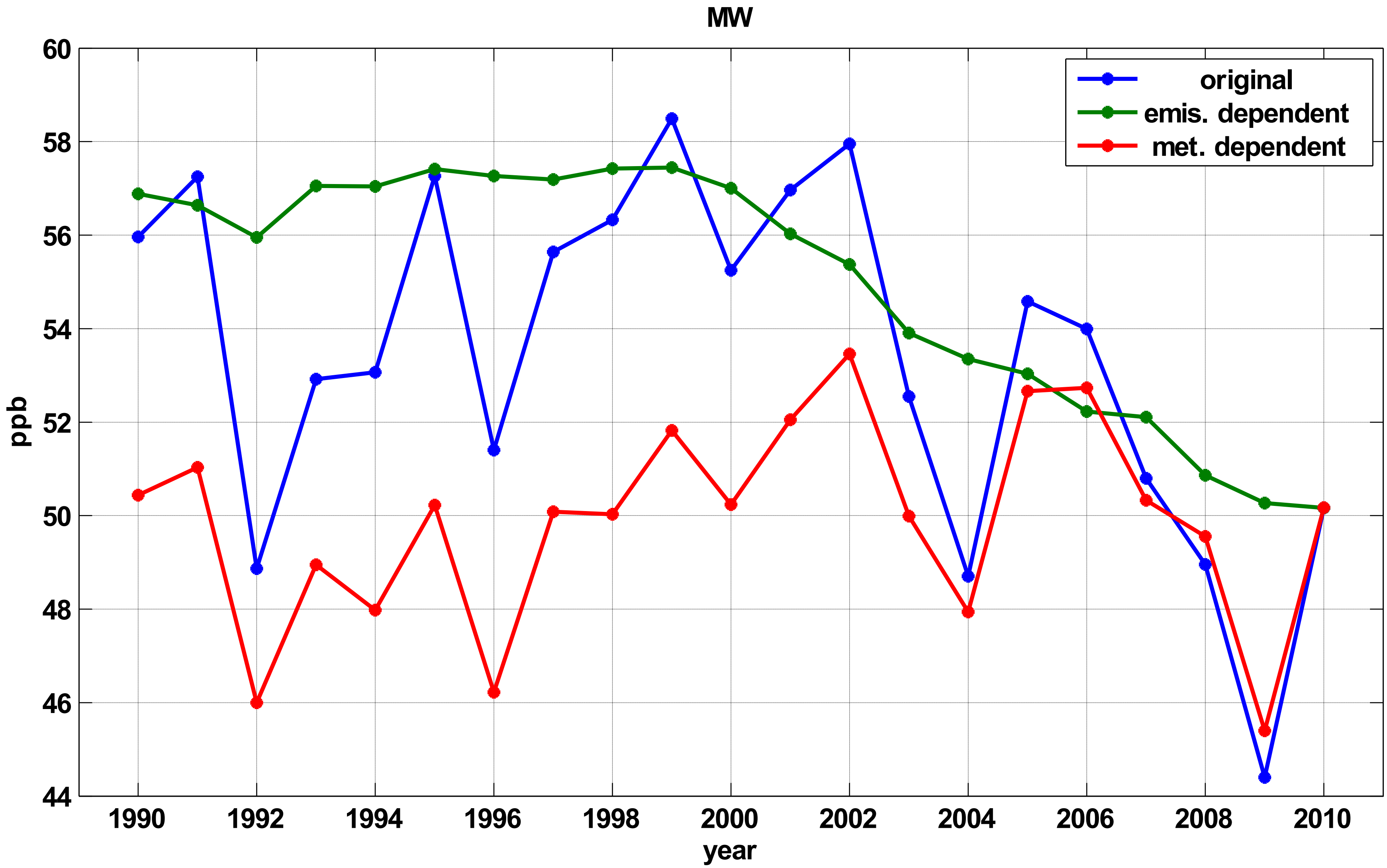

Figure 19. MW region: CMAQ ozone (CMAQ, blue), emission-dependent ozone (green), and meteorologically-dependent ozone (red).

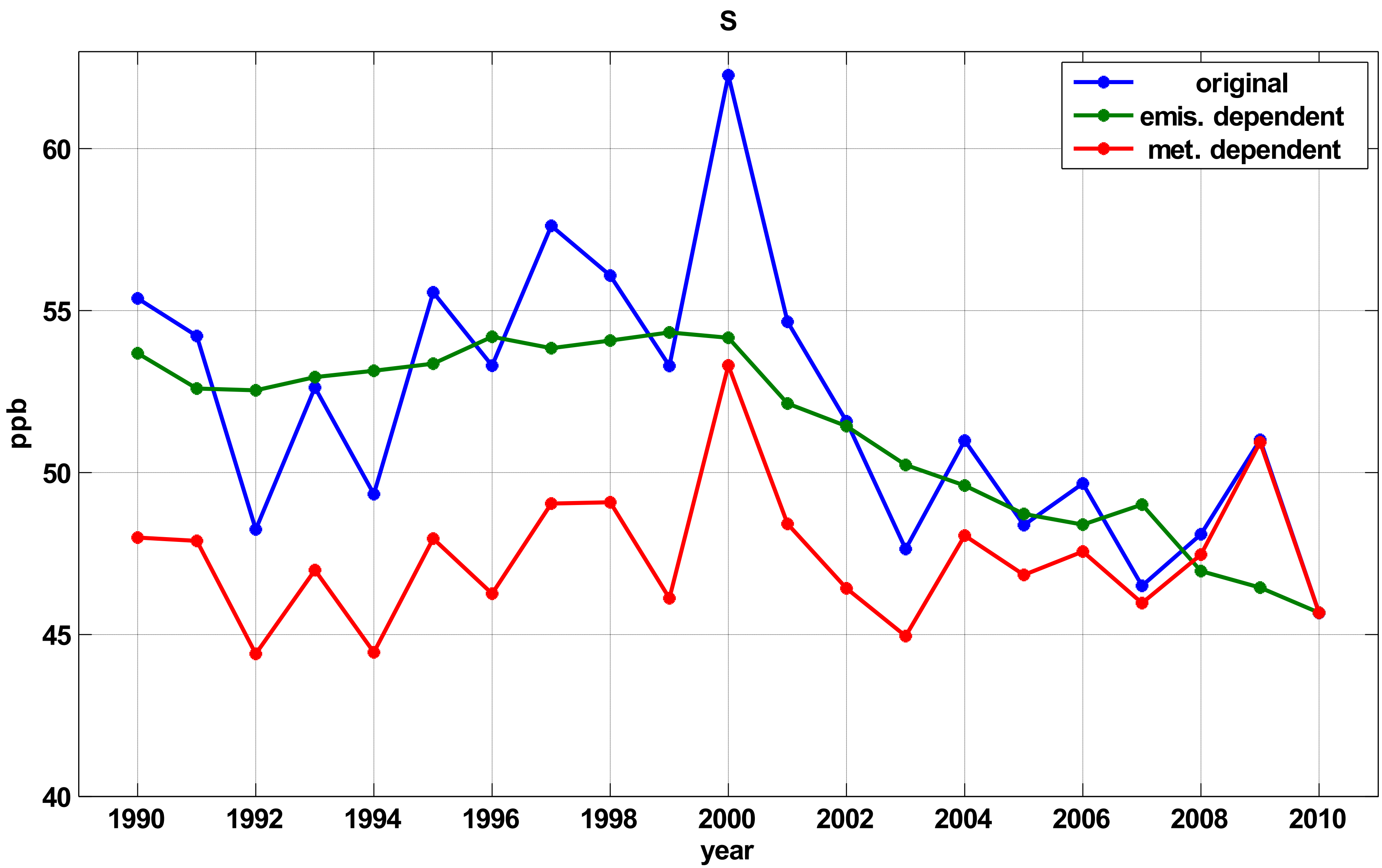

Figure 20. S region: CMAQ ozone (CMAQ, blue), emission-dependent ozone (green), and meteorologically-dependent ozone (red).

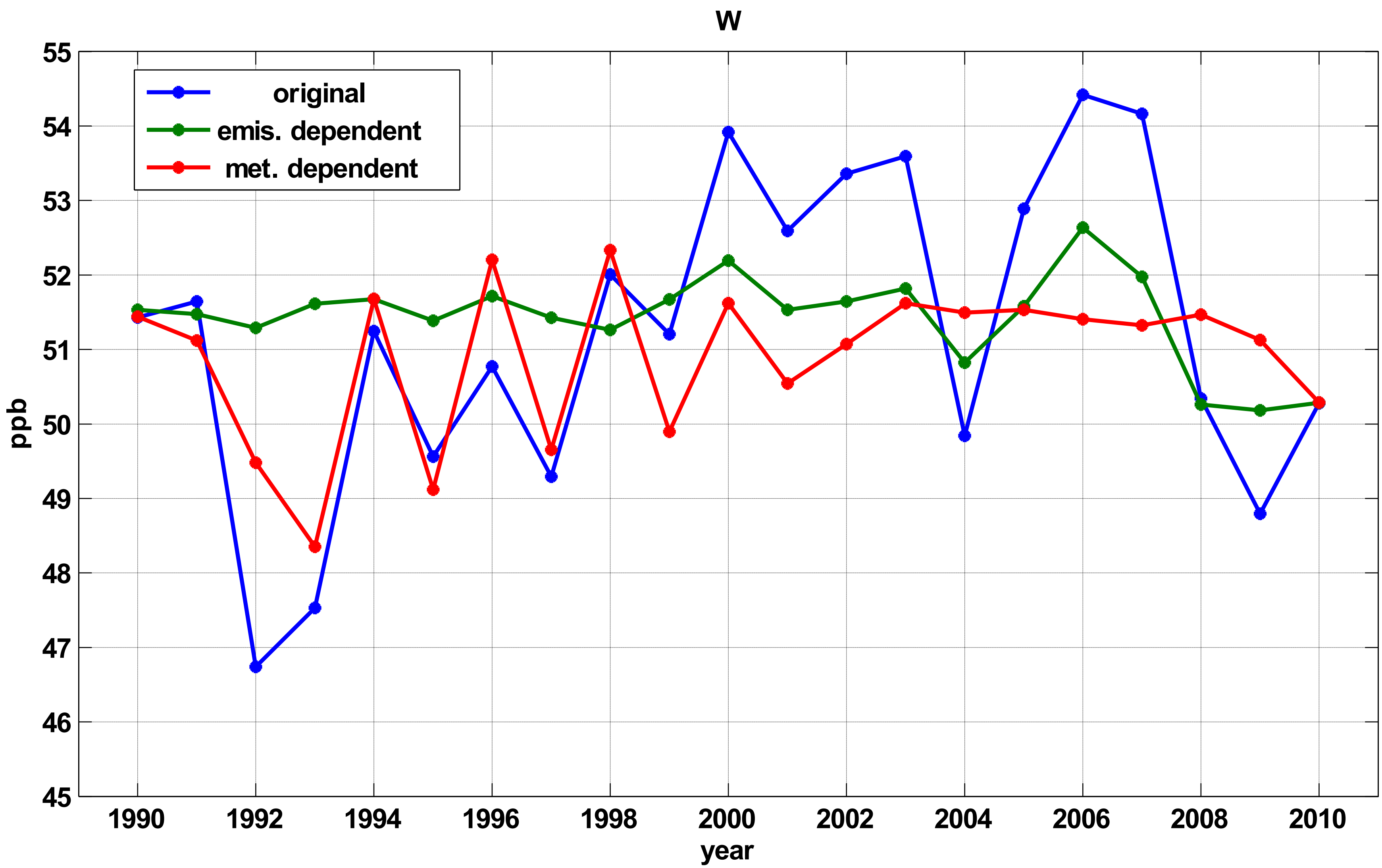

Figure 21. W region: CMAQ ozone (CMAQ, blue), emission-dependent ozone (green), and meteorologically-dependent ozone (red).

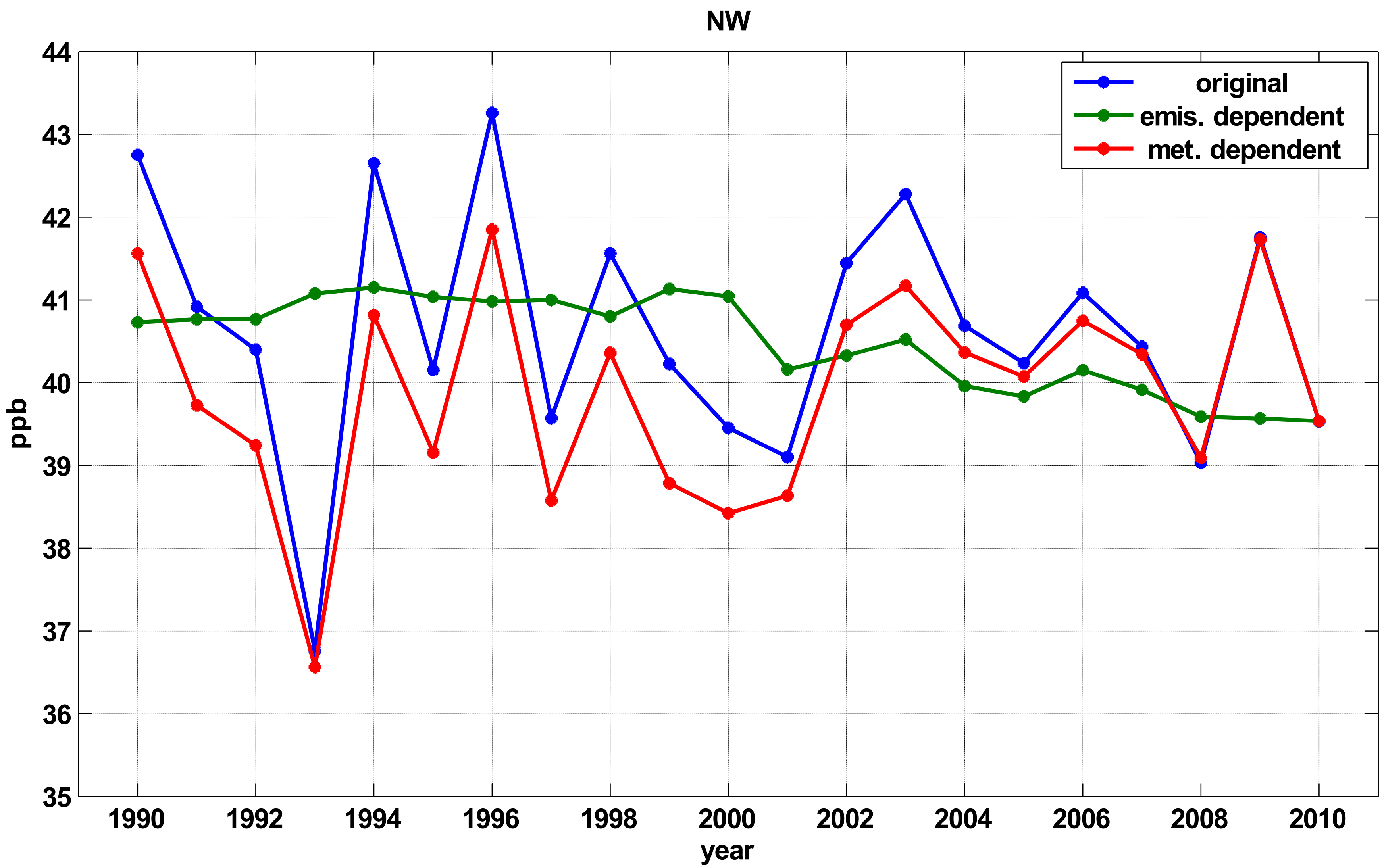

Figure 22. NW region: CMAQ ozone (CMAQ, blue), emission-dependent ozone (green), and meteorologically-dependent ozone (red).

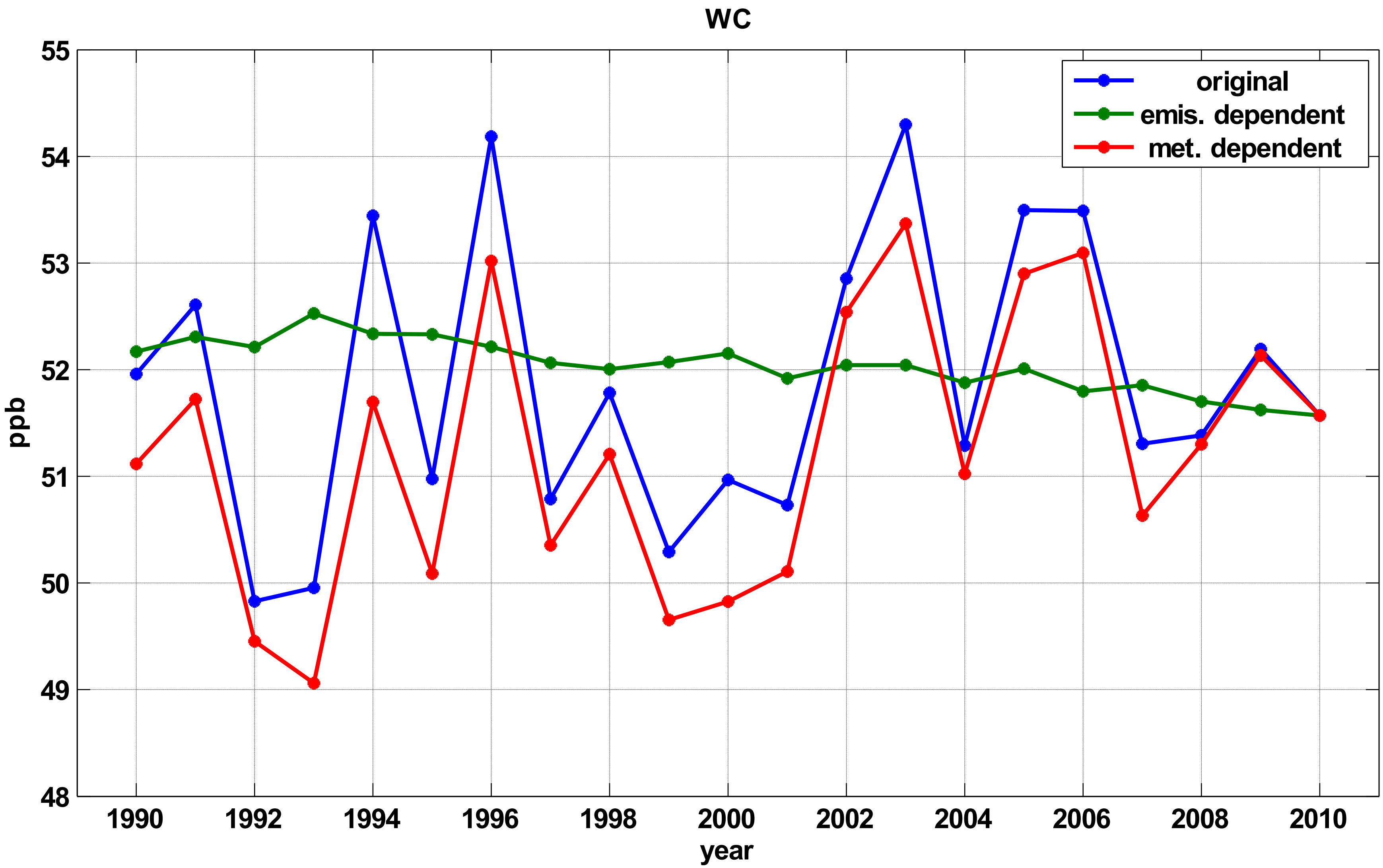

Figure 23. WC region: CMAQ ozone (CMAQ, blue), emission-dependent ozone (green), and meteorologically-dependent ozone (red).

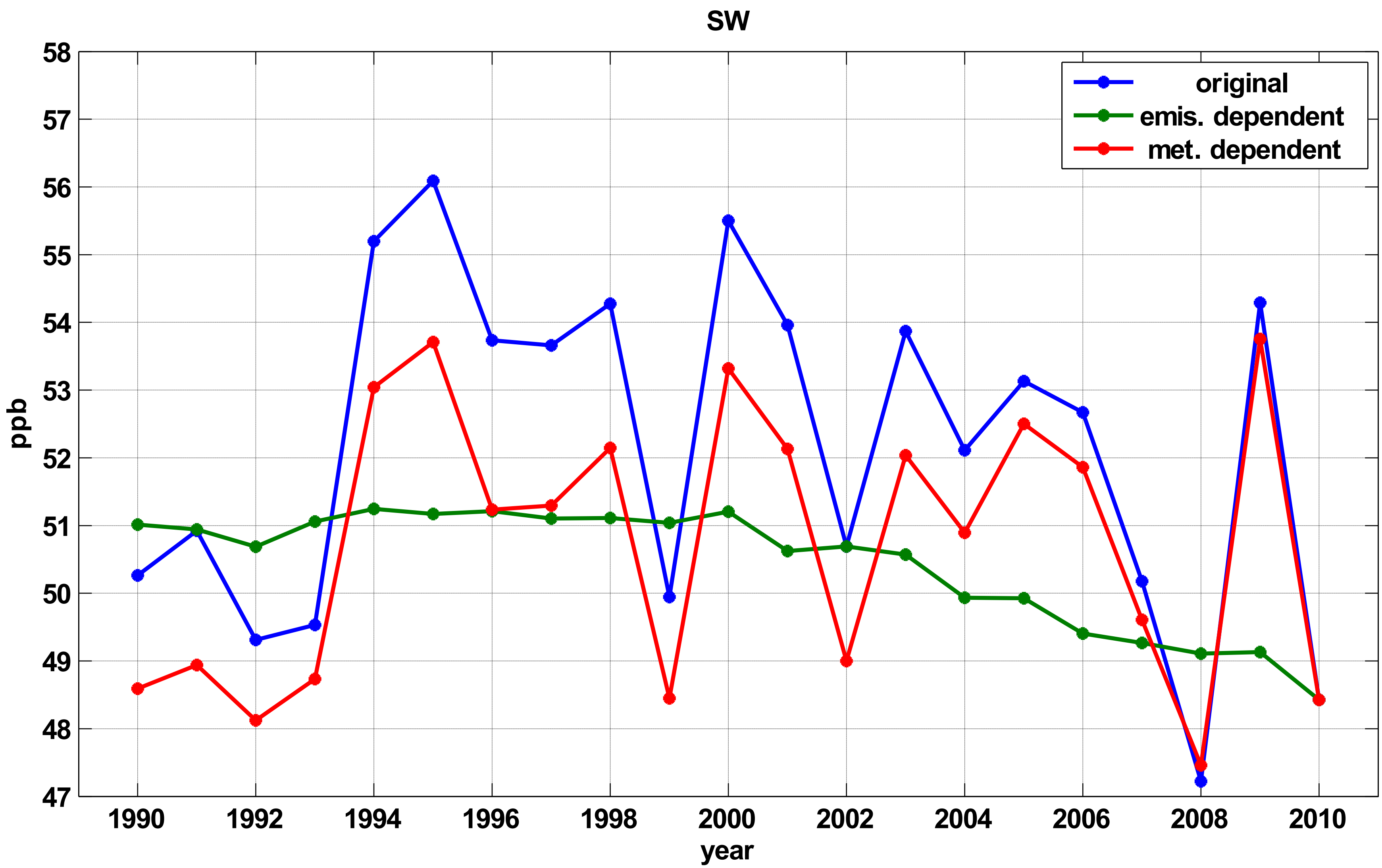

Figure 24. SW region: CMAQ ozone (CMAQ, blue), emission-dependent ozone (green), and meteorologically-dependent ozone (red).

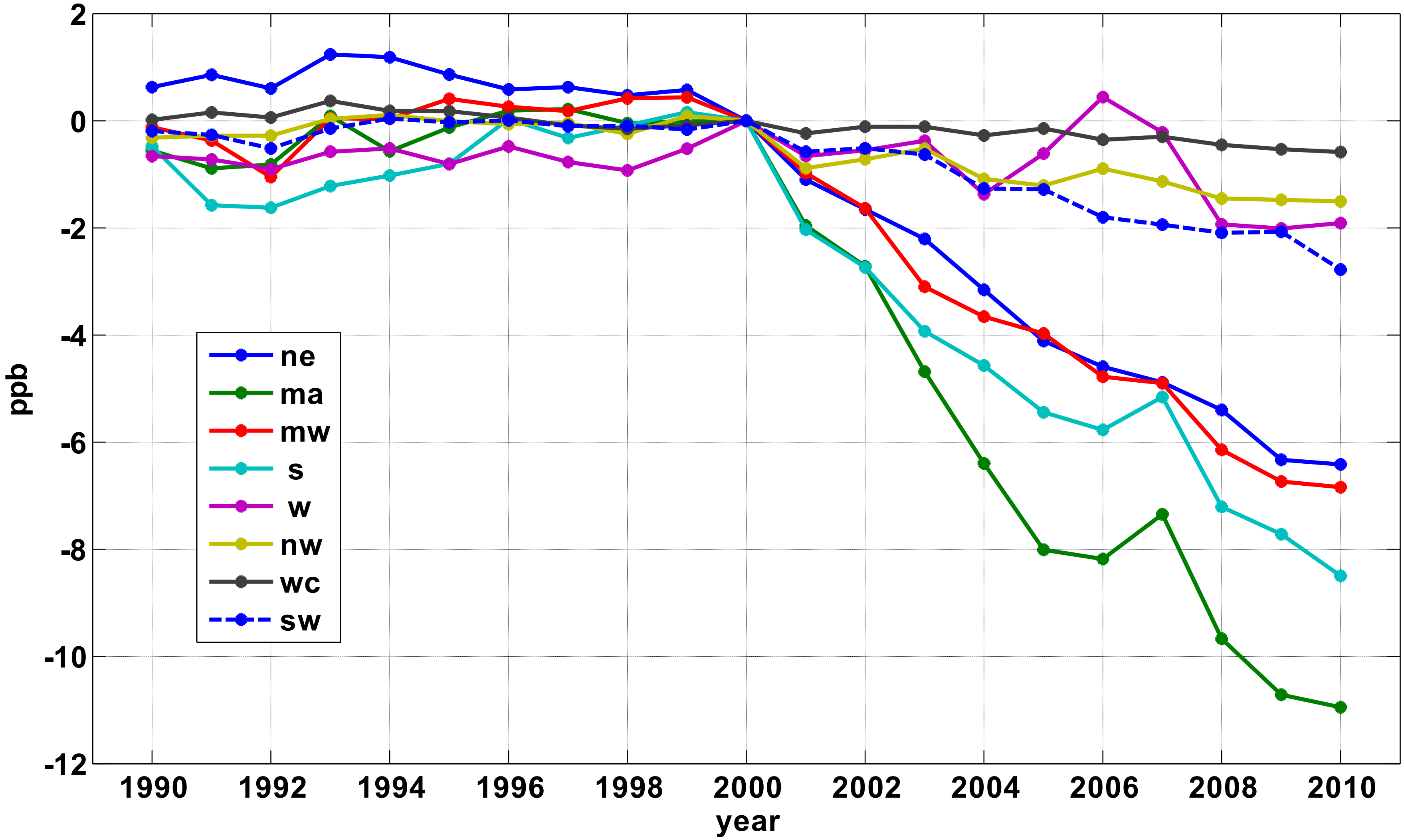

Figure 25. Emission-dependent ozone: regional means.

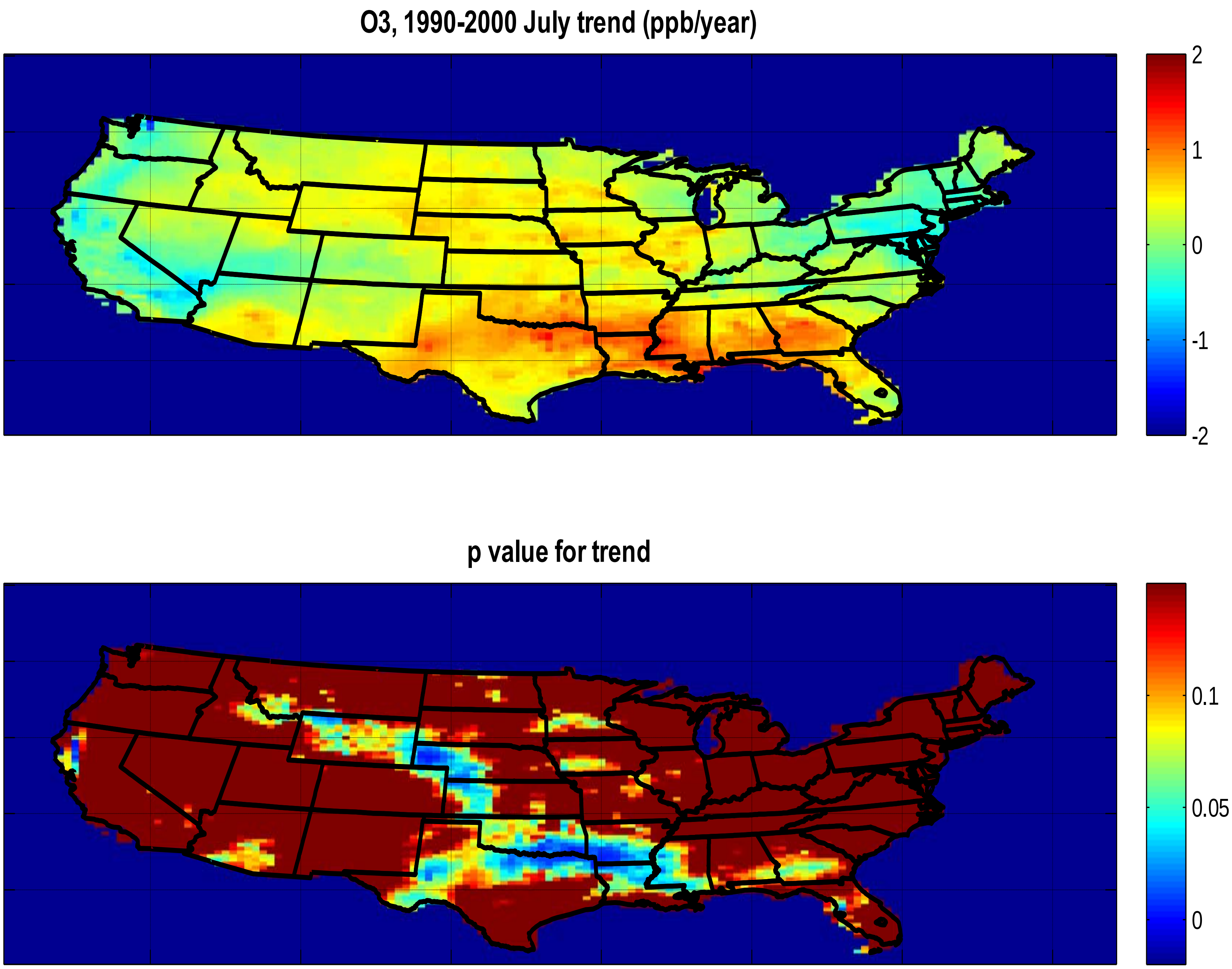

Figure 26. CMAQ ozone: 1990-2000 July trend (ppb/year, top panel), p value of slope estimate (lower panel)

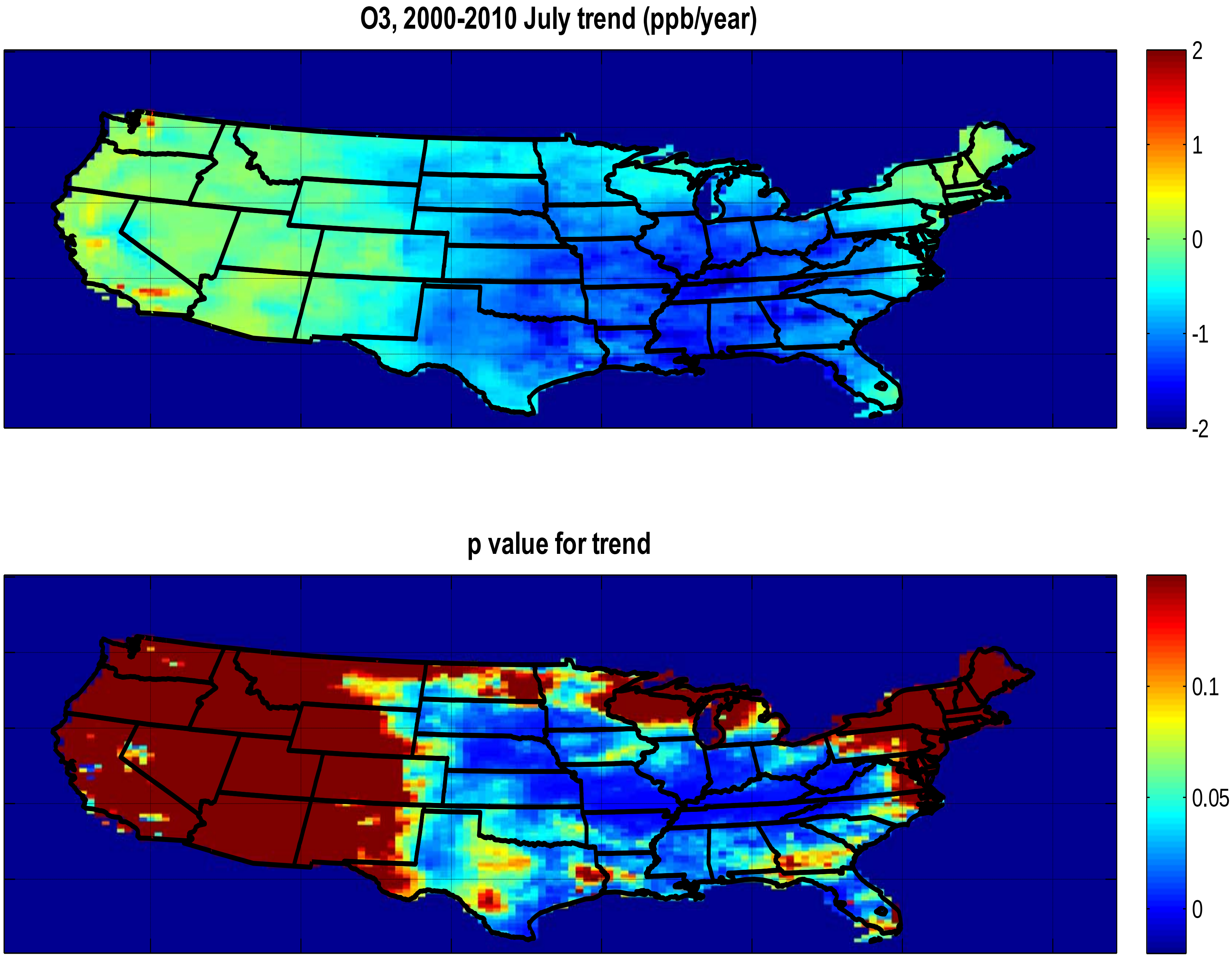

Figure 27. CMAQ ozone: 2000-2010 July trend (ppb/year, top panel), p value of slope estimate (lower panel)

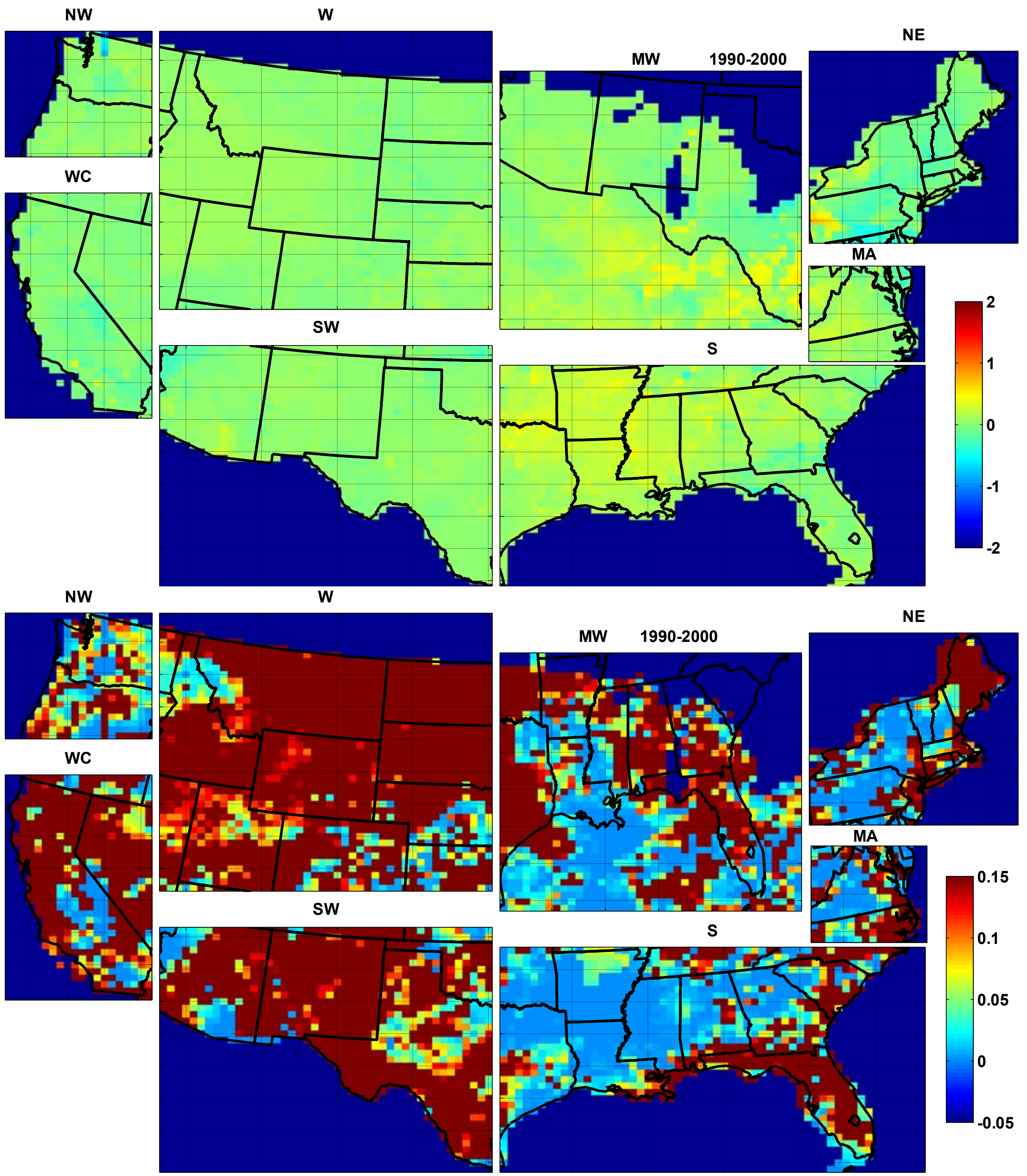

Figure 28. Emission-dependent ozone: temporal trend (ppb/year, 1990-2000) (upper panel), p value of slope estimate (lower panel)

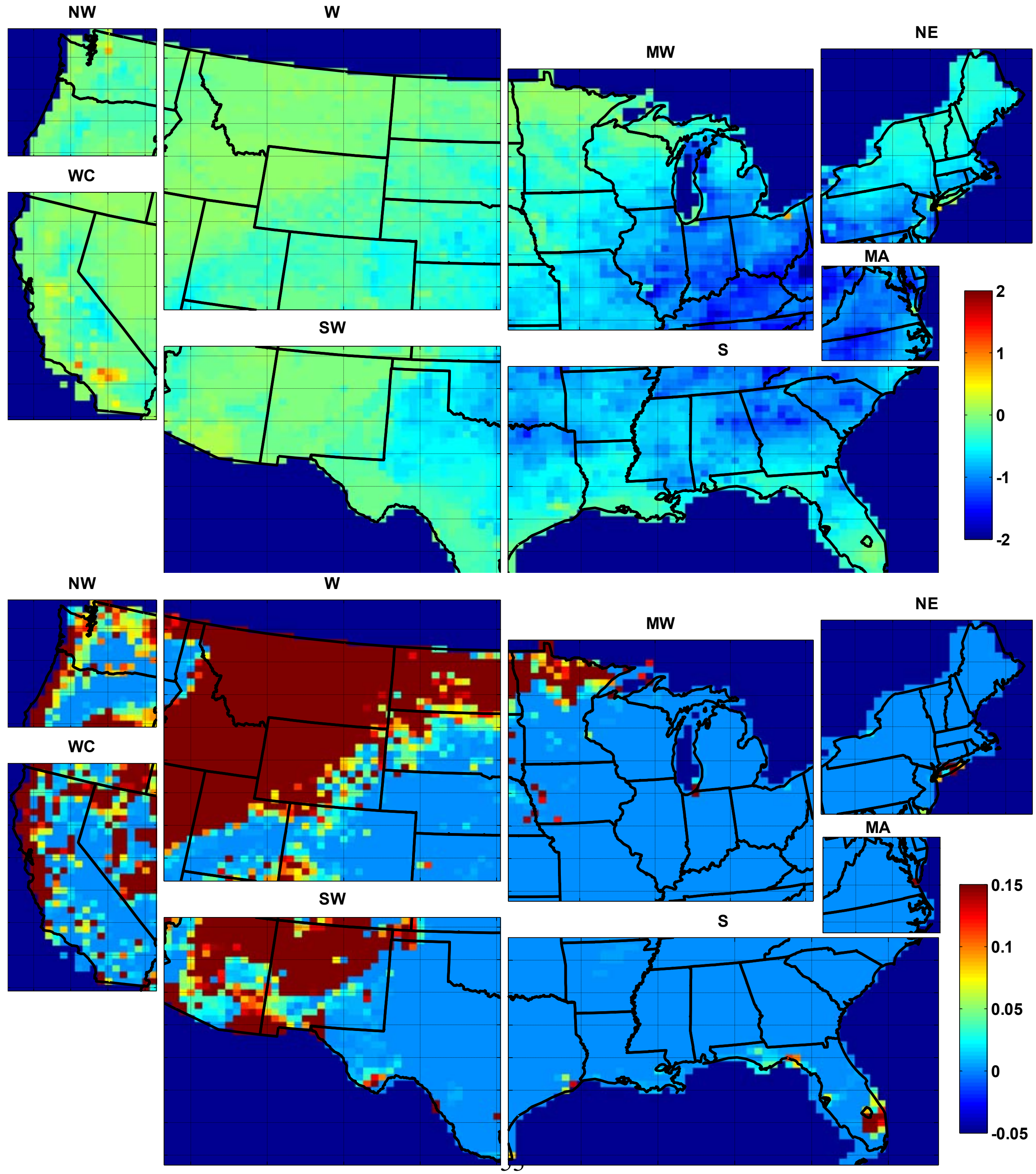

Figure 29. Emission-dependent ozone: temporal trend (ppb/year, 2000-2010) (upper panel), p value of slope estimate (lower panel)

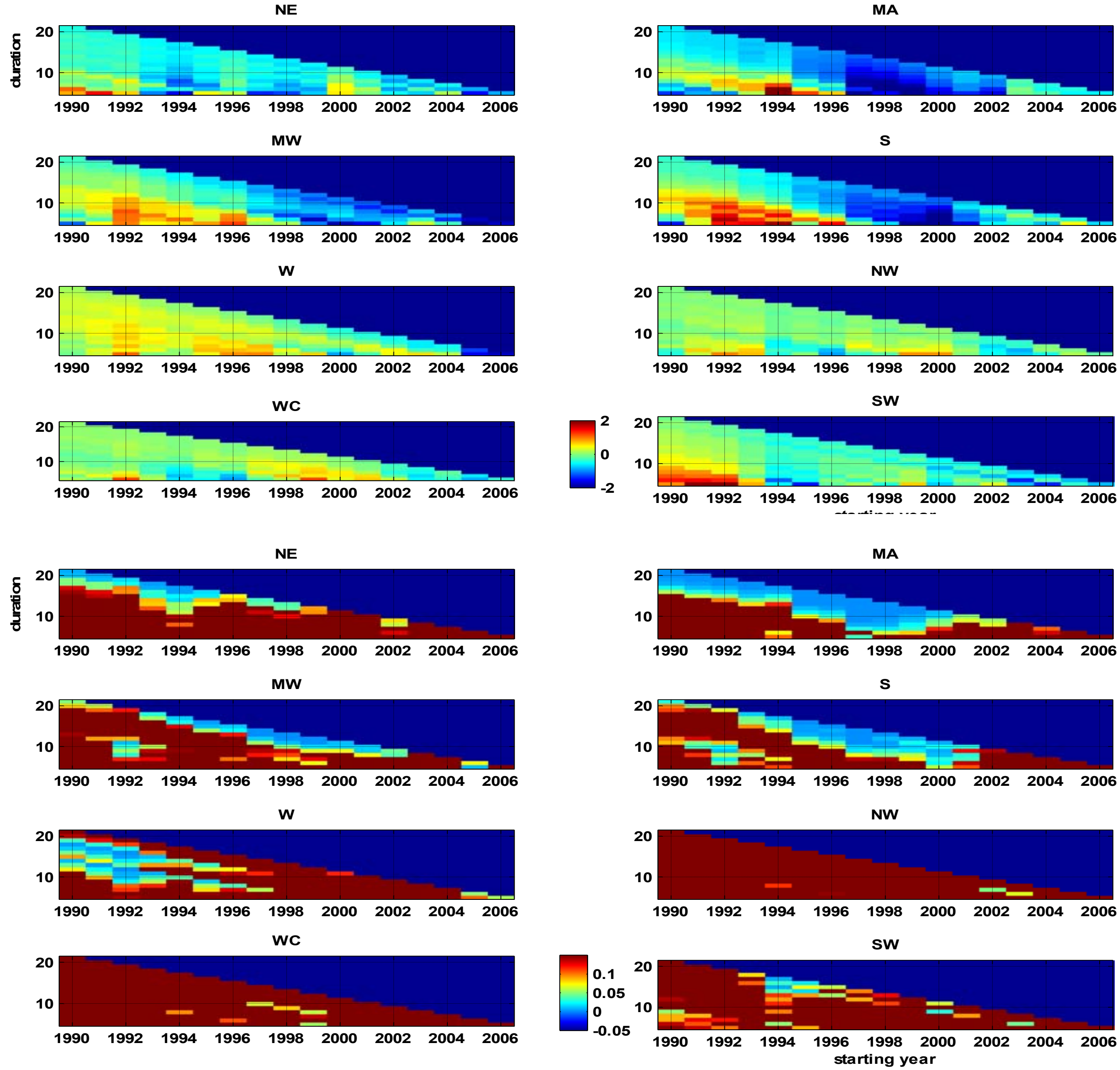

Figure 30. All CMAQ temporal trends in O3 (ppb/year) (upper panel), p value of slope estimate (lower panel). The x axis is the starting year for the trend estimate, the y axis is the duration of the trend.

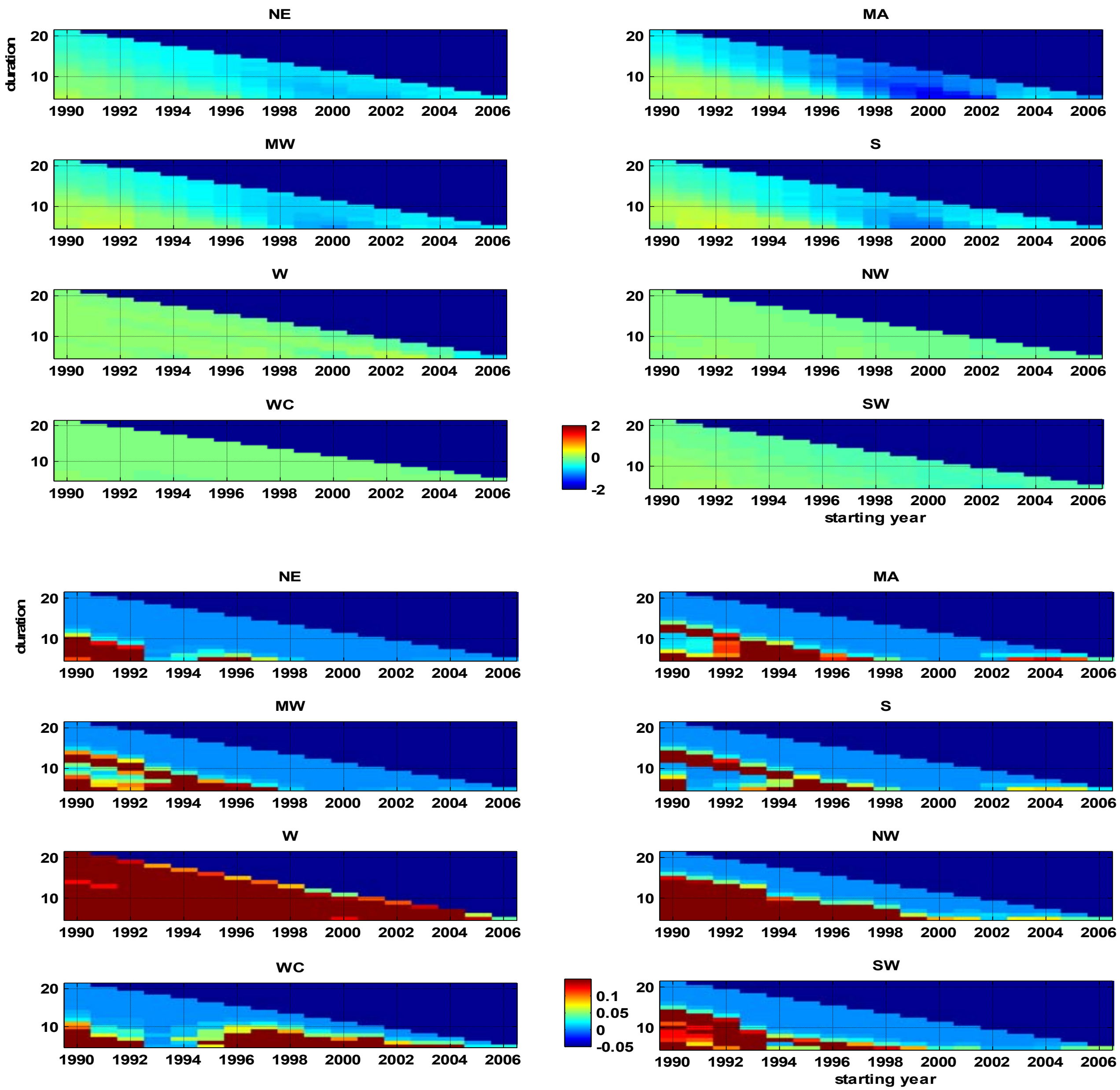

Figure 31. All emission-dependent temporal trends in O3 (ppb/year) (upper panel), p value of slope estimate (lower panel). The x axis is the starting year for the trend estimate, the y axis is the duration of the trend.

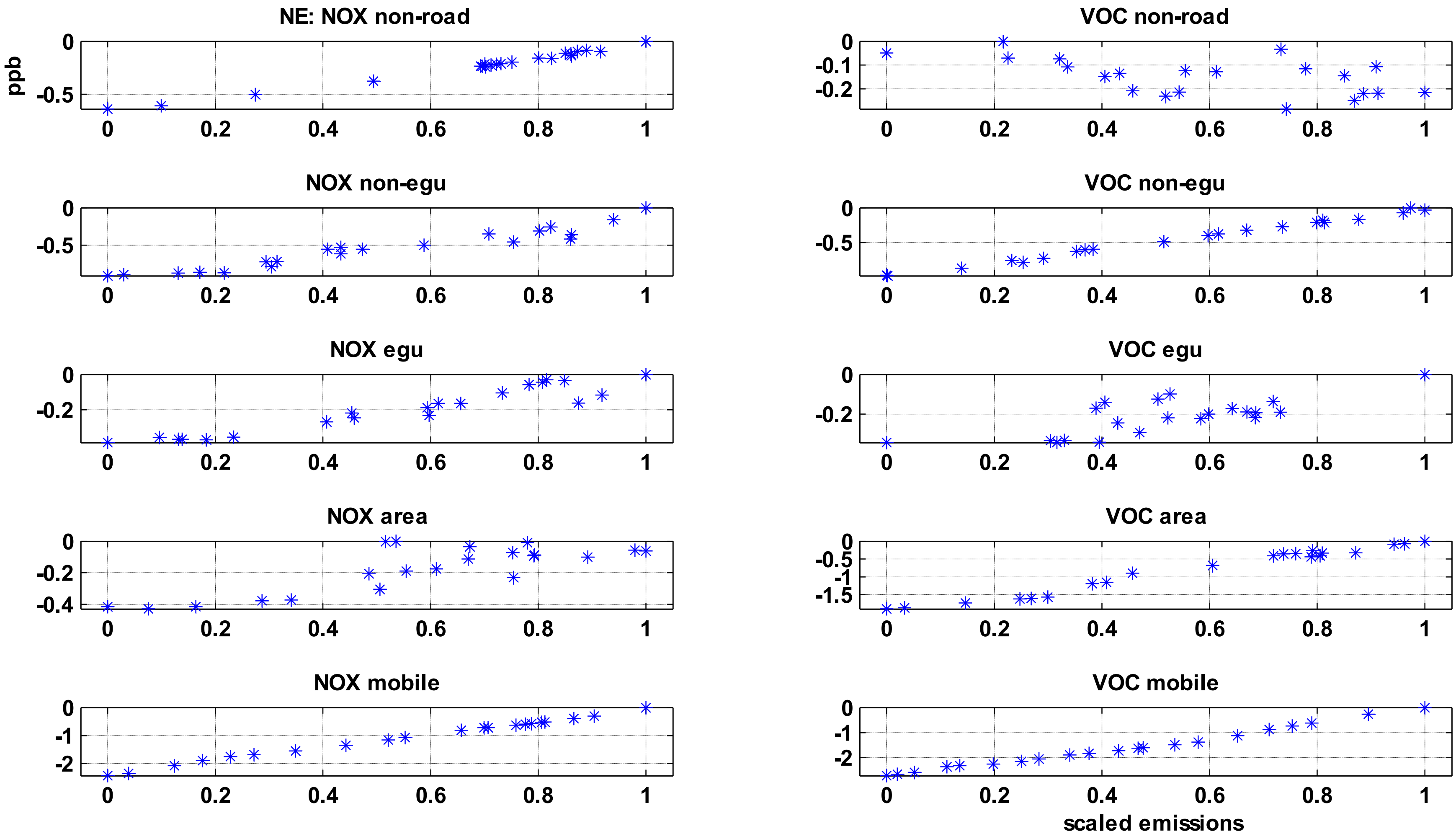

Figure 32. NE region: Emission-dependent ozone by source (ppb) vs. emission (scaled from 0 to 1).

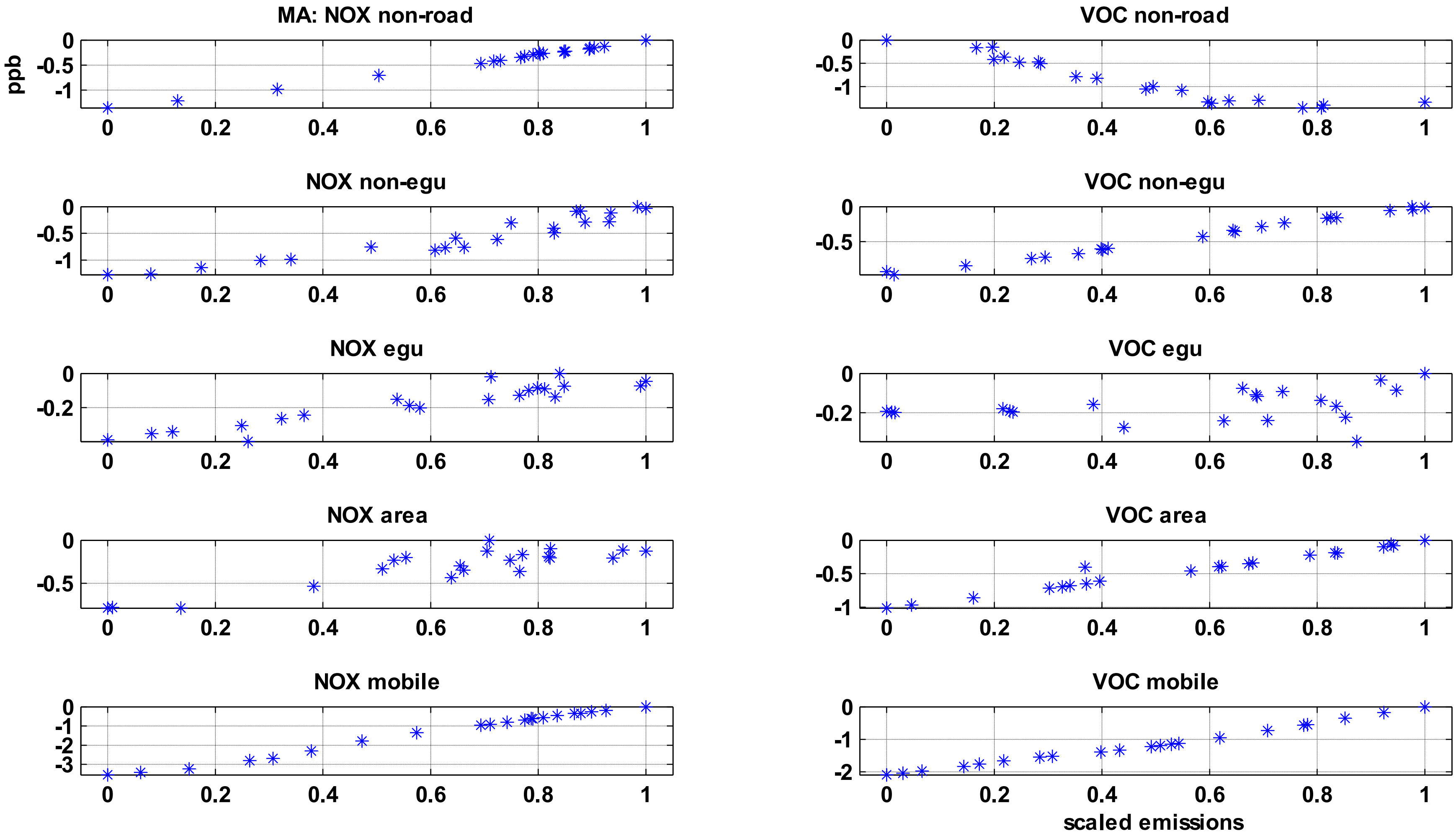

Figure 33. MA region: Emission-dependent ozone by source (ppb) vs. emission (scaled from 0 to 1).

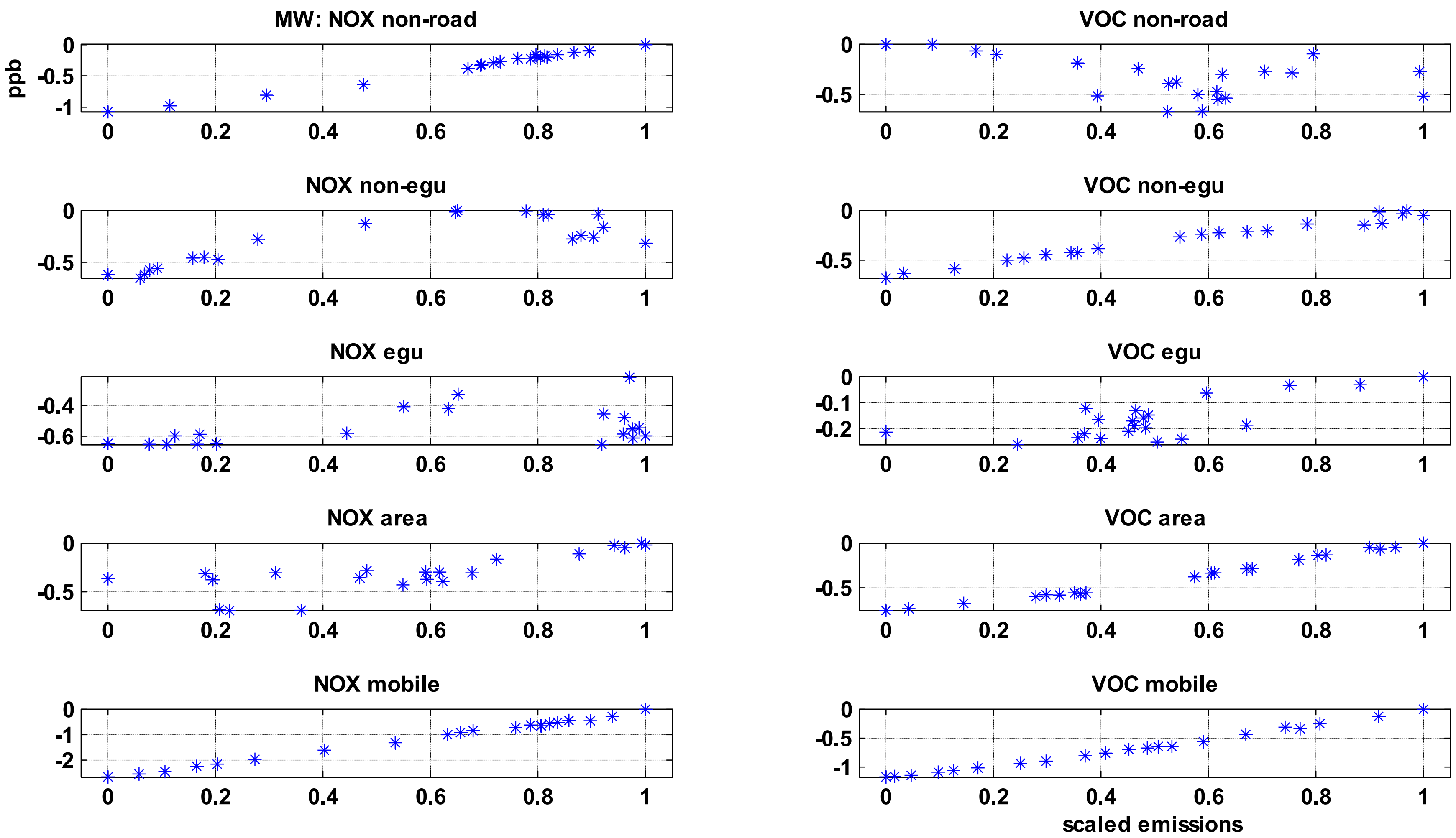

Figure 34. MW region: Emission-dependent ozone by source (ppb) vs. emission (scaled from 0 to 1).

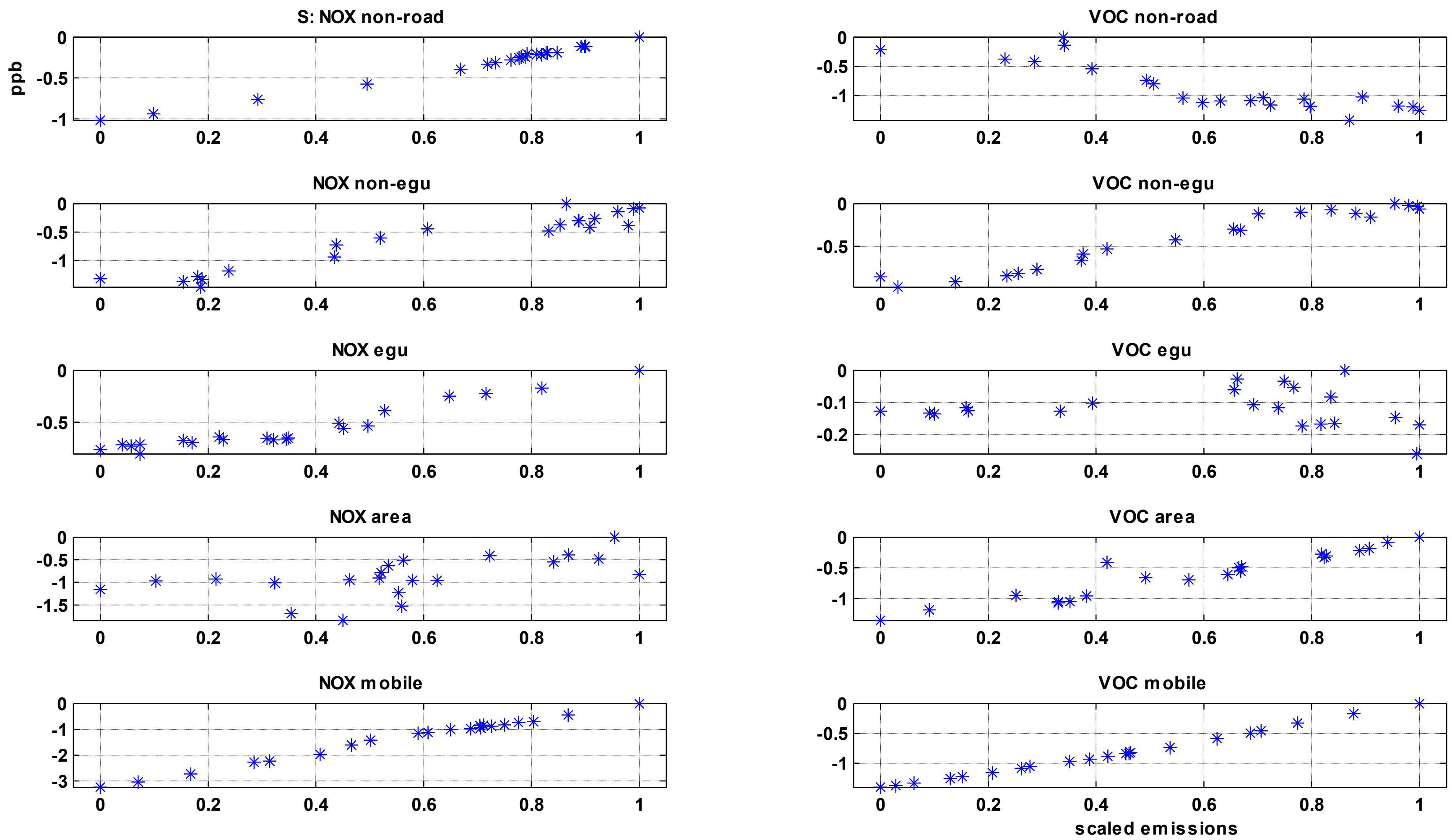

Figure 35. S region: Emission-dependent ozone by source (ppb) vs. emission (scaled from 0 to 1).

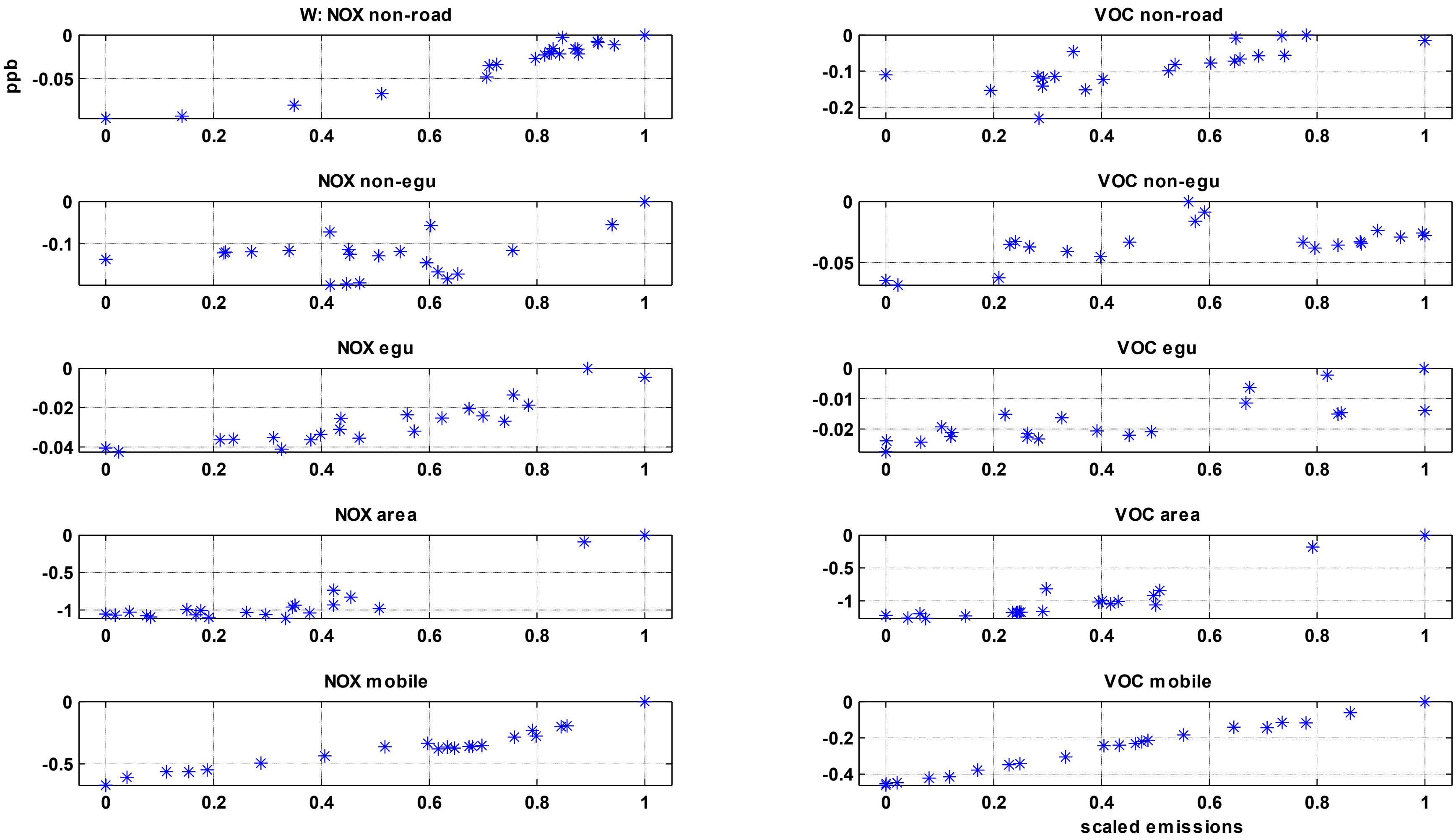

Figure 36. W region: Emission-dependent ozone by source (ppb) vs. emission (scaled from 0 to 1).

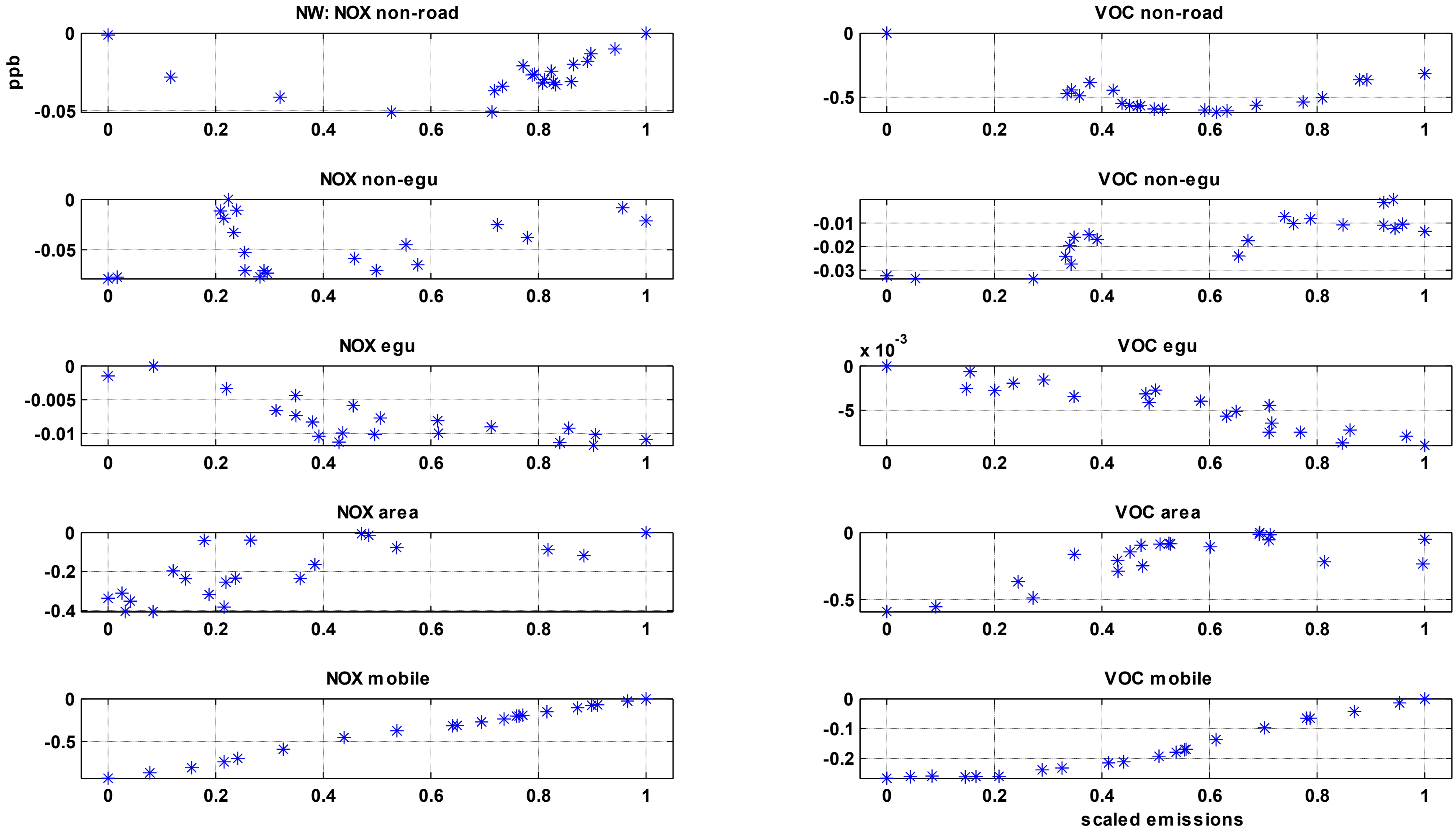

Figure 37. NW region: Emission-dependent ozone by source (ppb) vs. emission (scaled from 0 to 1).

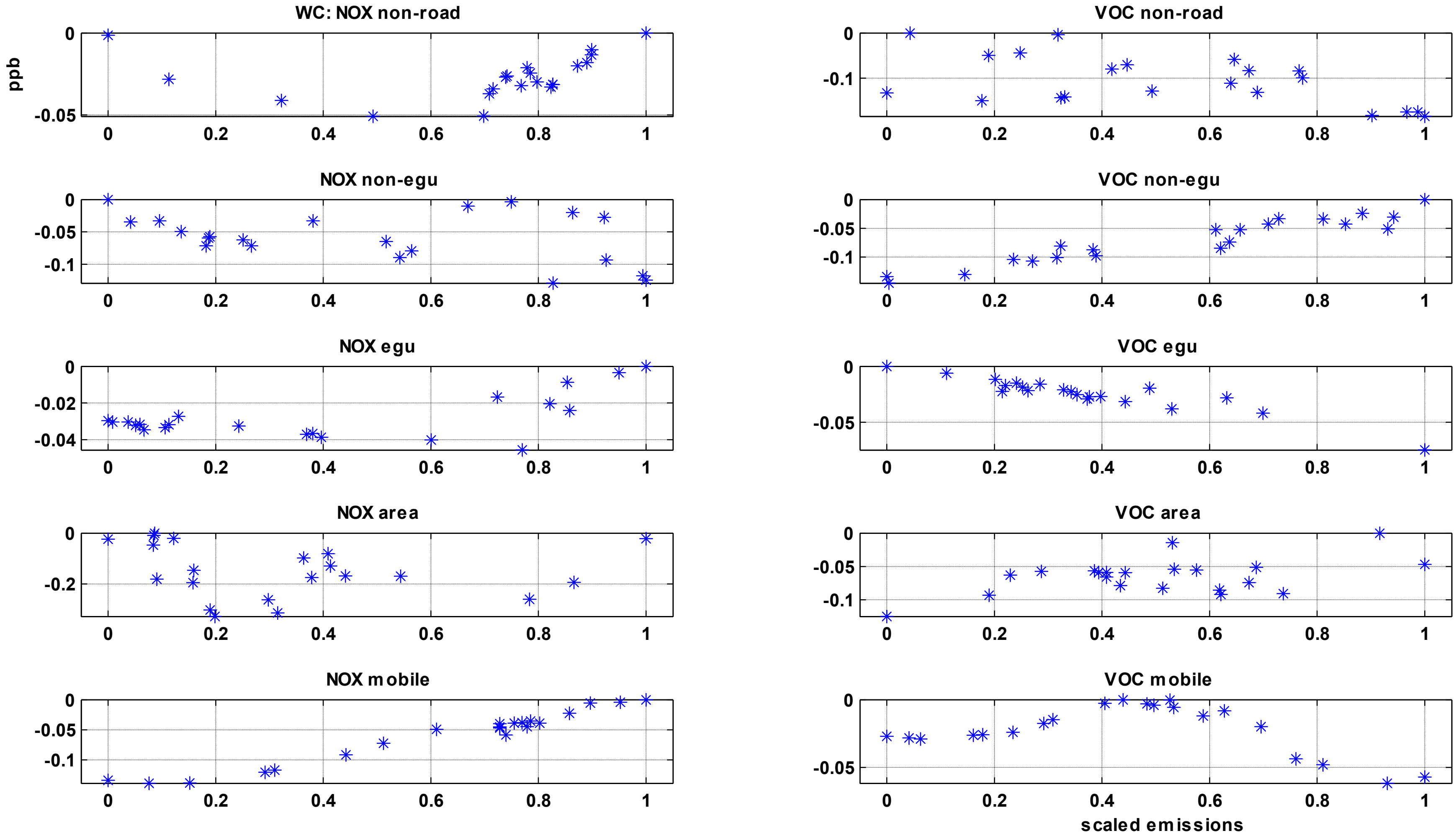

Figure 38. WC region: Emission-dependent ozone by source (ppb) vs. emission (scaled from 0 to 1).

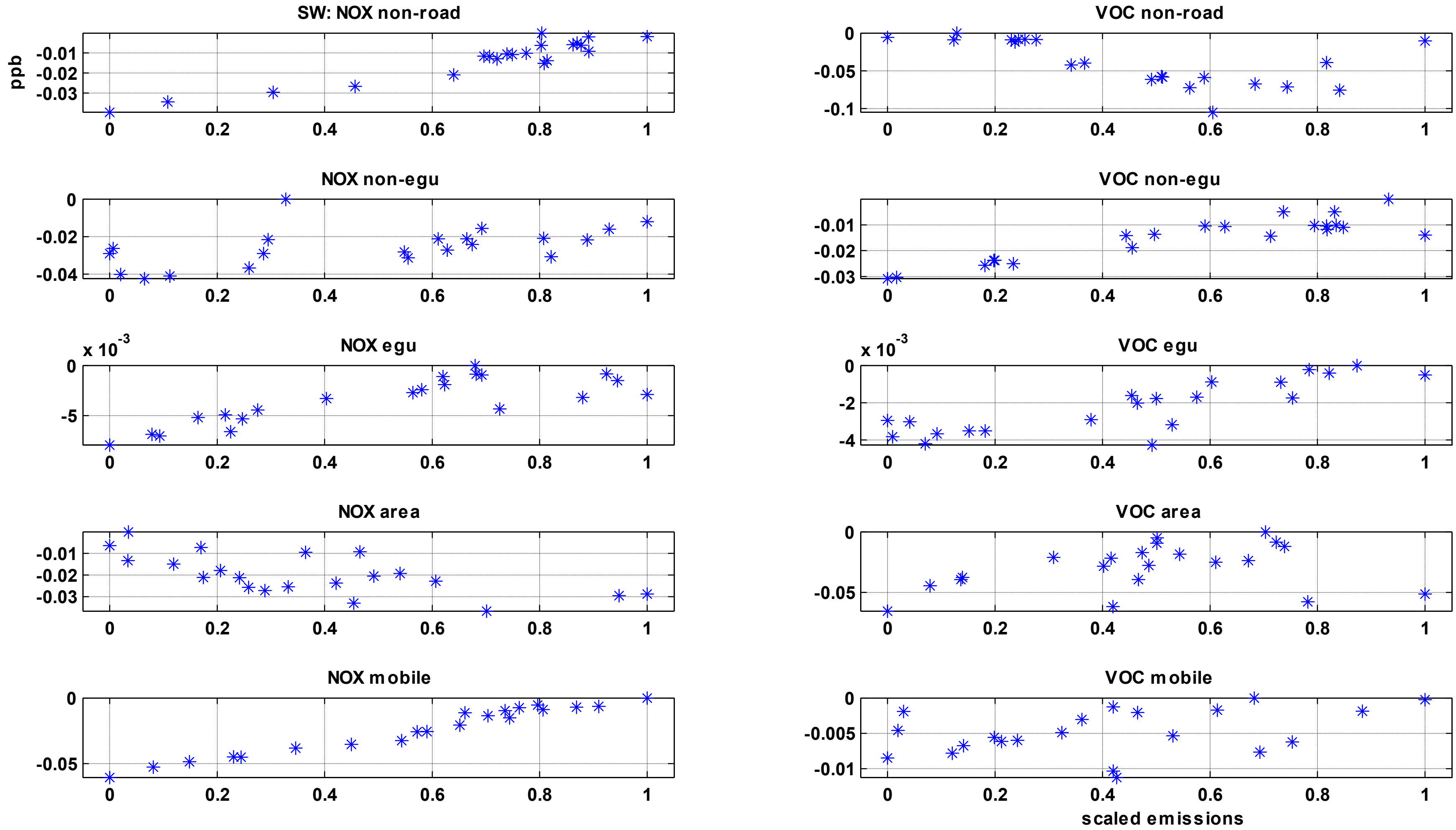

Figure 39. SW region: Emission-dependent ozone by source (ppb) vs. emission (scaled from 0 to 1).

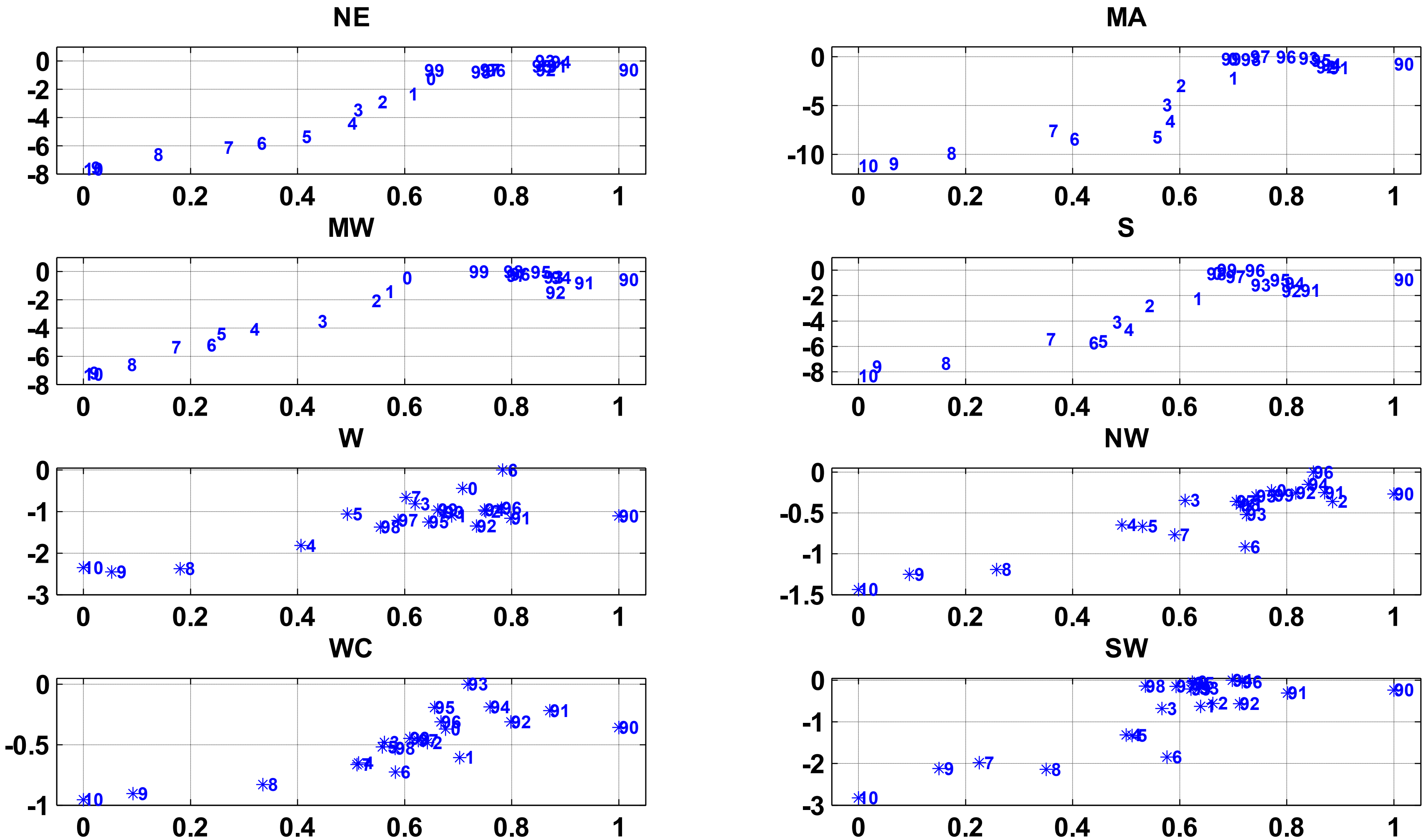

Figure 40. Ozone response to all anthropogenic emissions (numbers indicate year; ‘98’=1998, ‘6’ = 2006, etc.).

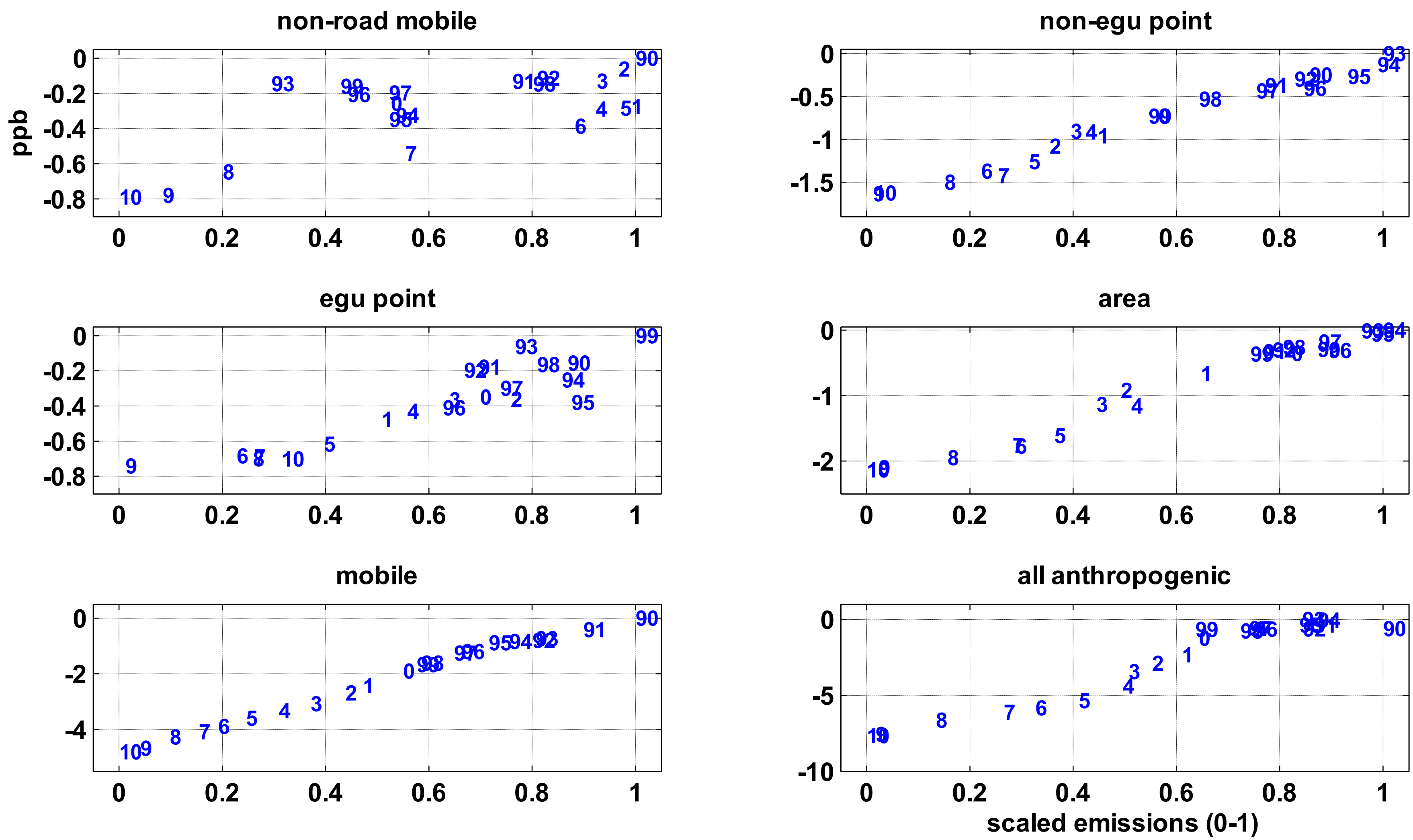

Figure 41. NE region: V+C emission-dependent ozone by source (ppb) vs. combined NOx and VOC emissions (scaled from 0 to 1) (numbers indicate year; ‘98’=1998, ‘6’ = 2006, etc.).

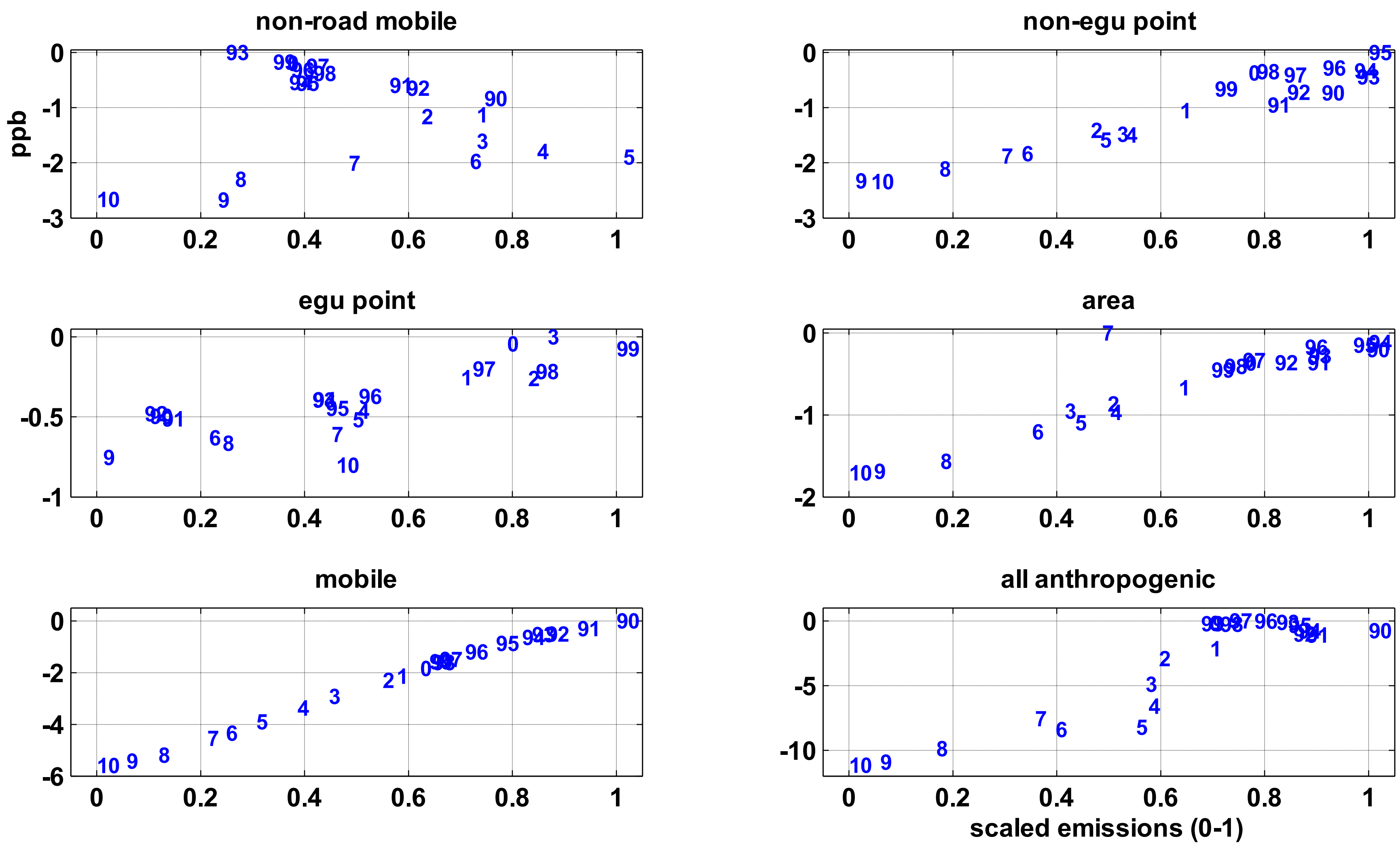

Figure 42. MA region: V+C emission-dependent ozone by source (ppb) vs. combined NOx and VOC emissions (scaled from 0 to 1) (numbers indicate year; '98'=1998, '6' = 2006, etc.).

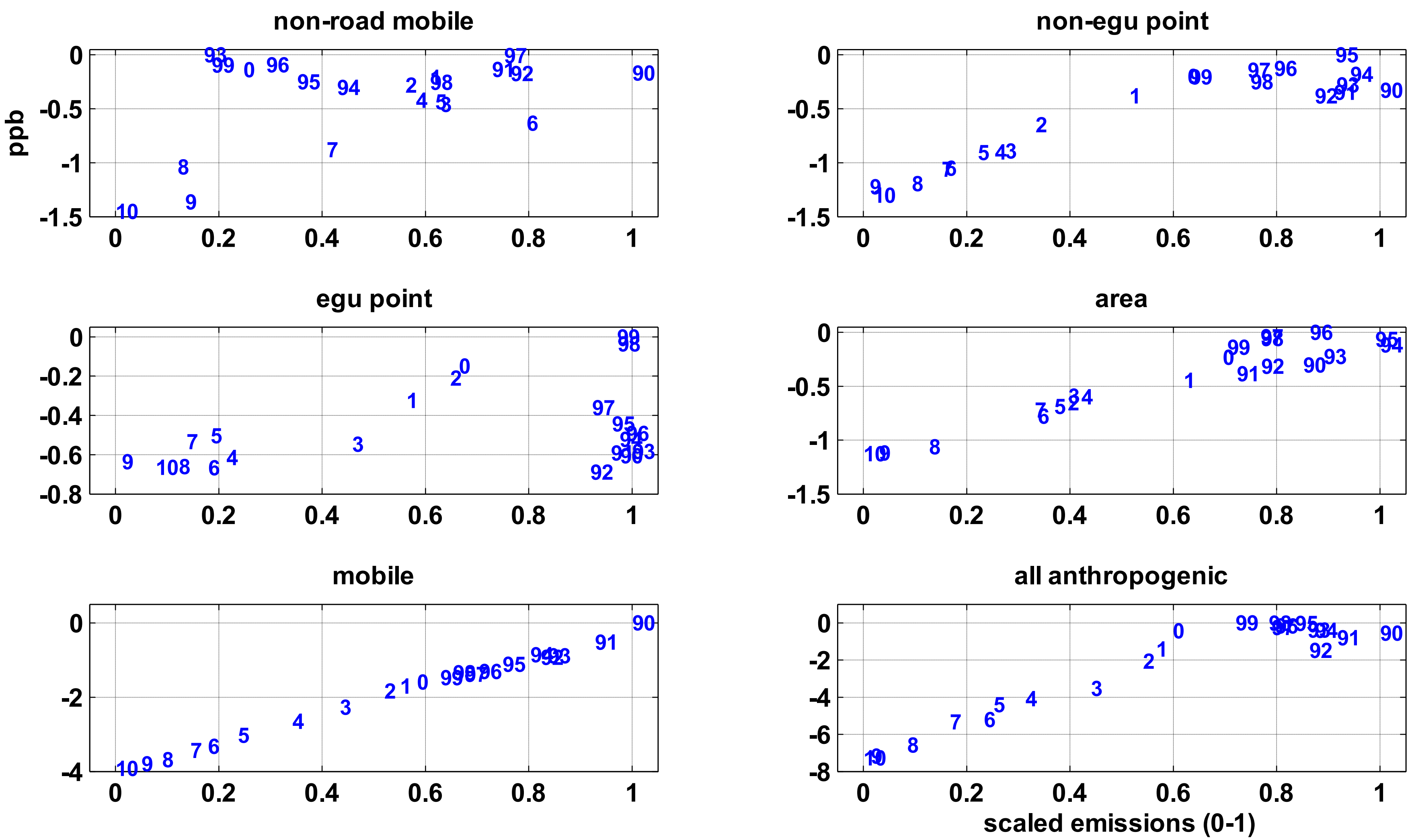

Figure 43. MW region: V+C emission-dependent ozone by source (ppb) vs. combined NOx and VOC emissions (scaled from 0 to 1) (numbers indicate year; ‘98’=1998, ‘6’ = 2006, etc.).

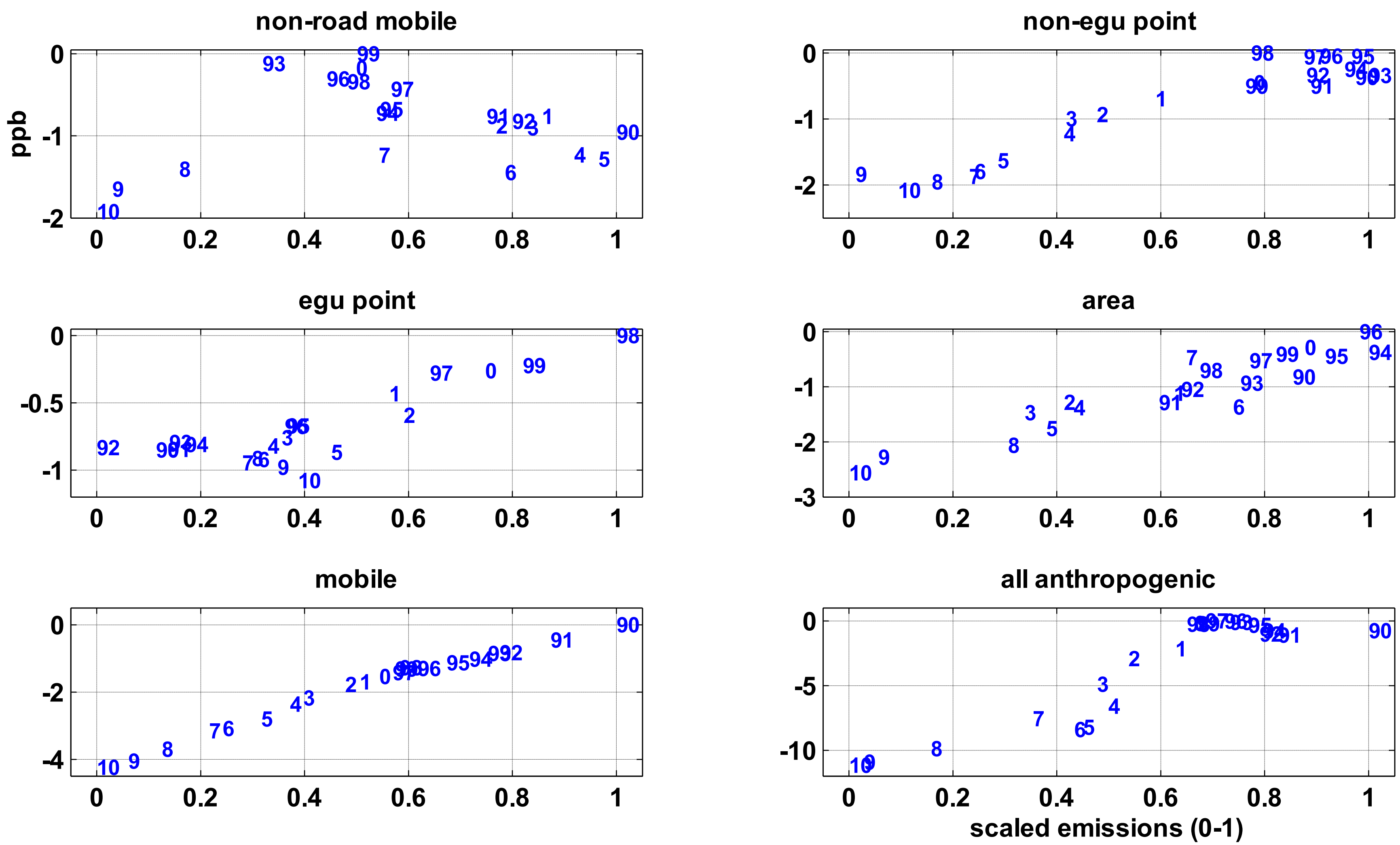

Figure 44. S region: V+C emission-dependent ozone by source (ppb) vs. combined NOx and VOC emissions (scaled from 0 to 1) (numbers indicate year; '98'=1998, '6' = 2006, etc.).

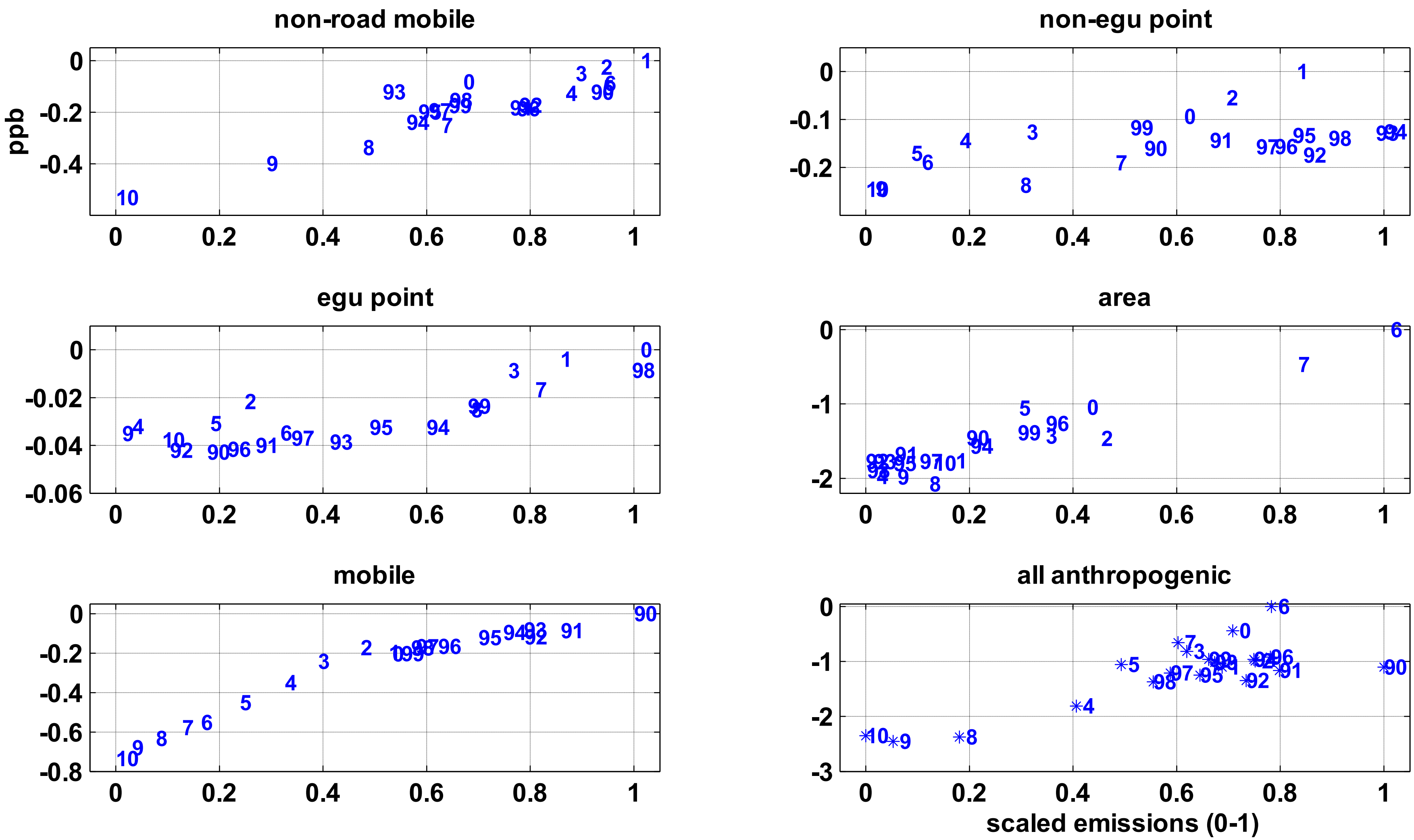

Figure 45. W region: V+C emission-dependent ozone by source (ppb) vs. combined NOx and VOC emissions (scaled from 0 to 1) (numbers indicate year; '98'=1998, '6' = 2006, etc.).

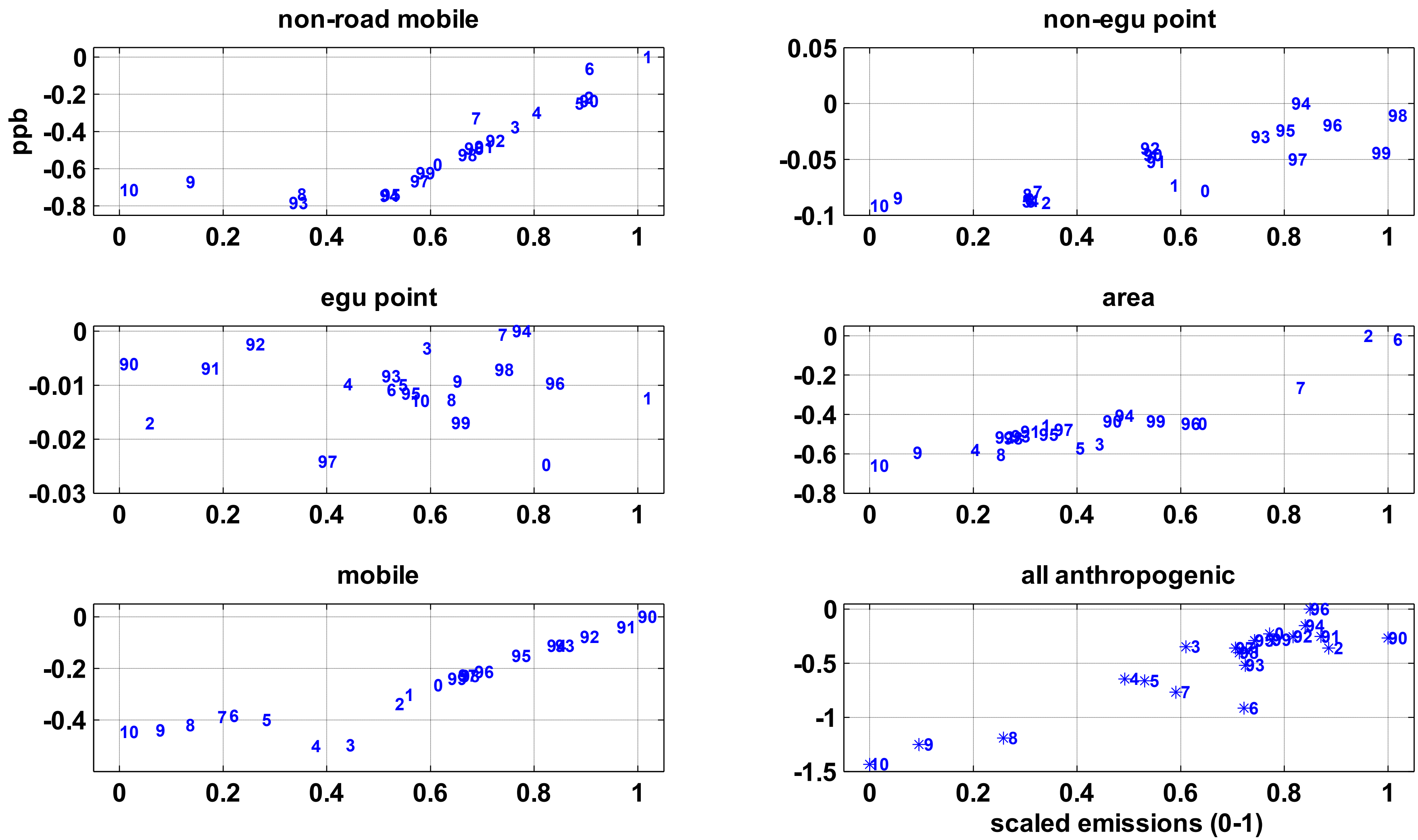

Figure 46. NW region: V+C emission-dependent ozone by source (ppb) vs. combined NOx and VOC emissions (scaled from 0 to 1) (numbers indicate year; '98'=1998, '6' = 2006, etc.).

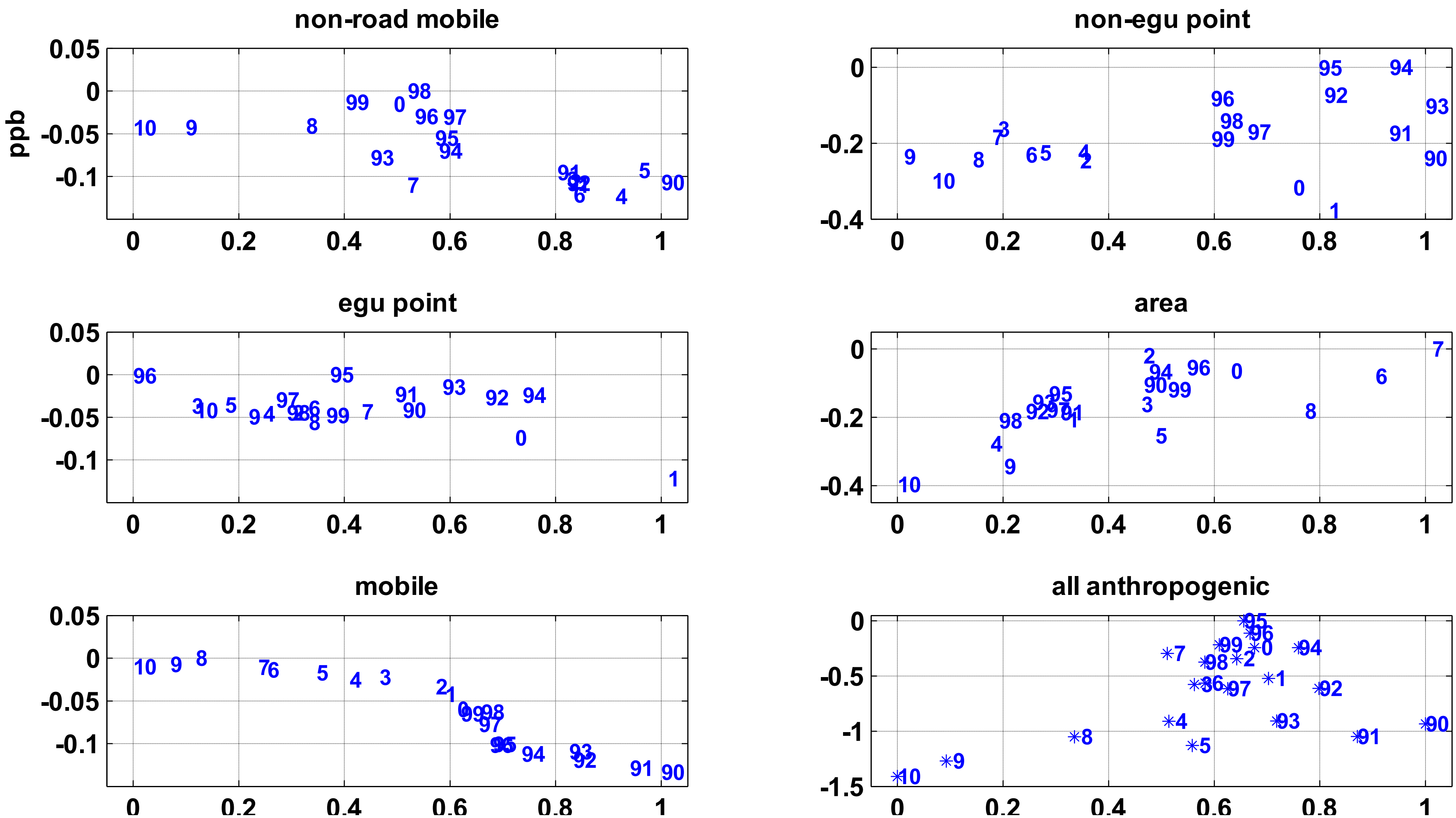

Figure 47. WC region: V+C emission-dependent ozone by source (ppb) vs. combined NOx and VOC emissions (scaled from 0 to 1) (numbers indicate year; '98'=1998, '6' = 2006, etc.).

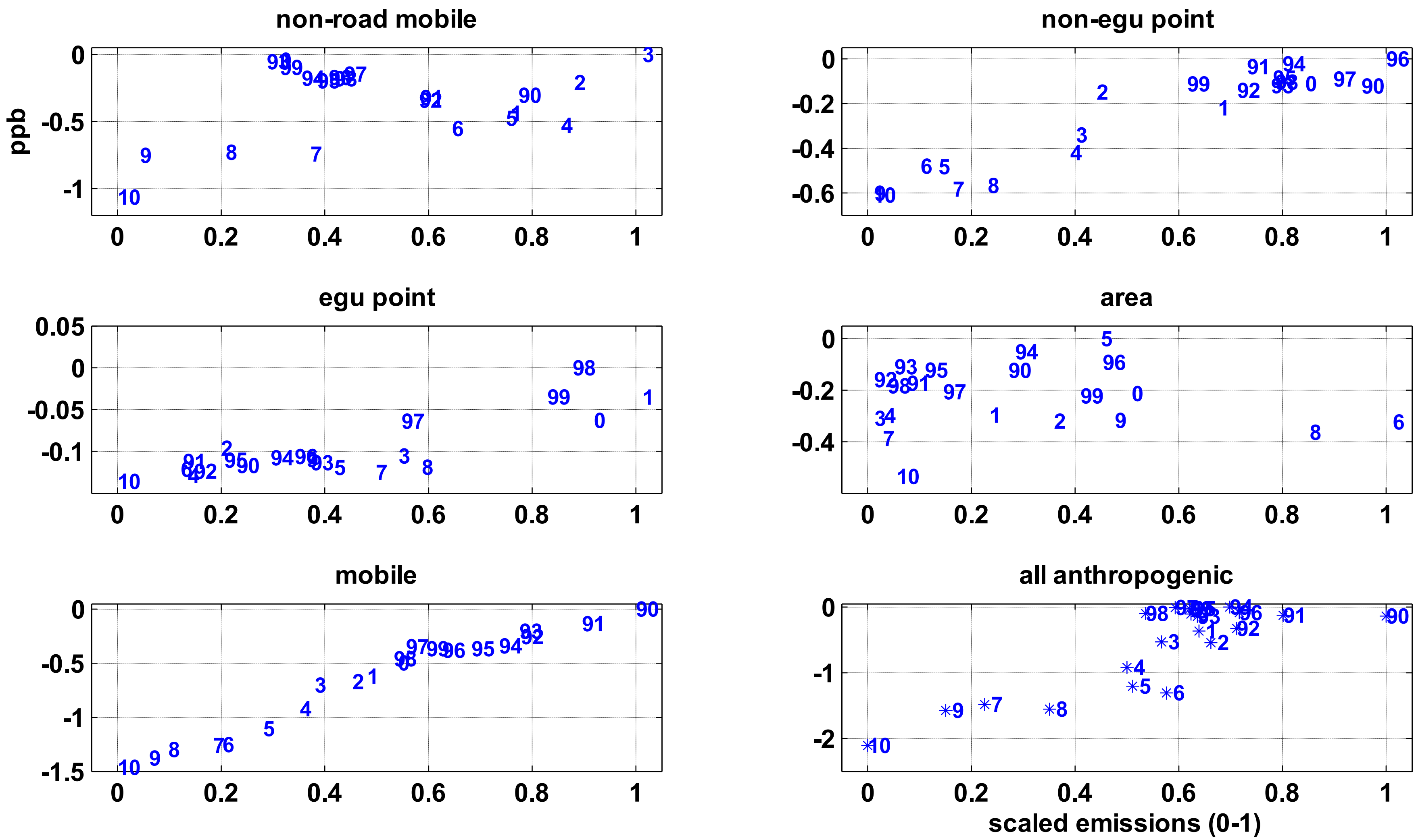

Figure 48. SW region: V+C emission-dependent ozone by source (ppb) vs. combined NOx and VOC emissions (scaled from 0 to 1) (numbers indicate year; '98'=1998, '6' = 2006, etc.).

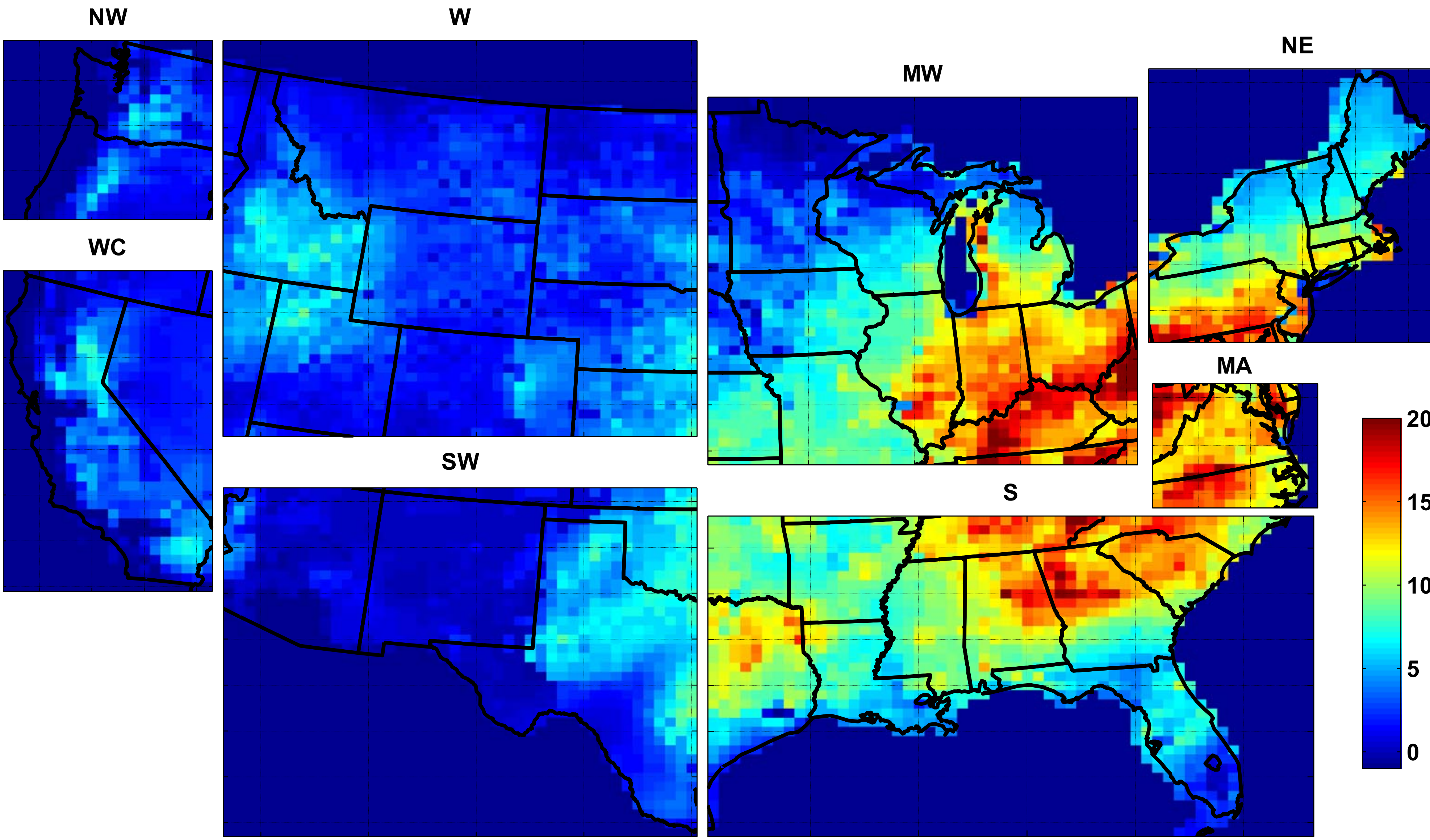

Figure 49. Ozone response to change in all anthropogenic emissions (ppb).

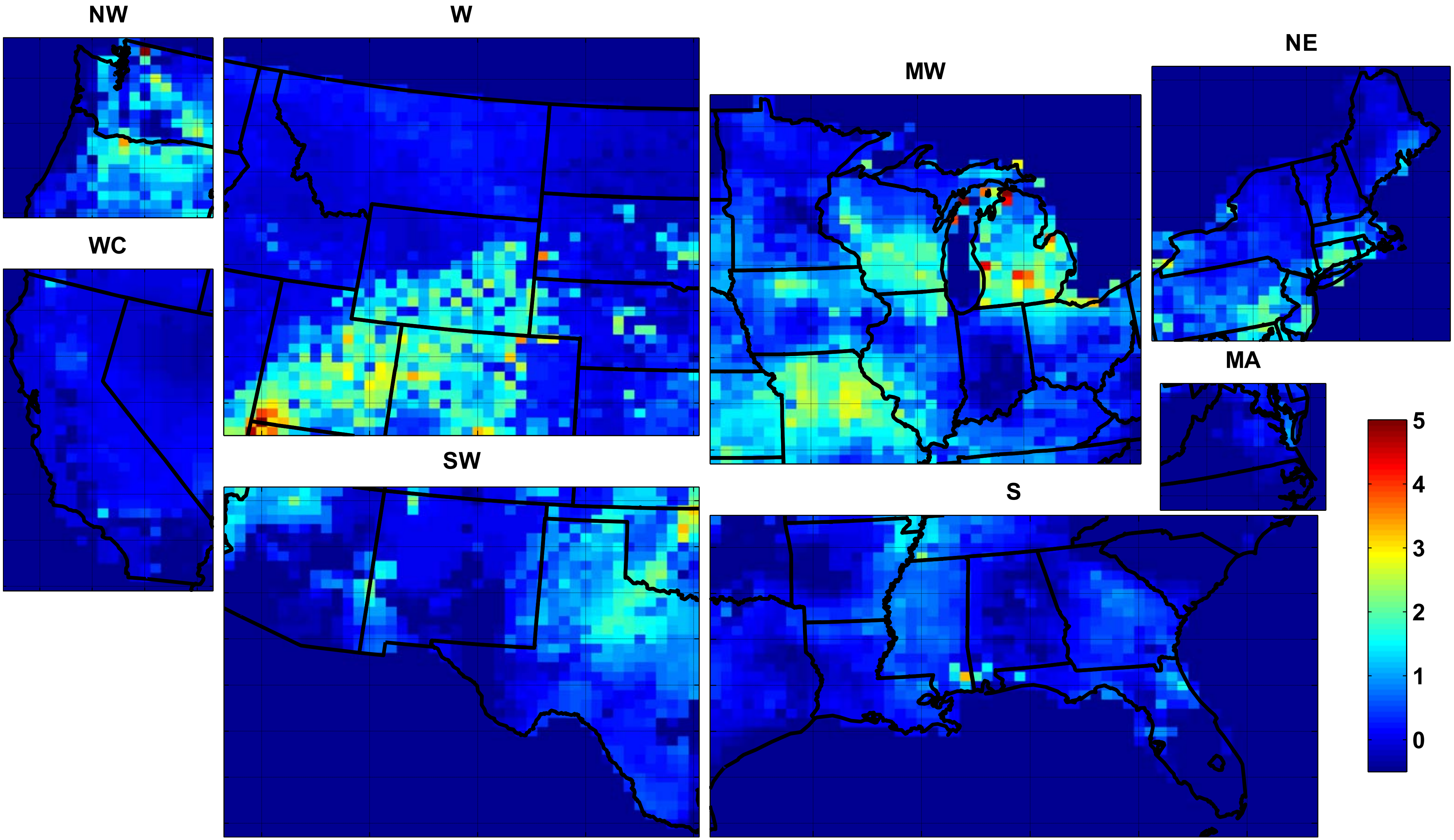

Figure 50. Ozone response to change in non-road mobile emissions (ppb).

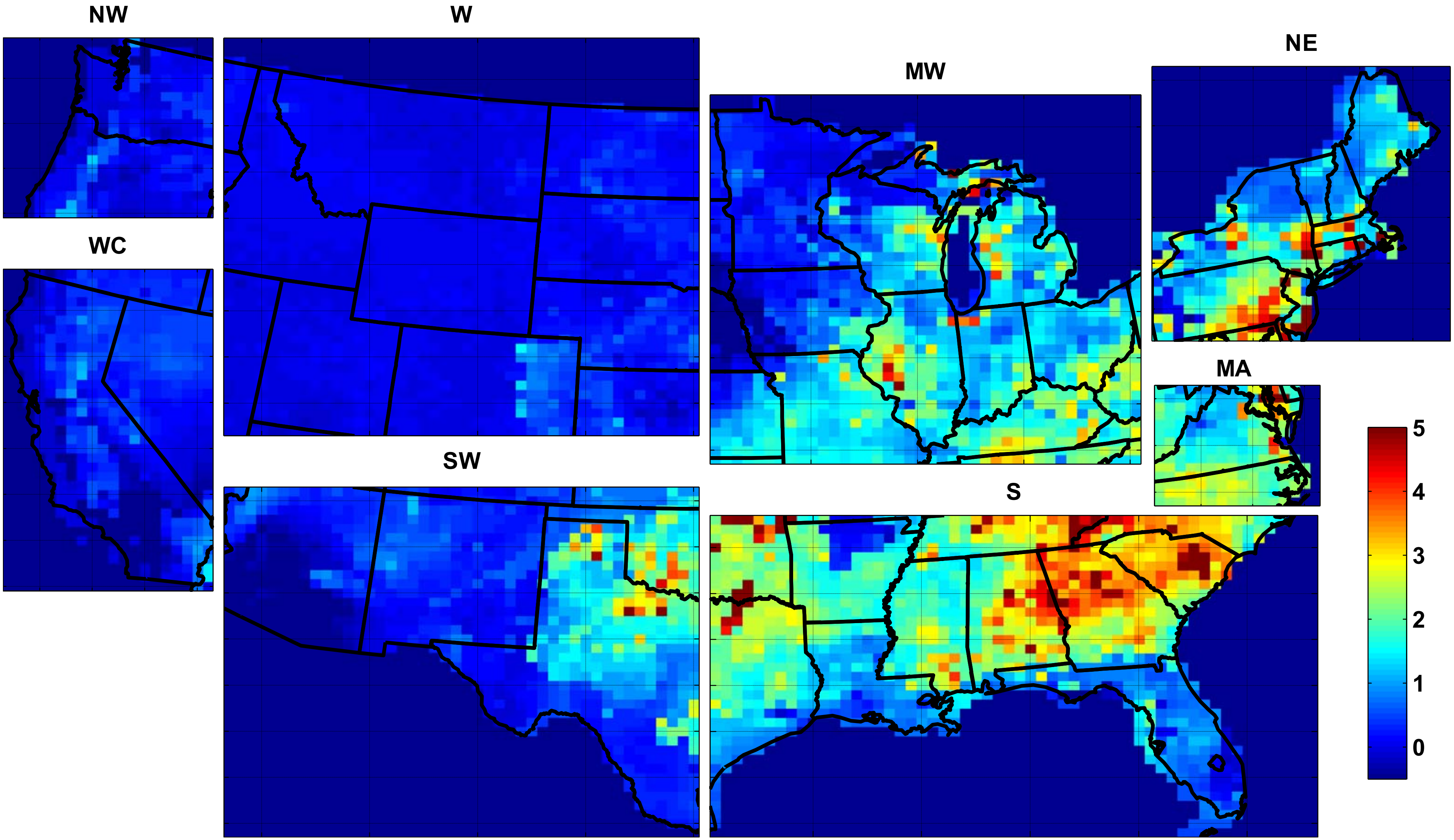

Figure 51. Ozone response to change in non-EGU point source emissions (ppb).

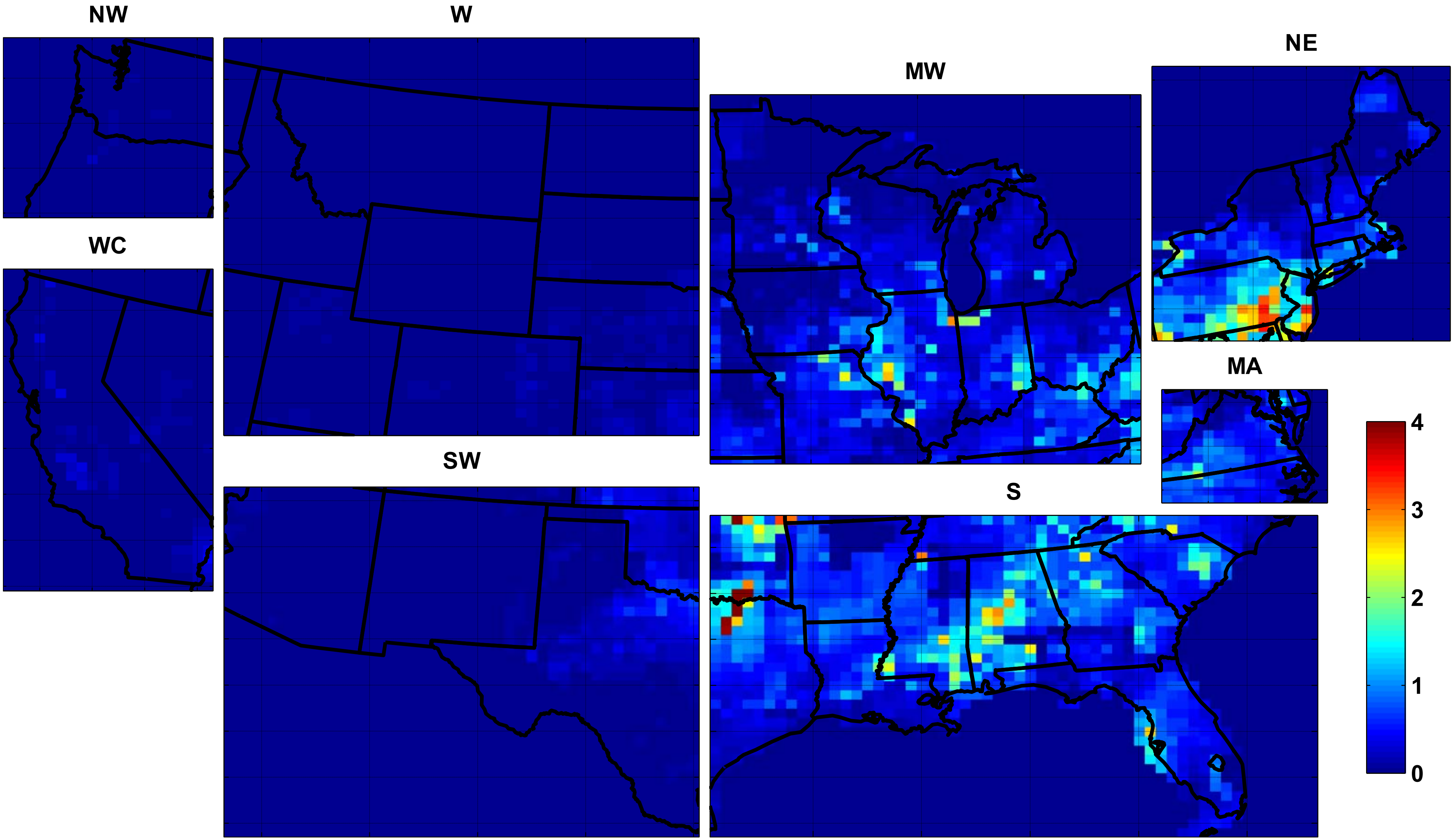

Figure 52. Ozone response to change in EGU emissions (ppb).

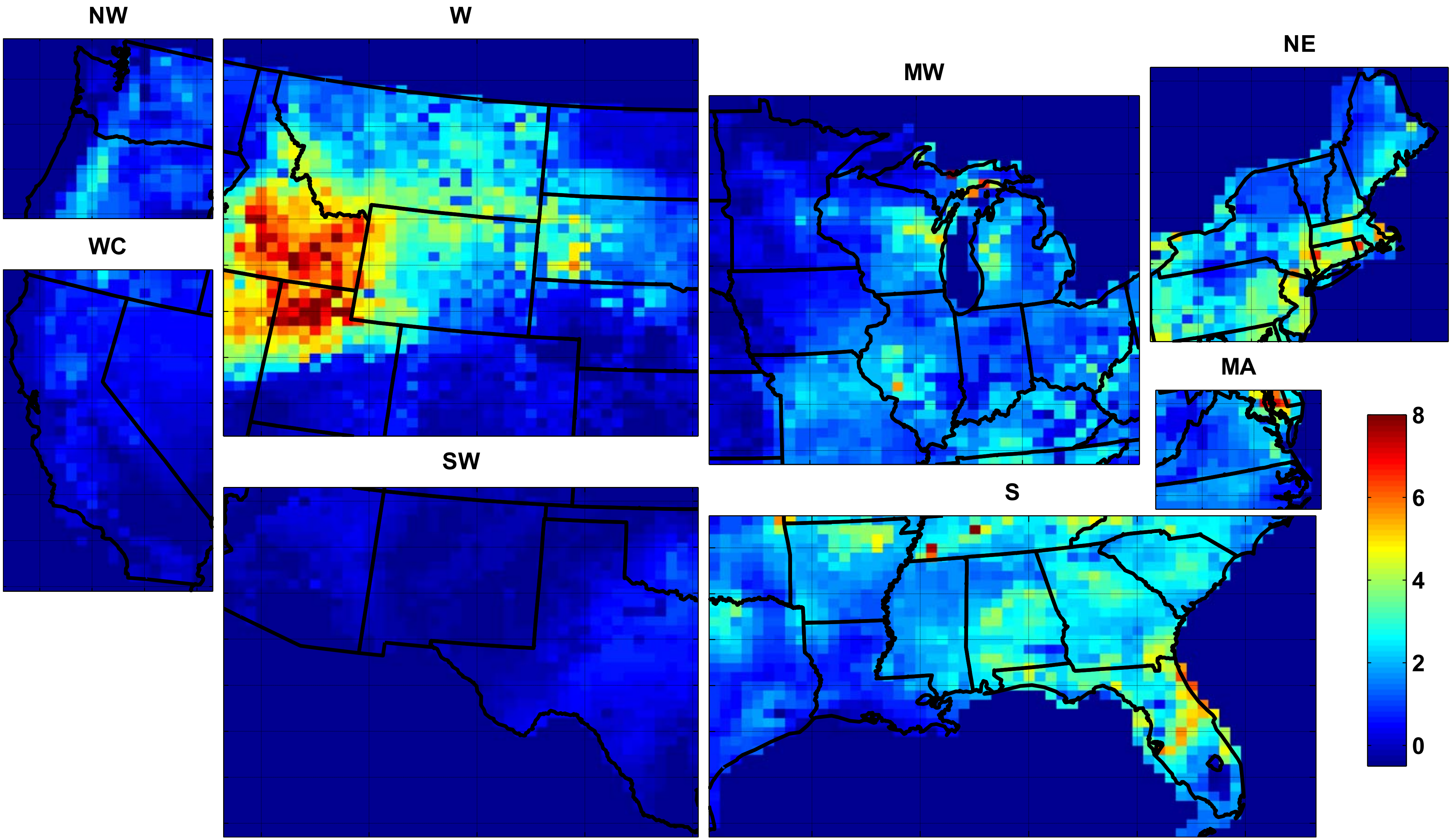

Figure 53. Ozone response to change in area emissions (ppb).

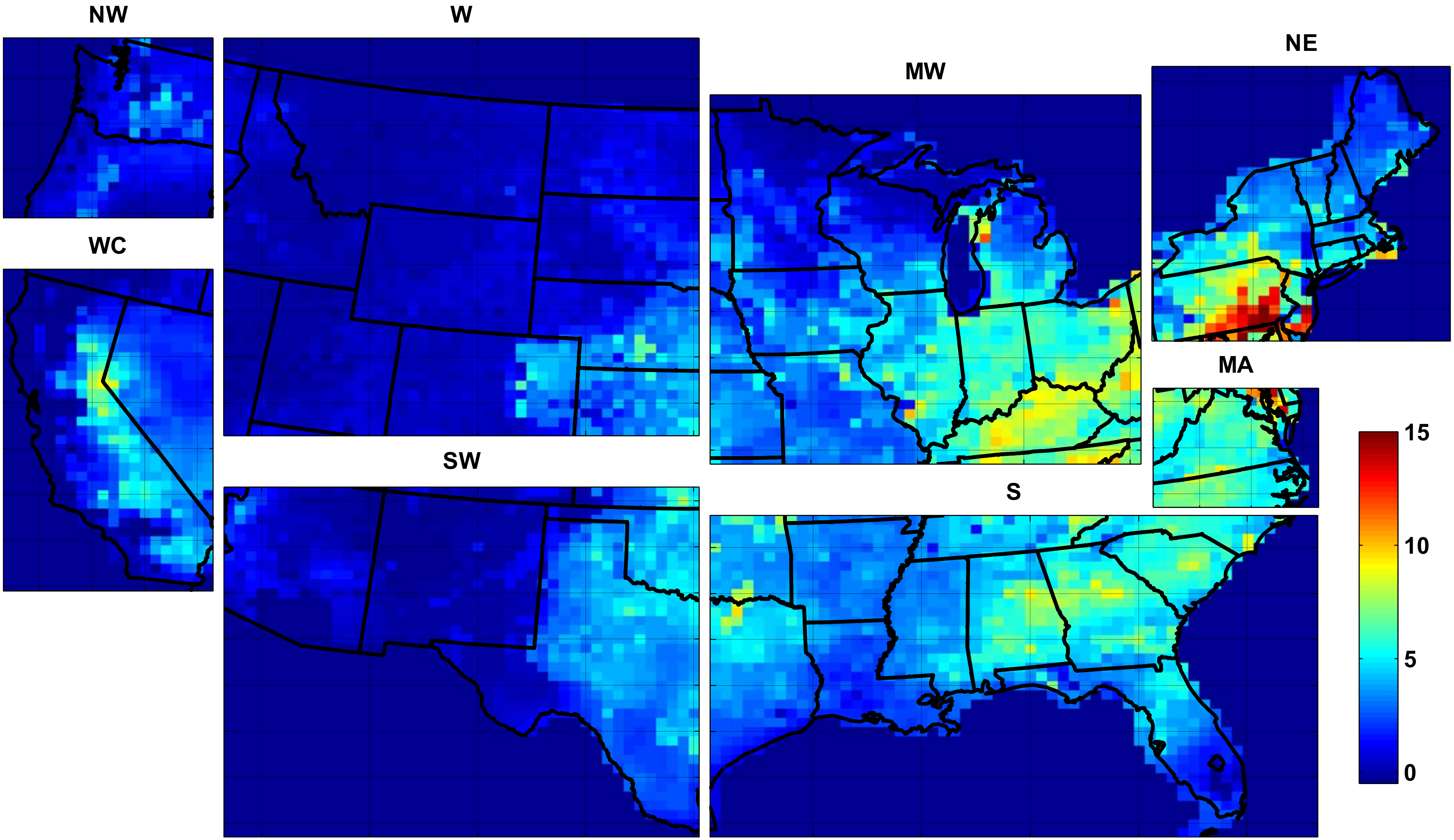

Figure 54. Ozone response to change in mobile source emissions (ppb).